GRADUATE AERONAUTICAL LABORATORIES
CALIFORNIA INSTITUTE OF TECHNOLOGY

AFOSR-83-0213 Interim Report

for the Period Ending 15-Apr-86

CHEMICAL REACTIONS in TURBULENT MIXING FLOWS

P. E. DIMOTAKIS, Professor, Aeronautics & Applied Physics

J. E. BROADWELL, Senior Scientist, Aeronautics

A. LEONARD, Professor, Aeronautics

Firestone Flight Sciences Laboratory

Guggenheim Aeronautical Laboratory

Karman Laboratory of Fluid Mechanics and Jet Propulsion

Pasadena

Unclassified
SECURITY CLASSIFICATION OF THIS PAGE

REPORT DOCUMENTATION PAGE

1a. REPORT SECURITY CLASSIFICATION: Unclassified	1b. RESTRICTIVE MARKINGS: None
2a. SECURITY CLASSIFICATION AUTHORITY	3. DISTRIBUTION/AVAILABILITY OF REPORT: Distribution unlimited; approved for public release
2b. DECLASSIFICATION/DOWNGRADING SCHEDULE	
4. PERFORMING ORGANIZATION REPORT NUMBER(S)	5. MONITORING ORGANIZATION REPORT NUMBER(S)
6a. NAME OF PERFORMING ORGANIZATION: California Institute of Technology; 6b. OFFICE SYMBOL (If applicable)	7a. NAME OF MONITORING ORGANIZATION: Air Force Office of Scientific Research
6c. ADDRESS (City, State and ZIP Code): Pasadena, CA 91125	7b. ADDRESS (City, State and ZIP Code): Bolling AFB DC 20332-6448
8a. NAME OF FUNDING/SPONSORING ORGANIZATION: Air Force Office of Sci. Res.; 8b. OFFICE SYMBOL (If applicable): AFOSR/NA	9. PROCUREMENT INSTRUMENT IDENTIFICATION NUMBER: AFOSR - 83 - 0213
8c. ADDRESS (City, State and ZIP Code): Bolling AFB DC 20332-6448	10. SOURCE OF FUNDING NOS.

PROGRAM ELEMENT NO.	PROJECT NO.	TASK NO.	WORK UNIT NO.
61102F	2308	A2	

11. TITLE (Include Security Classification): Chemical Reactions in Turbulent Mixing Flows (uncl)

12. PERSONAL AUTHOR(S): P.E. Dimotakis, J. E. Broadwell, A. Leonard

13a. TYPE OF REPORT	13b. TIME COVERED	14. DATE OF REPORT (Yr., Mo., Day)	15. PAGE COUNT
Interim	FROM Apr. '85 TO Apr. '86	15 June 1986	112

16. SUPPLEMENTARY NOTATION

17. COSATI CODES			18. SUBJECT TERMS (Continue on reverse if necessary and identify by block number)
FIELD	GROUP	SUB. GR.	Turbulence, Shear Flow, Combustion
20	04		
21	01		

19. ABSTRACT (Continue on reverse if necessary and identify by block number)

Work is continuing primarily in gas phase turbulent mixing and chemical reactions. The liquid phase work to date is in its final stages of being analyzed and documented for dissemination in the form of archival publications. In the gas phase shear layer work, our investigations are concentrating on shear layer free stream density ratio effects, finite kinetic rate (Damköhler number) effects, and a design effort in support of the planned extension of the work to supersonic flows. In jet flows, progress has been made in the gas phase laser Rayleigh scattering techniques developed for conserved scalar measurements down to diffusion space and time scales. A new technique has been developed under joint support with the Gas Research Institute that permits the imaging of soot sheets in turbulent flames and is being used to describe the combustion flame sheets in methane flames. Theoretical work in progress is addressing the finite chemical rate problem as well as the diffusion-limited shear layer mixing problem. Advances in our data acquisition capabilities during the last year are permitting higher temporal resolution

20. DISTRIBUTION/AVAILABILITY OF ABSTRACT	21. ABSTRACT SECURITY CLASSIFICATION
UNCLASSIFIED/UNLIMITED ☒ SAME AS RPT. ☐ DTIC USERS ☐	Unclassified

22a. NAME OF RESPONSIBLE INDIVIDUAL	22b. TELEPHONE NUMBER (Include Area Code)	22c. OFFICE SYMBOL
Julian M. Tishkoff	(202)767-4935	AFOSR/NA

DD FORM 1473, 83 APR EDITION OF 1 JAN 73 IS OBSOLETE.

Unclassified
SECURITY CLASSIFICATION OF THIS PAGE

GRADUATE AERONAUTICAL LABORATORIES
of the
CALIFORNIA INSTITUTE of TECHNOLOGY
Pasadena, California 91125

AFOSR-83-0213 Interim Report

for the Period Ending 15-Apr-86

CHEMICAL REACTIONS in TURBULENT MIXING FLOWS

Principal investigators:

P. E. DIMOTAKIS, Professor, Aeronautics & Applied Physics

J. E. BROADWELL, Senior Scientist, Aeronautics

A. LEONARD, Professor, Aeronautics

15-Jun-86

ABSTRACT

Work is continuing primarily in gas phase turbulent mixing and chemical reactions. The liquid phase work to date is in its final stages of being analyzed and documented for dissemination in the form of archival publications. In the gas phase shear layer work, our investigations are concentrating on shear layer free stream density ratio effects, finite kinetic rate (Damköhler number) effects, and a design effort in support of the planned extension of the work to supersonic flows. In jet flows, progress has been made in the gas phase laser Rayleigh scattering techniques developed for conserved scalar measurements down to diffusion space and time scales. A new technique has been developed under joint support with the Gas Research Institute that permits the imaging of soot sheets in turbulent flames and is being used to describe the combustion flame sheets in methane flames. Theoretical work in progress is addressing the finite chemical rate problem as well as the diffusion-limited shear layer mixing problem. Advances in our data acquisition capabilities during the last year are permitting higher temporal resolution measurements to be taken with digital image arrays.

1.0 INTRODUCTION

Work is continuing primarily in gas phase turbulent mixing, chemical reactions and combustion, while the work in liquid phase systems is in its final stages of being analyzed and published. A review paper has just appeared (Broadwell & Dimotakis 1986) summarizing these early results and their implications for modeling chemically reacting flows. Both experimental and analytical/modeling investigations are in progress, as well as an accompanying effort to develop and augment diagnostic techniques, on an as needed basis, in support of the experimental program. Progress in these areas, realized during the reporting period ending 15-Apr-86 will be described below.

2.0 HF COMBUSTING SHEAR LAYER

2.1 Heat release effects

The experimental investigation of the effects of heat release (and moderate pressure gradients) on equal free stream density shear layers has been completed. See discussion in our Interim Report for the period ending 15-Apr-1985 (Liepmann, Broadwell & Dimotakis 1985, section 2.4 and appendix). A documentation of that work has appeared during the period covered by this report in the form of a GALCIT Ph.D. thesis (Hermanson 1985). Minor revisions of the first announcement of that research (Hermanson, Mungal & Dimotakis 1985) are in progress for publication in the AIAA Journal.

2.2 Stability analysis

A study was carried out to determine the effect of large density ratios on the initial stability characteristics of the plane mixing layer. In this study, the inviscid, linear, parallel-flow stability

analysis of spatially growing disturbances was utilized to calculate the range of unstable frequencies and wave-numbers in a non-uniform density plane shear layer taking into account the wake component of the initial velocity profile. This work has been submitted for the AIAA 25th Aerospace Sciences Meeting in Reno, Nevada, January 1987 (see appendix A). The most important result is that when the high density is on the low-speed side, there exist two instability branches of comparable growth rate. One of these, the shear layer mode, leads to the usual Kelvin-Helmholtz roll-up patterns. The second branch, the wake mode, corresponds to roll-up patterns that resemble those found in pure wake flows. These results indicate that, under the right conditions, a shear layer of non-uniform density may transition to turbulence more like a wake than like a shear layer through the Kelvin-Helmholtz vortices. That this can, in fact, happen was confirmed in an acoustically-forced shear layer between a high-speed stream of helium and low-speed stream of argon. Both shear layer and wake type flow patterns were generated depending on the forcing frequency. See figure 4 in appendix A.

2.3 Damköhler number effects

A property of the hydrogen-fluorine reaction system that has proved to be most useful is that its overall rate is determined by the hydrogen atom concentration, which, in turn, can be controlled by the initial nitric oxide concentration. This system is, therefore, almost ideal for studying finite rate chemistry: the potential heat release can be small and fixed as the rate is changed from zero to values so high that the reaction is mixing limited. Previous extensive studies (Mungal & Dimotakis 1984, Mungal, Hermanson & Dimotakis 1985) at the high rate provide a set of results against which those obtained at "finite rates" can be compared.

In the past year, a series of experiments were carried out in the H_2-F_2 shear layer combustion facility using this reaction to investigate

the effects of reaction rate in a high Reynolds number shear layer. In addition, the finite reaction rate was incorporated into the model proposed by Broadwell and Breidenthal (1982) and which has been used in the interpretation of the earlier H_2-F_2 high reaction rate experiments. These studies are described in Mungal & Frieler (1985) and Broadwell & Mungal (1986), which are attached as Appendices B and C.

The primary experimental results were sets of temperature-time traces recorded at eight stations distributed laterally across the layer at one axial location. From these, mean temperature profiles can be constructed and the total amount of product in the layer calculated. In the model, the parameter which arises naturally to characterize the reaction rate is the first Dahköhler number, Da_x, the ratio of two times: the mean flow time between the measuring station and the transition location and a characterisitc reaction time. The first time is $2x/(U_1 + U_2)$, where the U's are the free stream velocities and x the distance just mentioned. The reaction time was determined from the CHEMKIN code for the various free stream reactant concentrations.

The experimental and analytical results are shown in figure 1 taken from Broadwell & Mungal (1986). We see that, for the fastest rates, the experiments and the model agree in showing that the reaction is nearly independent of Da_x, i.e., nearly mixing-limited at the highest rates. Finite rate effects become significant for $Da_x \sim 30$ (a result of critical importance for the design of the supersonic facility).

In addition, the changes in the shapes of the time traces and of the mean profiles with reaction rate in the experiment are important clues to the nature of the turbulent mixing process. The results of a preliminary evaluation in Broadwell & Mungal (1986) shows, again, the central role of the large scale structures in the first stages of the mixing process. The observations are also consistent with the ideas underlying the model. Interestingly, these ideas explain why the *time-traces and profile shapes for a slow reaction in a gas are similar* to those for a fast reaction in water.

With regard to the model we note that there are two empirical constants (one of which, however, can be estimated from the turbulence theory on which the model is based). For the same values of the constants, the model satisfactorily accounts for the effects of:

1. stoichiometric mixture (equivalence) ratio (Mungal & Dimotakis 1984),
2. Schmidt number (Koochesfahani 1984),
3. Reynolds number (Mungal, Hermanson & Dimotakis 1985) — not so satisfactorily,
4. the "flip" in liquids (Koochesfahani 1984, Koochesfahani, Dimotakis & Broadwell 1985),

and, now,

5. the Damköhler number.

When the same ideas are used in a model of fuel jets burning in air, it explains (Broadwell 1982):

1. the independence of flame length from Reynolds and Schmidt numbers at high Reynolds number,
2. the linear dependence of flame length on the stoichiometric mixture ratio,

and,

3. the dependence of nitric oxide generation in hydrogen and methane flames on Reynolds number.

Finally, if the influence of strain rate on the chemical reaction is introduced,

4. the parameters governing blow-out of hydrocarbon flames can be deduced (Broadwell, Dahm and Mungal 1984).

These results suggest that the single idea on which the model is based, namely that molecular mixing takes place in a succession of a Kolmogorov-like cascades between the largest and smallest scales in the flow, embodies most (or all) of the essential features of the turbulent mixing process. The model, as presently formulated, describes the mean behavior, the average over the cascade processes. The underlying processes are unsteady and the observed large scale flame length fluctuations are the best evidence of the individual cascade. A more detailed examination of the results of several experimental investigations will be undertaken to determine to what degree this conclusion is justified.

2.4 Chemical kinetics calculations with mass addition

In our extension of the work to date to supersonic flows, we would like to retain the considerable advantage of being in a position to measure the extent of turbulent mixing to a molecular scale using fast, irreversible chemical reactions Accordingly, the need for fast chemical kinetics in the supersonic shear layer flow was recognized as being the primary design driver since, for supersonic flow, the residence time of the reactant gases in the test section can be very short (order of 1 to 10 milliseconds). It is this consideration which motivated our selection of the $F_2/H_2/NO$ reaction system and our intention to have the flow test section as near as feasible to atmospheric pressure.

Our goal is to be able to perform experiments in the mixing-limited regime, in which the chemical kinetic rates are large relative to the mixing rate, that is in the limit of infinitely fast chemical kinetics. In order to predict whether or not this will be possible, we have resorted to a two-step analysis. First, we have assumed that the

experimental results of Mungal and Frieler (1985) can be reasonably extended to supersonic shear layers. This study indicated that the mixing limited regime is attained in flows for which Da_x (Damkohler number based on length) is greater than 40. Second, we performed computer calculations to estimate characteristic chemical times for reactant compositions that we expect in our supersonic experiments. These calculations enable us to estimate the maximum attainable Damkohler number under the least favorable flow conditions, namely those at the highest flow Mach number of 3.0 .

Our original computer calculations followed those of Mungal and Frieler in that they simulated a constant mass, homogeneous chemical reactor. As was previously reported, those results suggested that our new supersonic facility would be capable of a mixing-limited chemical kinetic environment, with approximately an order of magnitude safety margin. We are presently exploring a more realistic chemical kinetics reactor model in which we are simulating the continuous mass (reactant) addition that results from the entrainment and mixing processes and which proceeds concurrently with the chemical reaction. The new results demonstrate that characteristic chemical times can be significantly longer when mass addition is included. See figure 2 . These preliminary results, however, indicate that it may still be possible to operate in the mixing-limited regime, albeit with a somewhat reduced margin with respect to the fast chemistry requirement.

There are two caveats that must be stated with regards to the fast chemistry criterion as it relates to the supersonic shear layer. First, it is not clear that the subsonic results of Mungal and Frieler can be applied directly to supersonic shear layer flows. The turbulent interface generation under supersonic flow conditions could be qualitatively and quantitatively different and, as a consequence, our estimated margins for fast chemistry could prove optimistic. Second, fast chemical kinetics can only be attained with relatively high concentrations of reactant gases; for example, the fluorine gas

concentration must be 10 to 15 molar percent. This results in elevated gas temperatures (in excess of 1300 K) which may make it difficult to study the mixing-limited, supersonic shear layer as decoupled from the effects of heat release. These are important issues which will be addressed in the course of the research that will be undertaken. They have prompted us to consider, however, the additional flexibility that adding supersonic stream gas pre-heating capability to the design (subject to the availability of funding support) will permit.

2.5 Supersonic shear layer design

The GALCIT Reacting Shear Layer Combustion facility is in the process of being re-designed for supersonic flows. The new facility is being designed to produce a bisonic (supersonic/subsonic) reacting shear layer capable of handling the reactants of the $F_2/H_2/NO$ system. The fundamental design considerations behind this facility were described in some detail in our last report. For convenience, the supersonic stream plumbing schematic (figure 3) and the table of specifications (Table 1) are reproduced here. It should be recalled that the low speed (F_2) plumbing hardware in the existing laboratory will be used without significant modification in the new facility. Therefore, our design efforts have primarily dealt with the new supersonic leg and test section.

Four segments of the facility for the new supersoinc leg have received attention since our last report. They are: the reactant tank, the (possible) pre-heater, the fast acting valve, and the main pressure regulator. Although none of these items are ready for fabrication or purchase, it is hoped that only one more design iteration for each will be required.

The desirability of a gas pre-heater was explained in the previous section. The current design calls for the reactant tank to be wrapped

with electrical heating tape and thermal insulation. The total heating capability will be 10 kW. Prior to the experiment, the tank and its packing will be heated to maximum temperature of 600 K. After the desired temperature is reached, the supersonic gas mixture will be added to the tank. During the tank discharge, the tank and its packing should limit the temperature drop to approximately 20 K.

A new vendor for the fast acting valve has been located (Fox Valve Development Corporation, East Hanover, NJ). This valve, which was recommended to us by Paul Waltrup of the Applied Physics Laboratory of Johns Hopkins University, is of the venturi-type with much improved performance over the original device. Opening times on the order of 100 ms or less are claimed for this valve.

Another product from the Fox Corporation could potentially serve as a main pressure regulator. The device is an adjustable area venturi valve which could be combined with an electronic controller so as to provide mass flow regulation and hence pressure regulation. The feasibility of such an actively controlled device is in the process of being evaluated. After the feasibility study, the relative merits of that device will be compared with those of the commercial pressure regulators already located, and a final device selected.

2.6 Density Ratio Effects

By selecting the free-stream diluents in the HF shear layer combustion facility it is possible to study the effects of density differences on entrainment, mixing and reaction. Keeping the velocity ratio, flame temperature and molar specific heats constant, experiments will eventually be performed for the range of density ratios $1/8 < s < 8$ ($s = \rho_2/\rho_1$). Pressure gradients due to displacement effects can be removed by properly adjusting the test section side walls.

Several important questions are addressed in this work. Among these is the dependence of the shear layer volumetric entrainment ratio and mixed fluid composition on density ratio. The flux of fluid into the turbulent region can be estimated from the orientation of the free-stream streamlines and the boundaries of the mixing layer (Dimotakis 1984, Hermanson 1985). The ratio of the fluid flux from the two streams is the volume entrainment ratio (E_V) and has been shown to be sensitively dependent upon the density ratio (Konrad 1976, Mungal & Dimotakis 1984). Shown in figure 4 are preliminary data for E_V for a number of density ratios, along with a similarly derived empirical value from the Brown & Roshko (1974) data. It should be noted that theoretical analyses by Brown (1974) and Dimotakis (1984) predict a $\sqrt{s}$ dependence on density ratio for this quantity. The dashed line in figure 4 is a plot of the theoretical expression (Dimotakis 1984)

$$E_V = \sqrt{s}\left(1 + 0.68\,\frac{1-r}{1+r}\right)$$

where $r = U_2/U_1$ is the velocity ratio which was set in the range of 0.38-0.40 for the data in figure 4. (note that $E_V > 1$ for $\rho_2/\rho_1 = 1$). While this estimate is in good agreement with the data for density ratios $s > 1$, the behavior for density ratios $s < 1$ appears to be less well described by this theory.

The anomalous point for $s = 10$ is worth elaborating upon. Detailed elsewhere within this report is recent work by Koochesfahani and Frieler which demonstrates the existence of a second fundamental mode of instability in the experimentally realizable shear layer. This corresponds to an instability of the splitter plate wake velocity profile arising from the merging of the boundary layers shed from the trailing edge of the splitter tip. The predominance of this mode in the cases with $s \gg 1$ appears to be responsible for significant changes in the structure and dynamics of the initial roll-up of the mixing layer, which seem to extend for a significant distance downstream. We believe

that factor of two to three decrease in E_v at $s = 10$, over the value that would have been anticipated by any reasonable extrapolation of the rest of the data, is a manifestation of this qualitative difference in shear layer behavior. This is also reflected in the layer growth rate and mean stagnation pressure profiles, which also indicate that the effects of this mode last for the extent of the HF facility test section. Further work on these extreme density ranges will rely on our ability to manipulate initial conditions to control this instability.

Using chemical reactions at stoichiometric mixture ratios both large and small compared to unity, e.g. $\phi = 8$ and $\phi = 1/8$, it is possible to estimate the volume ratio comprising the mean mixed fluid composition (see Koochesfahani 1984), denoted here by E_{vM}. In this work this is derived from pairs of "flip" experiments performed at the same density ratio at high and low free-stream reactant stoichiometric mixture (concentration) ratios ($\phi = 8, 1/8$). Also plotted in figure 4 are the estimates of the entrainment ratio derived in this manner (E_{vM}) from these "flip" experiments, along with the equal density experiments of Mungal & Dimotakis (1984, gas phase) and Koochesfahani (1984, liquid). Results from two (non-reacting) gas phase experiments by Konrad (1976, $s = 1, 7$) are also shown. Konrad attempted to measure the concentration field directly in dilution experiments in non-homogeneous shear layers. While he used the term entrainment ratio, his definition involving intermittency was an attempt to included the mixed fluid fraction only, and as a result will be called here the mixed fluid composition. While it can be seen that this assignement of a value to the entrainment ratio follows the (geometrically estimated) E_v trend, it is consistently lower. In fact, for $s < 4$, the mixed fluid ratio E_{vM} appears to be a nearly fixed fraction of the geometric entrainment ratio E_v, i.e. $E_{vM}/E_v \approx 0.7$.

There is, of course, no a priori reason to assume that the two quantities should be the same; the fluid need not necessarily be mixed in the ratio at which it crosses the shear layer boundaries.

Nevertheless, the difference in the behavior for density ratios greater than unity (low speed side denser) as compared to density ratios smaller than unity (high speed side denser) is noteworthy. As of this writing it is not clear whether this is a manifestation of the different kinds of instability modes that can be supported by shear layers at different density ratios or is an artifact of the methods we are using to estimate the entrainment ratio. If the former should prove to be the case, it would constitute a new result in the fluid mechanics of turbulent shear layer mixing.

This work is part of the on-going Ph.D. thesis work of Cliff Frieler.

3.0 LIQUID PHASE SHEAR LAYER

This work has been completed. An early announcement in the form of an AIAA Paper was published during the present reporting period (Koochefahani & Dimotakis 1985). A more extended paper documenting the results including those involving chemical reactions has been accepted for publication in the J. of Fluid Mech. (Koochesfahani & Dimotakis 1986).

4.0 TURBULENT JET MIXING & CHEMICAL REACTIONS

4.1 Gas Phase Jet Mixing - Laser Rayleigh Scattering

The characterization of Schmidt number (ratio of kinematic viscosity to species diffusivity) effects is important in understanding turbulent mixing and combusting flows. The gas phase mixing experiments described here are directed towards determining quantitatively the differences between gases and liquids for turbulent jets and plumes. Since we expect that the effects of varying diffusivity would be

confined to the smallest scales of the flow, high resolution measurements, in both time and space, have been undertaken. The development of a laser Rayleigh scattering diagnostic for these measurements was reviewed in the interim report of last year. This year all of our work has focused on the full scale experiment in which we will make the high resolution measurements. A schematic of this facility has been included as figure 5.

The construction of the full scale experiment facility has been completed. This includes all of the sub-systems for manipulation of the gases and optics. Testing of these systems has been completed with good results in all but one case. A few preliminary runs were made as a check of system integration. What follows in this section is a summary of the completed work.

The main enclosure on which the laser is mounted and in which the gases are mixed was fabricated, varnished, painted, sealed and placed in a laboratory which has the proper electrical capability for the laser system. Unfortunately, this was in the sub-basement and it was necessary to install a special explosion proof suction line to the roof (five stories up) in order to safely vent the exhaust gases from the experiment. The large optical traverse and the laser beam manipulation optics were installed and tested. The resolution of the collection optics was extensively tested and the results were in agreement with the calculated values. The nozzle assembly was completed and installed. The exit turbulence level was found to be less than 0.2%. The exit velocity profile was found to be uniform to within the accuracy of the pressure transducer (0.2%). Combustible gas detectors were installed in the laboratory as a safety precaution since some of the gases we plan to use are volatile (explosive) hydrocarbons. Appropriate data acquisition and processing software was developed. The construction of the gas delivery systems has been completed. Their testing has not been completed since the required long time stability of the flows from these systems was not achieved. The gas delivery system for the jet was

modified to include a driver vessel which would assure a constant driving pressure which was unattainable by an earlier design. The temperature of the gas delivered by the coflow system was found to drop by about 1.5 K during one minute. Unfortunately this temperature difference, in addition to the density differences resulting from air left in the main enclosure from inadequate purging, was sufficient to cause unsteady buoyancy currents in the main enclosure after about 15 seconds of run when argon was used as the reservoir gas. This problem is being addressed with a feedback heating system and a new purging procedure.

Since the troubles with the gas delivery system are only a consideration affecting longer run times, some short preliminary runs were made. This was a useful test of all aspects of the entire experiment and has yielded some data that already suggest qualitative differences between gas phase and liquid phase ($Sc \gg 1$) mixing. In particular, the gas phase data suggest that reservoir fluid is not found on the centerline of the jet as frequently as in liquids and gradients in the concentration field of the gas phase jet are seen to be smaller for the same Reynolds number. We should repeat here that the temporal and spatial resolution in these measurements is adequate to resolve the theoretically computed corresponding scales in the flow. A time trace of some data from these runs has been included as figure 6.

The work planned for next year is to correct the remaining minor problems with the gas delivery systems and make the detailed measurements that will yield quantitative information about the differences between gas and liquid phase turbulent jet mixing.

This work is part of the on-going Ph.D. research by David Dowling.

4.2 Liquid Phase Jet Mixing & Chemical Reactions

The liquid phase jet mixing experiments were completed during this reporting period. The results have been documented in the form of a GALCIT Ph.D. thesis (Dahm 1985). A first paper of aspects of these data that was presented earlier (Dahm & Dimotakis 1985) is in the final stages of preparation to be submitted for publication in the AIAA Journal.

4.3 Soot scattering measurements in turbulent flames

We are finishing a report (Miake-Lye & Toner 1986) on the experimental soot-scattering investigation carried out during the the past year on a large turbulent buoyant diffusion flame. The experimental apparatus, the soot-scattering data, and the data analysis procedures are described in in this report. Several important conclusions can be drawn about the soot distribution in the large buoyant diffusion (methane) flame we have been studying at the initial phases of this effort.

In our report, we have set forth arguments justifying the use of soot as a marker for the combustion interface in the flame under study. These arguments are based on the facts that

1. essentially all the soot generated by the flame is consumed by the flame tip and, further,

2. there is no evidence for cold soot that is formed at one stage and consumed at a later stage.

These data, in conjunction with our r-t images, lead us to conclude that the soot is localized in a thin layer close to and locally following the reaction interface surface.

Thus, our imaging measurements of the soot distribution, wherein we have imaged a line segment within the flame as a function of time, allow us to make inferences about the nature of the topology of the combustion zone itself. Construction of r-t images from many individual scans of the imaged line segment indicates that the soot is found in relatively thin, contorted zones which we interpret to be convoluted laminar diffusion flamelets. The flamelets are continuous near the burner, but are broken and discontinuous further downstream in the flame where the velocities are greater.

Based on our r-t data, we have calculated the soot intermittency, or fraction of time that soot is present, at each radial station. The soot intermittency is highest near the center and falls to zero at the edges of the flame. By determining the instantaneous flame boundary, we have also calculated the conditional soot intermittency, which we define to be the fraction of time that soot is present within the flame boundary at any radial station. The conditional soot intermittency is nearly constant across the flame. These conclusions hold true for the various axial stations and the range of fuel flow rates that we have investigated.

Our measurements to date lead us to a picture of the flame made up of thin laminar diffusion flamelets distributed fairly uniformly within the large puff-like envelope of the flame. The interior of the puff is entirely free of soot for 40 to 60% of the time; the remainder of the time some part of a relatively thin soot-sheet is present. Since the width of the reaction zone is probably smaller than the width of the soot-sheet and since soot may strain out before the reaction is quenched, the fraction of time that the reaction interface is present may be different.

Investigations to follow will make use of a new burner designed to permit the illuminating laser beam to be directed parallel to the burner axis at several radial stations. The burner construction is now complete and we are integrating it into our experimental apparatus. By

permitting tthe laser beam to be directed parallel to the axis of the burner, this burner will allow us to measure the celerity of the puff structures. Modifications of our optical geometry are presently in progress.

We will also make higher resolution r-t measurements beyond x/D of 0.75 to complement our work to date. We will have to observe a smaller section of the flame in order to resolve the smallest soot-sheets but, since our previous data include images of the entire flame diameter, we will be able to piece together a more complete view of the soot structure even at these axial stations. These experiments will make use of the existing experimental apparatus and recent improvements in our real-time digital image acquisition capabilities. Subsequent, planned for experiments will push the flow from the buoyancy-driven regime into one that is more closely momentum driven.

These studies are co-sponsored by the Gas Research Institute (GRI).

5.0 COMPUTATIONAL EFFORT

The objective of this research is to numerically simulate a 2-D incompressible shear layer with the capability of including chemical reactions. By Kelvin and Helmholtz's theorems, the inviscid motion of vorticity at high Reynolds numbers is determined by the local fluid velocity which is itself based on the vorticity field. The techniques of discretizing vorticity and calculating the mutual interactions have been frequently used to simulate the flow. The point vortex and vortex blob are two typical methods of discretization.

The effort so far has mainly concentrated on improving the computational efficiency and accuracy. There are several ways to accomplish this purpose. One of the methods of improving the computational efficiency is to use special algorithms which can reduce the calculations of the vortex interactions from $O(N^2)$ to $O(N \log N)$,

where N is the number of computational elements (vortices). An independent method (which can be used in conjunction with the N^2 to N logN reduction) is to modify the blob method itself.

We have been investigating the possibility of using an elliptical guassian vortex blob instead of the regular circular guassian vortex blob, in the hope that the number of vortices, required for the same accuracy, can be reduced to model the same flow. The reason for this is as follows. Since a concentration of vorticity causes a strain field around itself, the effects on the motion of the other vortices from that strain field should be considered. The analytical result by Kida (1981) shows that an elliptic vortex of uniform vorticity in a uniform strain field rotates around its center, preserves the elliptical shape and keeps the area constant. However, the rates of changes in the aspect ratio and rotation angle are not constant. See figure 7. Consequently, to model the fluid precisely, the blobs should be allowed to deform in response to the strain fields from the other vortices.

By analysis, the motion of the elliptical guassian blob vortex in the region of super-imposed strain fields is decomposed into three parts.

1. translation with the local fluid velocity caused by vortex interaction

2. self-induced rotation

3. deformation caused by strain fields.

It can also be shown that the motion of each blob depends only on the present value of the strain fields and the state of the blob itself. The rate of deformation can be obtained analytically if the velocity field around the blobs are known and those effects from the strain fields are linearly summed up. See figure 8.

We are currently studying the self-induced rotation and the velocity field around an elliptical guassian core. Unfortunately, exact solutions are not available. However, the self-induced rotation of the blob is asymptotic to that of the uniform vorticity and the velocity field may be obtained by multipole expansion methods. It is clear that this new blob method needs more calculations and bookkeeping per vortex blob than the regular blob method. It is anticipated, however, that the total CPU time will be less as a result of the reduction, for a given required accuracy, of the required number of vortices.

This effort is part of the on-going Ph.D. thesis work of Kayo Ide.

6.0 REPORTS and PUBLICATIONS DURING REPORTING PERIOD

Reports and publications of work supported under this Grant that have appeared during the reporting period (16-Apr-85 to 15-Apr-86) are as follows (see reference list for complete bibliographical references):

1. Broadwell & Mungal 1986,
2. Dahm 1985,
3. Hermanson 1985,
4. Koochesfahani & Dimotakis 1985,
5. Koochesfahani, Dimotakis & Broadwell 1985,
6. Liepmann, Broadwell & Dimotakis 1985
7. Mungal & Frieler 1985,
8. Mungal, Hermanson & Dimotakis 1985.

In addition, the following have been accepted for publication in the near future.

9. Broadwell & Dimotakis 1986,

10. Dimotakis 1984 (accepted for publication in the AIAA J.),

11. Koochesfahani & Dimotakis 1986.

7.0 References

BROADWELL, J. E. [1982] "A Model of Turbulent Diffusion Flames and Nitric Oxide Generation. Part I", TRW Document No. 38515-6001-UT-00, EERC Final Report, PO No. 18889.

BROADWELL, J. E. and BREIDENTHAL, R. E. [1982] "A Simple Model of Mixing and Chemical Reaction in a Turbulent Shear Layer", J. Fluid Mech. 125, 397-410.

BROADWELL, J. E. and DIMOTAKIS, P. E. [1986] "Implications of Recent Experimental Results for Modeling Reactions in Turbulent Flows", AIAA J. 24(6), 885-889.

BROADWELL, J. E., DAHM, W. J. A., and MUNGAL, M. G. [1984] "Blow-Out of Turbulent Diffusion Flames", 20th International Symposium on Combustion (Ann Arbor, Michigan, August 1984), 303-310.

BROADWELL, J. E. and MUNGAL, M. G. [1986] "The effects of Damköhler number in a turbulent shear layer", GALCIT Report FM86-01 (4-Jun-86).

BROWN, G. L. [1974] "The Entrainment and Large Structure in Turbulent Mixing Layers", 5th Australasian Conf. on Hydraulics and Fluid Mech., 352-359.

BROWN, G. L. and ROSHKO, A. [1974] "On Density Effects and Large Structure in Turbulent Mixing Layers", J. Fluid Mech. 64(4), 775-816.

DAHM, W. J. A. [1985] Experiments on Entrainment, Mixing and Chemical Reactions in Turbulent Jets at Large Schmidt Numbers, California Institute of Technology, Ph. D. thesis.

DAHM, W. J. A. and DIMOTAKIS, P. E. [1985] "Measurements of Entrainment and Mixing in Turbulent Jets", AIAA 23rd Aerospace Sciences Meeting 14-17 January 1985 (Reno, Nevada), AIAA Paper No. 85-0056.

DIMOTAKIS, P. E. [1984] "Entrainment into a Fully Developed, Two-Dimensional Shear Layer", AIAA 22nd Aerospace Sciences Meeting (Reno, Nevada), AIAA Paper No. 84-0368. Accepted for publication in the AIAA J.

HERMANSON, J. C. [1985] Heat Release Effects in a Turbulent, Reacting Shear Layer, California Institute of Technology, Ph. D. thesis.

HERMANSON, J. C., MUNGAL, M. G. and DIMOTAKIS, P. E. [1985] "Heat Release Effects on Shear Layer Growth and Entrainment", AIAA 23rd Aerospace Sciences Meeting 14-17 January 1985 (Reno, Nevada), AIAA Paper No. 85-0142.

KIDA, S. [1981] "Motion of an Elliptic Vortex in a Uniform Shear Flow" J. Phys. Soc. Japan 50(10), 3517-3520.

KONRAD, J. H. [1976] An Experimental Investigation of Mixing in Two-Dimensional Turbulent Shear Flows with Applications to Diffusion-Limited Chemical Reactions, Ph.D. Thesis, California Institute of Technology, and Project SQUID Technical Report CIT-8-PU (December 1976).

KOOCHESFAHANI, M. M. [1984] Experiments on Turbulent Mixing and Chemical Reactions in a Liquid Mixing Layer, Ph. D. thesis, California Institute of Technology.

KOOCHESFAHANI, M. M. and DIMOTAKIS, P. E. [1985] "Laser Induced Fluorescence Measurements Concentration in a Plane Mixing Layer", AIAA 22nd Aerospace Sciences Meeting (Reno, Nevada), AIAA Paper No. 84-0198, published in the AIAA J. 23(11), 1700-1707.

KOOCHESFAHANI, M. M. and DIMOTAKIS, P. E. [1986] "Mixing and chemical reactions in a turbulent liquid mixing layer", accepted for publication in the J. Fluid Mech.

KOOCHESFAHANI, M. M., DIMOTAKIS, P. E. and BROADWELL, J. E. [1985] "A 'Flip' Experiment in a Chemically Reacting Turbulent Mixing Layer", AIAA J. 23(8), 1191-1194.

LIEPMANN, H. W., BROADWELL, J. E. and DIMOTAKIS [1985] "Chemical Reactions in Turbulent Mixing Flows", AFOSR-83-0213 Interim Report for the period ending 15-Apr-85.

MIAKE-LYE, R. C., and TONER, S. J. [1986] "Laser Soot-Scattering Imaging of a Large Buoyant Diffusion Flame", submitted to Combustion & Flame.

MUNGAL, M. G. and DIMOTAKIS, P. E. [1984] "Mixing and combustion with low heat release in a turbulent mixing layer", J. Fluid Mech. 148, 349-382.

MUNGAL, M. G. and FRIELER, C. E. [1985] "Chemical reactions in a turbulent mixing layer: The effects of the reaction rate coefficient - Part I", GALCIT report FM85-01 (31-Dec-85).

MUNGAL, M. G, HERMANSON, J. C. and DIMOTAKIS, P. E. [1985] "Reynolds Number Effects on Mixing and Combustion in a Reacting Shear Layer", AIAA J. 23(9), 1418-1423.

Bisonic Facility Specifications

	Supersonic Side (New)	Subsonic Side (Old *)
Test Section Mach Number	1.25 < M < 3.00	0.0 < M < 0.2
Reactant Gases	H2, NO	F2
Diluent Gases	N2, Ar, He	N2, Ar, He
Test Section Height Span Length	3 cm 15 cm 50 cm	5 cm 15 cm 50 cm
Maximum Mass Flow Rate	9.5 kg/sec (at M=3.00)	0.6 kg/sec (at M=0.2)
Reactant Tank Maximum Pressure	20.7 MPa (3000 psi)	0.8 MPa (115 psi)
Method Of Gas Delivery	Reactant Tank Blowdown With Pressure Regulation	Bladder Bag Compression From Outside Pressure Source
Temperature Control	Reactant Tank Pre-heating And Aluminum Packing	None
Except For Test Section		

TABLE 1

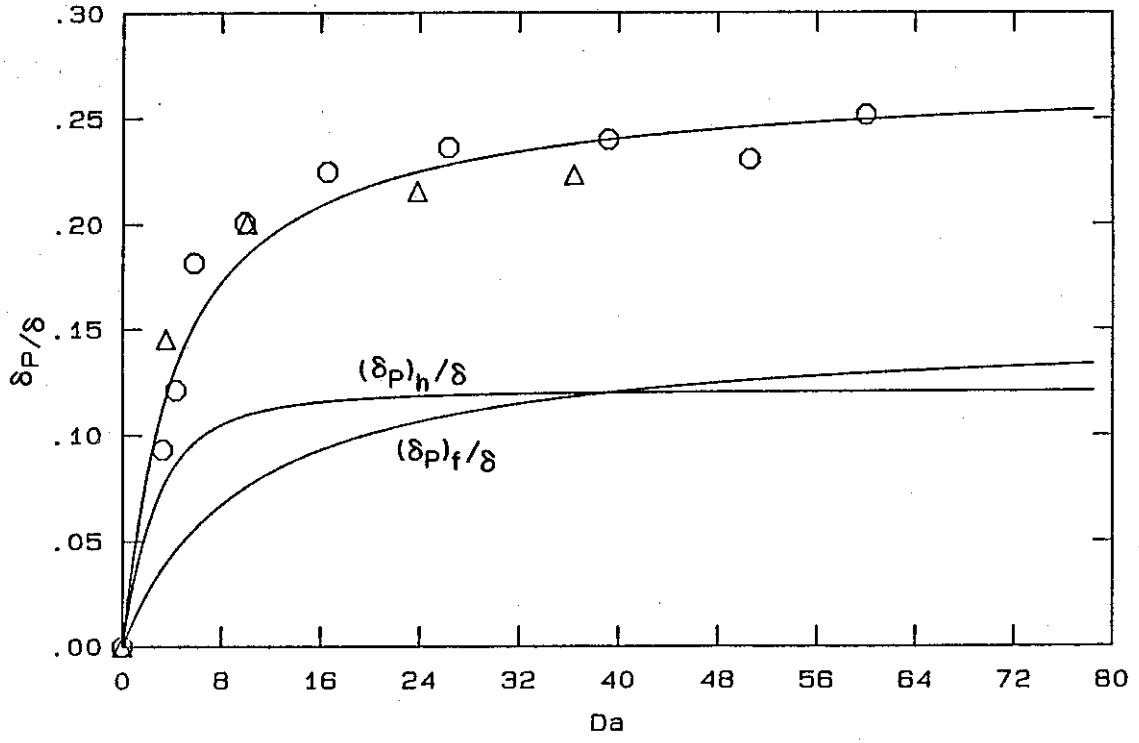

Figure 1. Dependence of integrated product concentration on Damköhler number, $Da = k\, C_{H_\infty}\, x/\bar{u}$. δ_P, total product; $(\delta_P)_f$, flame sheet product; $(\delta_P)_h$, homogeneous mixture product; δ, shear layer thickness; ○, experiment, u_1 = 22 m/sec, u_2 = 8.8 m/sec; △ u_1 = 44 m/sec, u_2 = 17.6 m/sec.

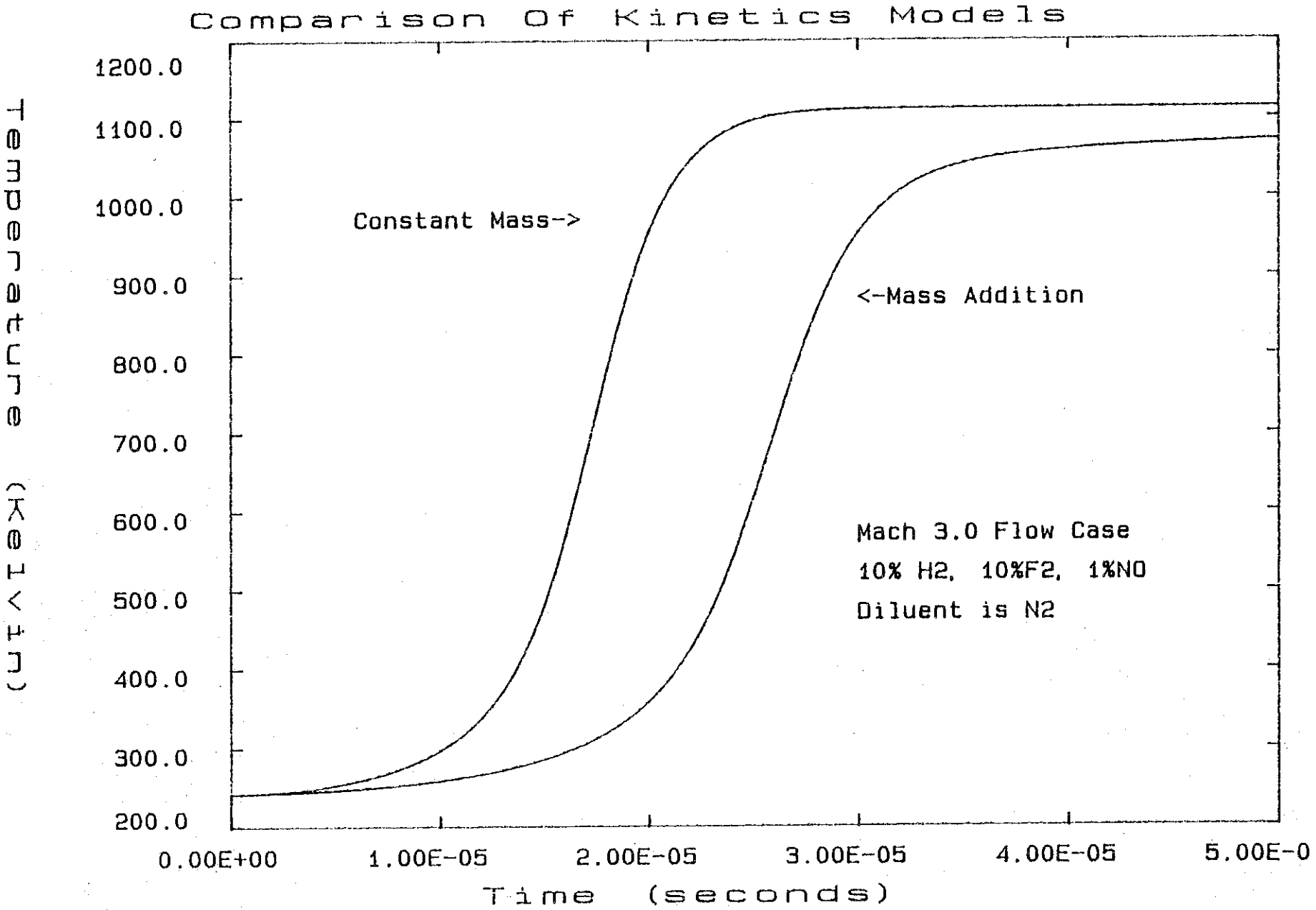
Comparison Of Kinetics Models
Temperature (Kelvin)
1200.0
1100.0
1000.0
900.0
800.0
700.0
600.0
500.0
400.0
300.0
200.0
Constant Mass->
<-Mass Addition
Mach 3.0 Flow Case
10% H2, 10%F2, 1%NO
Diluent is N2
0.00E+00
1.00E-05
2.00E-05
3.00E-05
4.00E-05
5.00E-0
Time (seconds)

SUPERSONIC STREAM PLUMBING SCHEMATIC

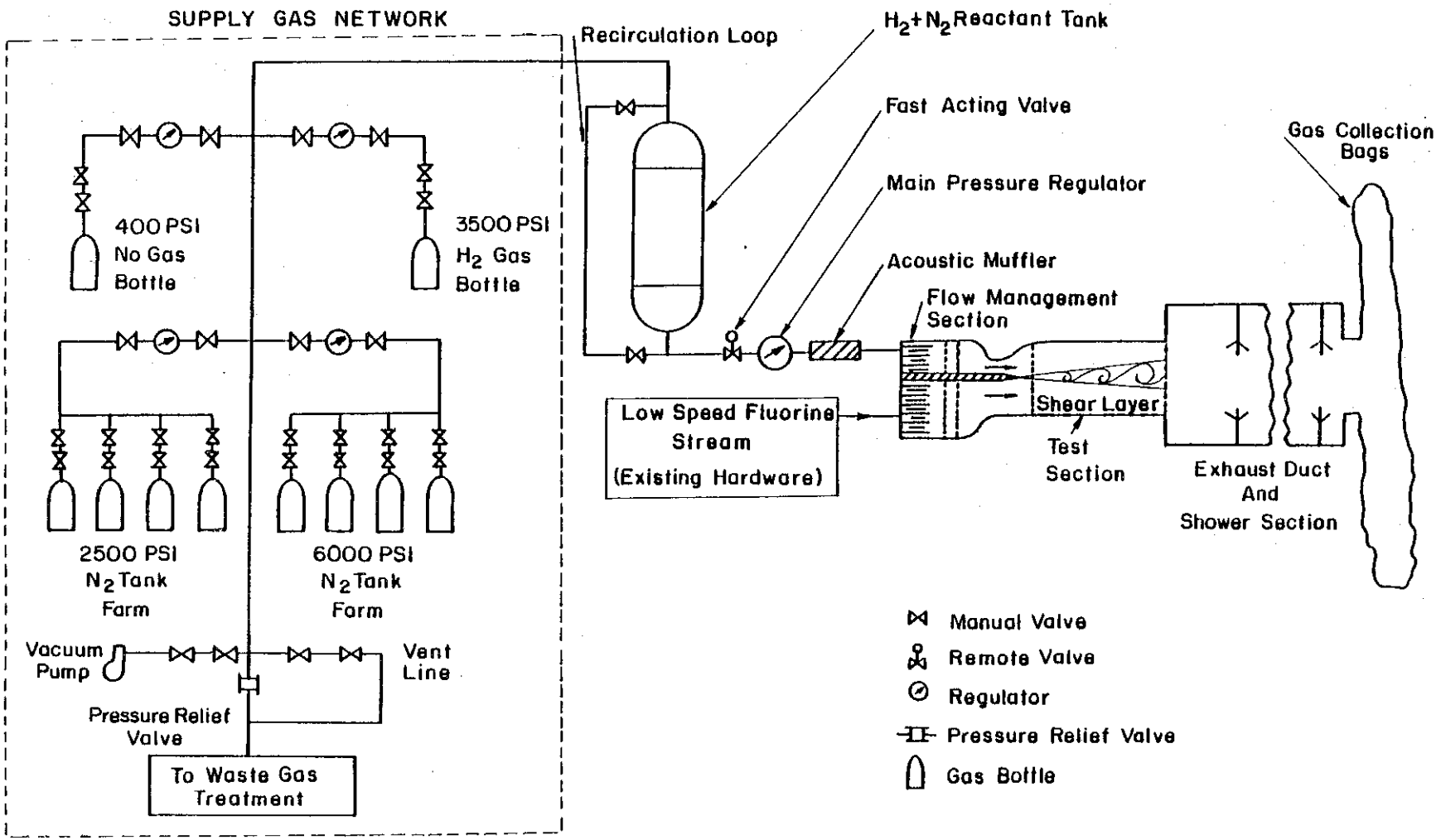

Figure 3

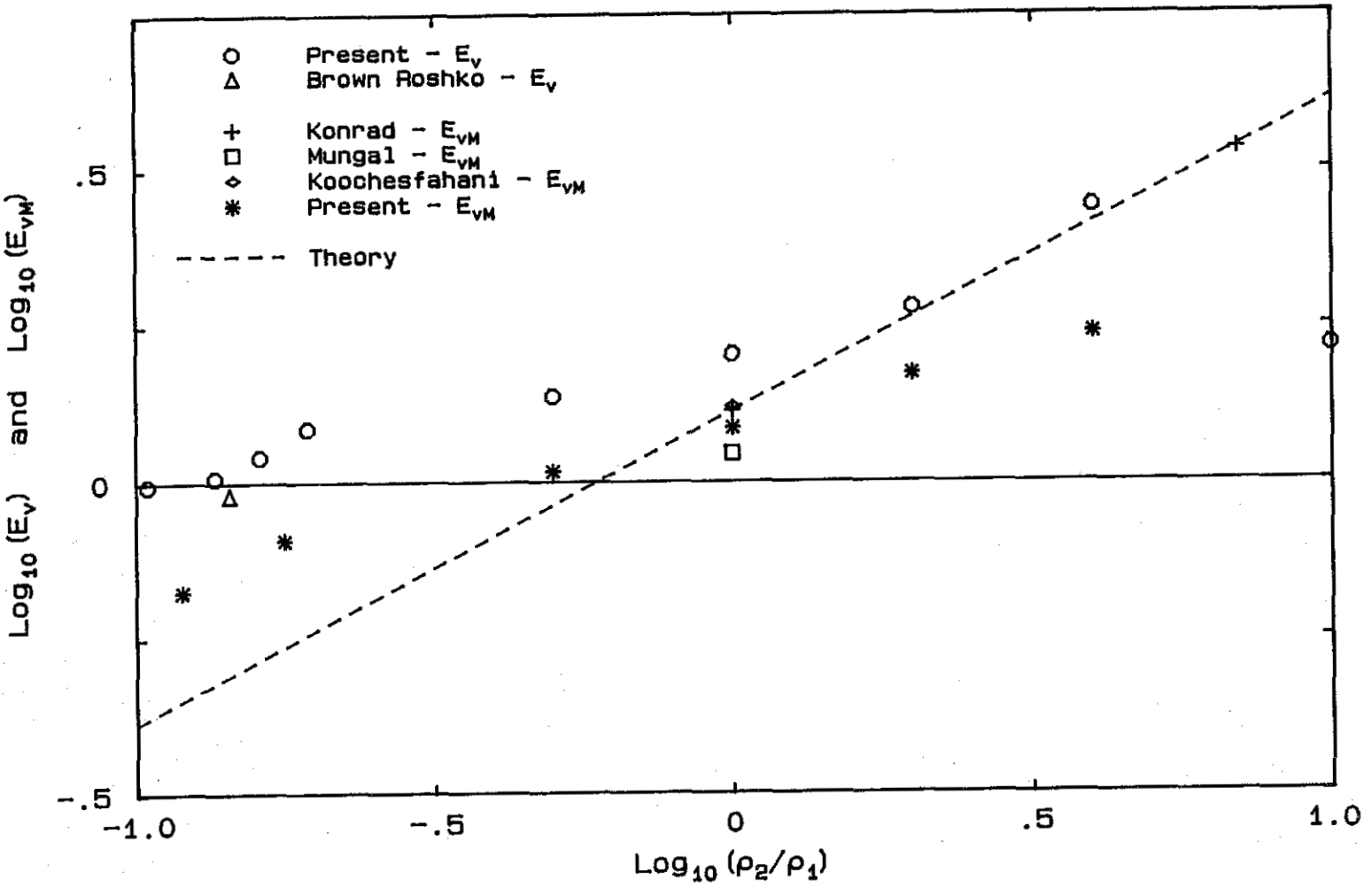

Effects of Density Ratio on Entrainment Ratio and Mixed Fluid Ratio

Figure 4

SCHEMATIC OF GAS PHASE RAYLEIGH SCATTERING EXPERIMENT

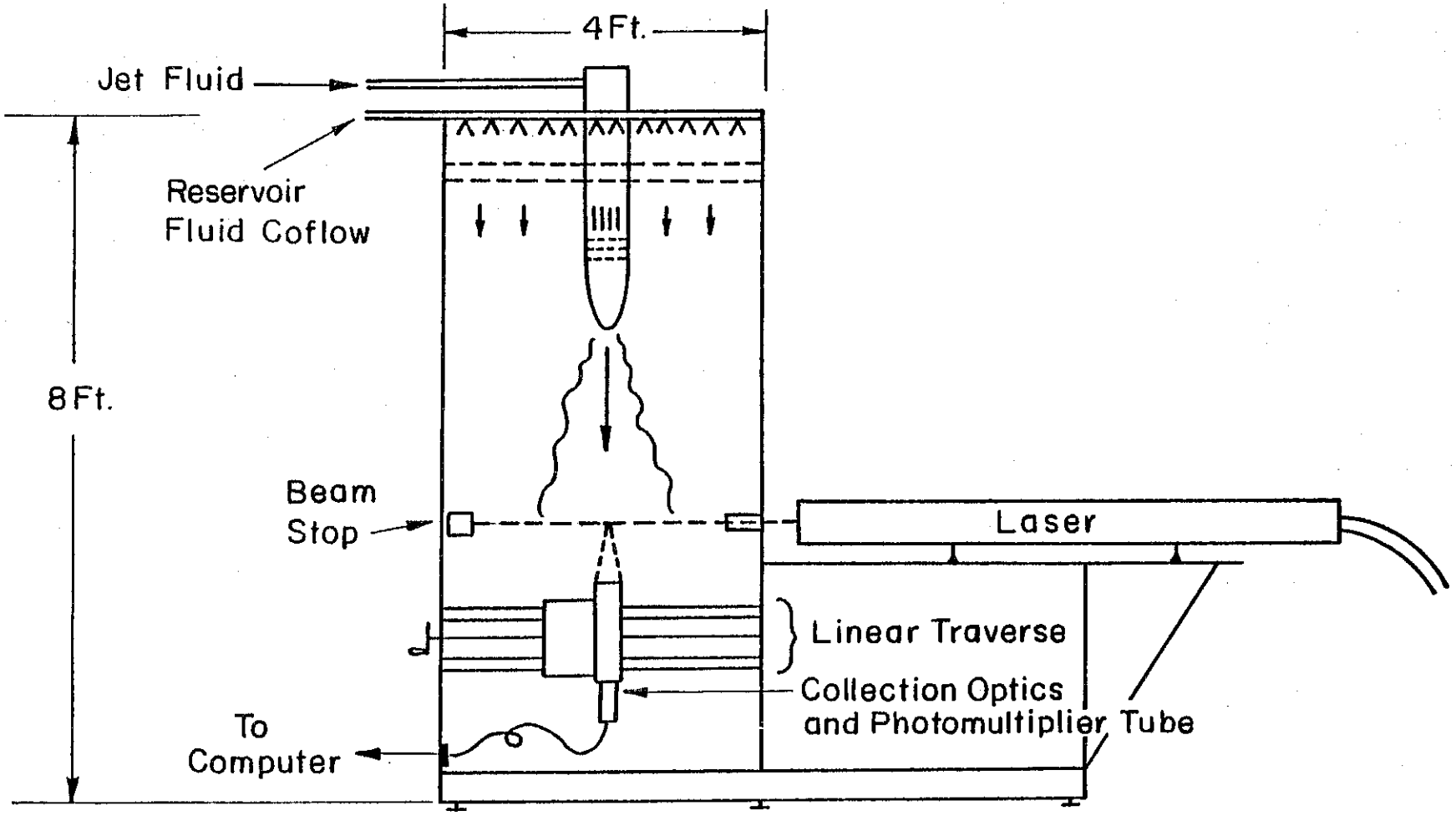

Figure 5

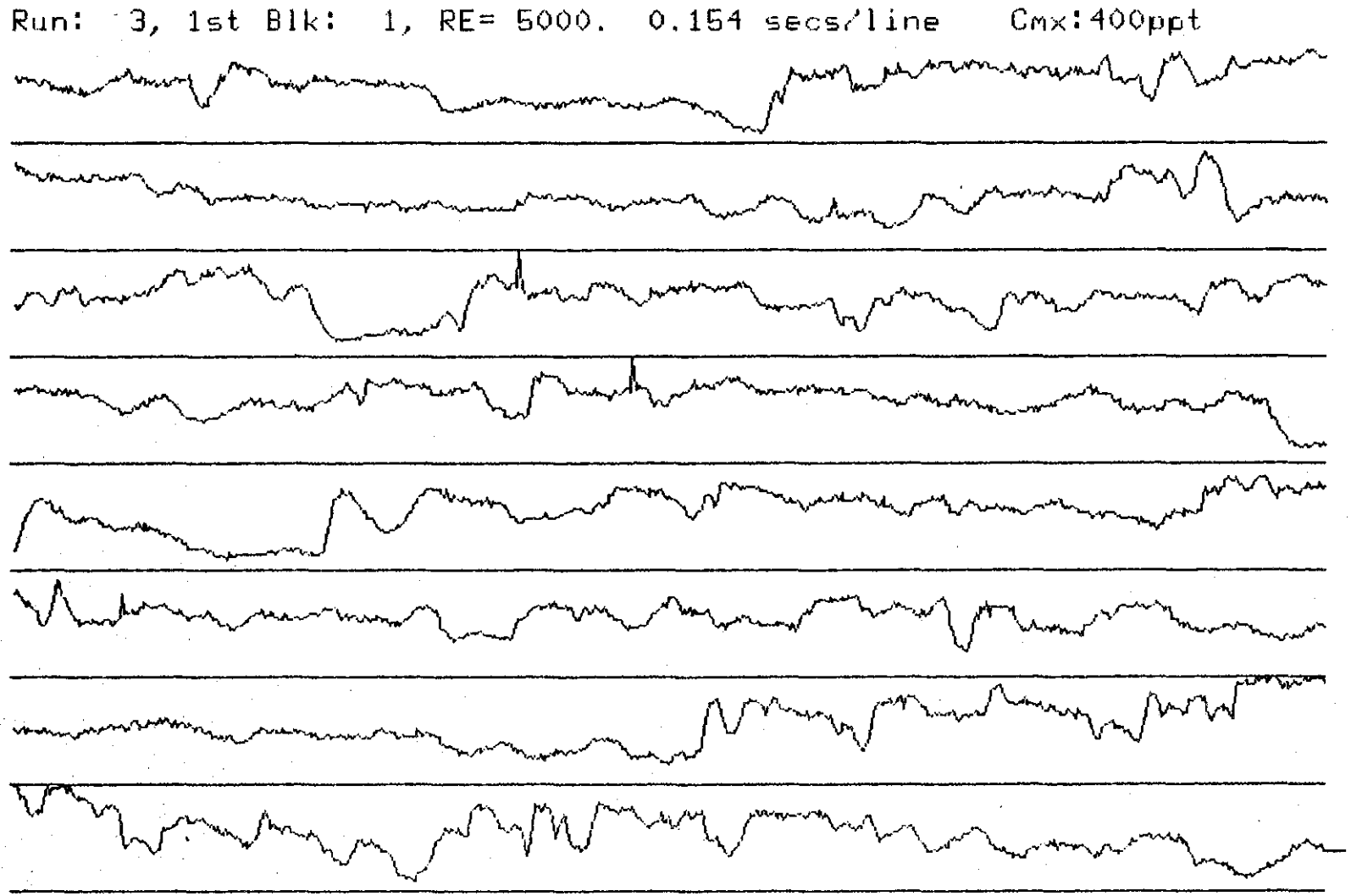

Figure 6

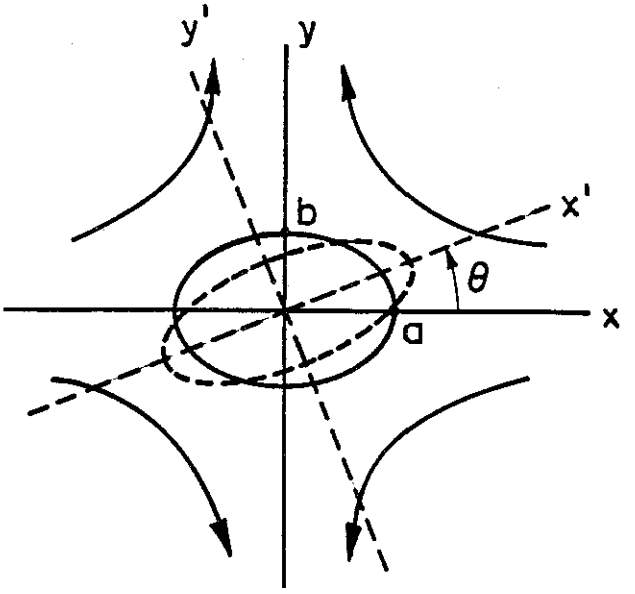

Figure 7

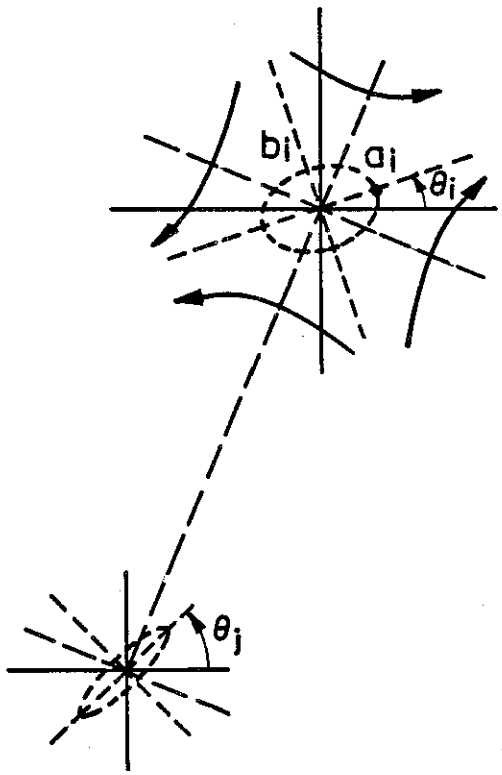

<i - th vortex>

<j - th vortex>

Figure 8

APPENDIX A

GRADUATE AERONAUTICAL LABORATORIES
of the
CALIFORNIA INSTITUTE of TECHNOLOGY
Pasadena, California 91125

INVISCID INSTABILITY CHARACTERISTICS OF FREE SHEAR LAYERS WITH NON-UNIFORM DENSITY

by

M. M. Koochesfahani* and C. E. Frieler#

Abstract submitted for the
AIAA 25th Aerospace Sciences Meeting
12-15 January 1987, Reno, Nevada

12-June-1986

---

* Post-Doctoral Research Fellow, Aeronautics. Member AIAA.
# Graduate Student, Aeronautics.

ABSTRACT

The linear spatial instability of two-dimensional two-stream plane mixing layers has been studied extensively in the past. In the case of uniform density, Michalke (1965) investigated the single-stream shear layer and Monkewitz & Huerre (1982) considered the effect of the velocity ratio. Maslowe & Kelly (1971) studied the stratified (non-uniform density) shear layers and showed that density variations can be destabilizing. In all these studies, the mean velocity profile has been assumed to be monotonically increasing from the value on the low-speed stream to that on the high-speed stream and usually the hyperbolic tangent form is used. It should be noted, however, that under experimental conditions the initial mean velocity profile almost always has a wake component due to the boundary layers on the two sides of the splitter plate. The effect of the wake component has only recently come into consideration with the investigations of Miau 1984 and Zhang et al. 1984 for the uniform density case.

The purpose of the present work is to study the instability characteristics of both uniform and non-uniform density plane shear layers taking into account the wake component of the initial velocity profile. The inviscid, linear, parallel-flow stability analysis of spatially growing disturbances is utilized to numerically calculate the range of unstable frequencies and wave-numbers.

We consider the general case of a two-stream plane shear layer with U_1, ρ_1 as the free-stream velocity and density on the high-speed stream and U_2, ρ_2 as the corresponding quantities on the low-speed side of the layer. All quantities used here are normalized with the average velocity $(U_1+U_2)/2$, average density $(\rho_1+\rho_2)/2$ and the local layer thickness δ as the length scale. The mean velocity profile is composed of the usual hyperbolic tangent profile plus a wake component represented by a Gaussian distribution and has the form

$$U(Y) = 1 + \lambda_u \tanh(Y) - W e^{-Y^2}$$

where $\lambda_U = (U_1-U_2)/(U_1+U_2)$ and W is the normalized wake deficit. The mean density profile has a hyperbolic tangent profile and is given by

$$\rho(Y) = 1 + \lambda_\rho \tanh[(Y-Y_o)/\sigma]$$

where $\lambda_\rho = (\rho_1-\rho_2)/(\rho_1+\rho_2)$ and Y_o and σ adjust the lateral position and thickness of the density profile relative to the velocity profile.

The disturbance stream function is written in the form

$$\psi = \phi(Y)\, e^{i(\alpha x - \beta t)}$$

where $\alpha = \alpha_r+i\alpha_i$ is the complex wave-number and β is frequency which is real for the spatial case. For the case of incompressible flow and negligible buoyancy effects (i.e. gravity is ignored), it can be shown that the disturbance eigenfunction ϕ satisfies the equation

$$\phi'' + (\rho'/\rho)\,\phi' - \left[\alpha^2 + \frac{U'' + \rho' U'/\rho}{U-\beta/\alpha}\right]\phi = 0$$

where $(\,)'$ corresponds to d/dY. The equation above reduces to the Rayleigh equation when the density is uniform. A "shooting" technique is used to solve this eigenvalue equation and calculate the spatial growth rate, $-\alpha_i$, of unstable disturbances and the corresponding wave-number, α_r, versus frequency β.

Representative results for the uniform density case are shown in figure 1. The main result is that when the wake component is present there are two unstable branches as opposed to one in the case of the hyperbolic tangent. These two branches do not have much in common with the "sinuous" and "varicose" modes of instability calculated by Mattingly & Criminale (1972) in the case of pure wakes since the symmetry conditions that exist in the pure wake do not hold here. The stronger branch leads to the usual Kelvin-Helmholtz roll-up patterns observed in shear layers and it is referred to here as the shear layer branch. The lower branch is suspected to correspond to roll-up patterns

that resemble those in pure wake flows and, therefore, we call it the wake branch. This branch, in the uniform density case, is rarely observed since its amplification rate is quite lower than the shear layer branch.

To investigate the effect of non-uniform density, we consider the case of low-speed stream having the higher density (see figure 2). The density profile has been arranged to have its inflection point at the minimum of the velocity profile and its thickness much thinner than that of the velocity profile. These conditions are expected to hold in the initial region of the flow near the splitter plate. The qualitative features of the results are not sensitive to these conditions as long as the density profile is reasonably thin relative to the velocity profile.

The results for the case of non-uniform density are shown in figure 3. In figure 3a, the uniform density case, the two instability branches similar to figure 1b can be seen. The most important result is that when the high density is on the low-speed side, the two branches have similar growth rates. In fact, the normally weak branch (wake branch) in the uniform density case, now seems to have a slightly larger growth rate than the shear layer branch. This means that, depending on the spectrum of disturbances in the flow and the extent of the persistence of the wake component in the downstream region, a shear layer of non-uniform density may not roll-up like the usual Kelvin-Helmholtz structures but more like a wake. The finding in figure 3 also suggests that, under the right flow conditions, both shear layer and wake modes of instability may exist simultaneously and interact with each other.

To show that the features described above are, in fact, possible, the shear layer between a high-speed stream of Helium and low-speed stream of Argon was forced acoustically. The flow visualization by Schlieren photography, figure 4, shows that both wake and shear layer modes can be generated in a two-stream shear layer.

REFERENCES

MASLOWE, S. A. & KELLY, R. E. 1971 Inviscid instability of an unbounded heterogeneous shear layer. J. Fluid Mech. 48(2), 405-415.

MATTINGLY, G. E. & CRIMINALE, W. O. 1972 The stability of an incompressible two-dimensional wake. J. Fluid Mech. 51(2), 233-272.

MIAU, J-J. 1984 An experimental study on the instability of a mixing-layer with laminar wake as the initial condition. Ph.D. thesis, Brown University.

MICHALKE, A. 1965 On spatially growing disturbances in an inviscid shear layer. J. Fluid Mech. 23(3), 521-544.

MONKEWITZ, P. & HUERRE, P. 1982 Influence of the velocity ratio on the spatial instability of mixing layers. Phys. FLuids 25(7), 1137-1143.

ZHANG, Y-Q., HO, C-H. & MONKEWITZ, P. 1984 The mixing layer forced by fundamental and subharmonic. LAMINAR-TURBULENT TRANSITION, Proc. IUTAM Symp., Novosibirsk, USSR, July 9-13, Springer-Verlag, 385-395.

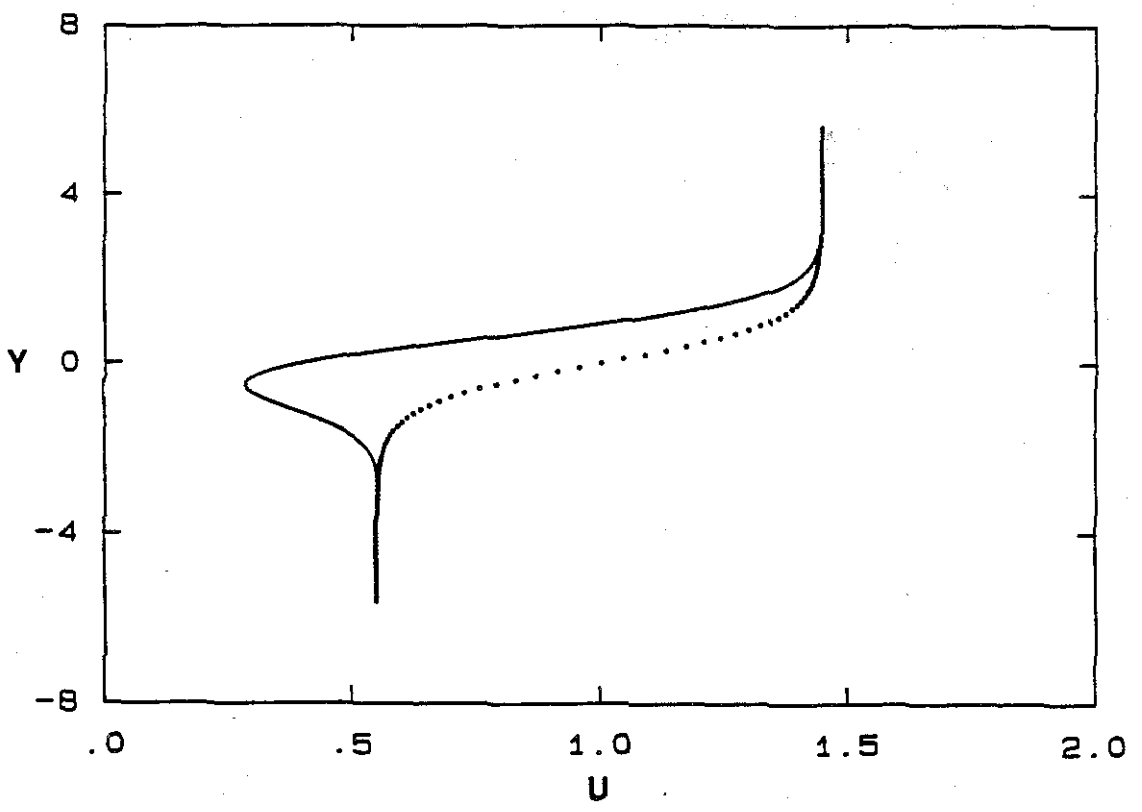

Figure 1a. Mean velocity profile, $\lambda_o = 0.45$ ($U_2/U_1 = 0.38$), ····· tanh profile, ——— tanh plus wake component.

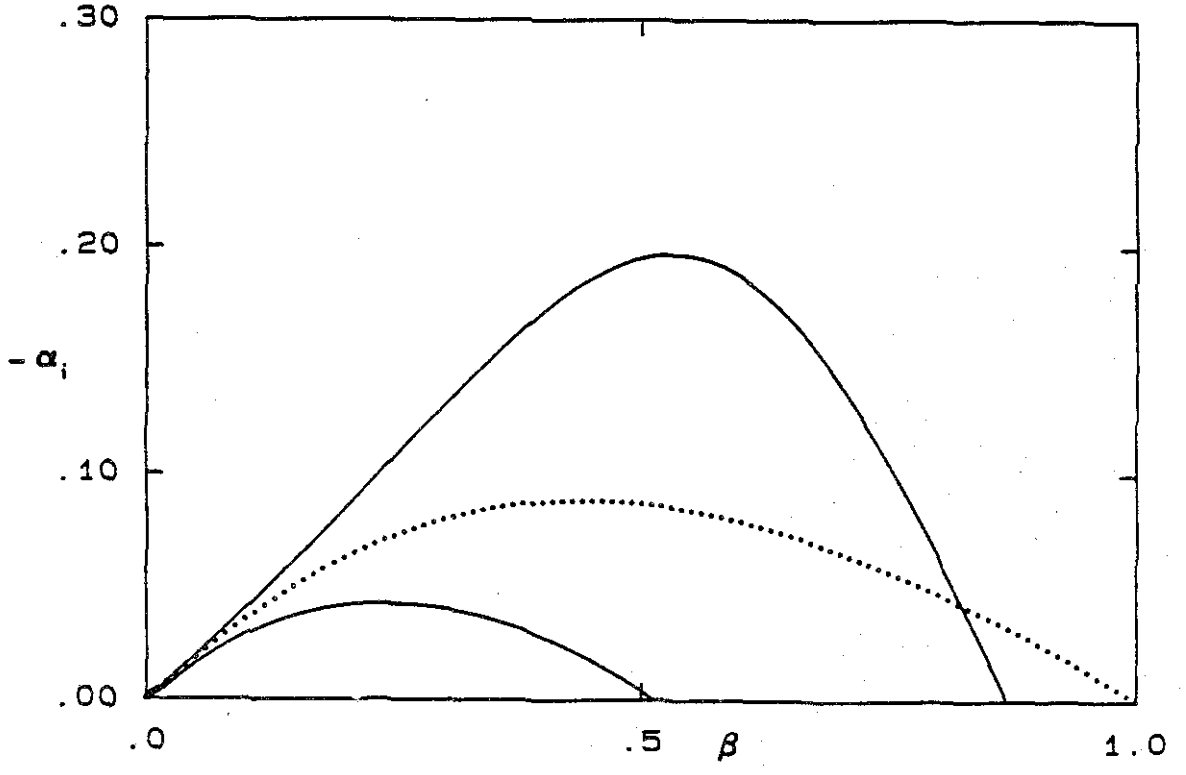

Figure 1b. Growth rate vs. frequency, same conditions as above.

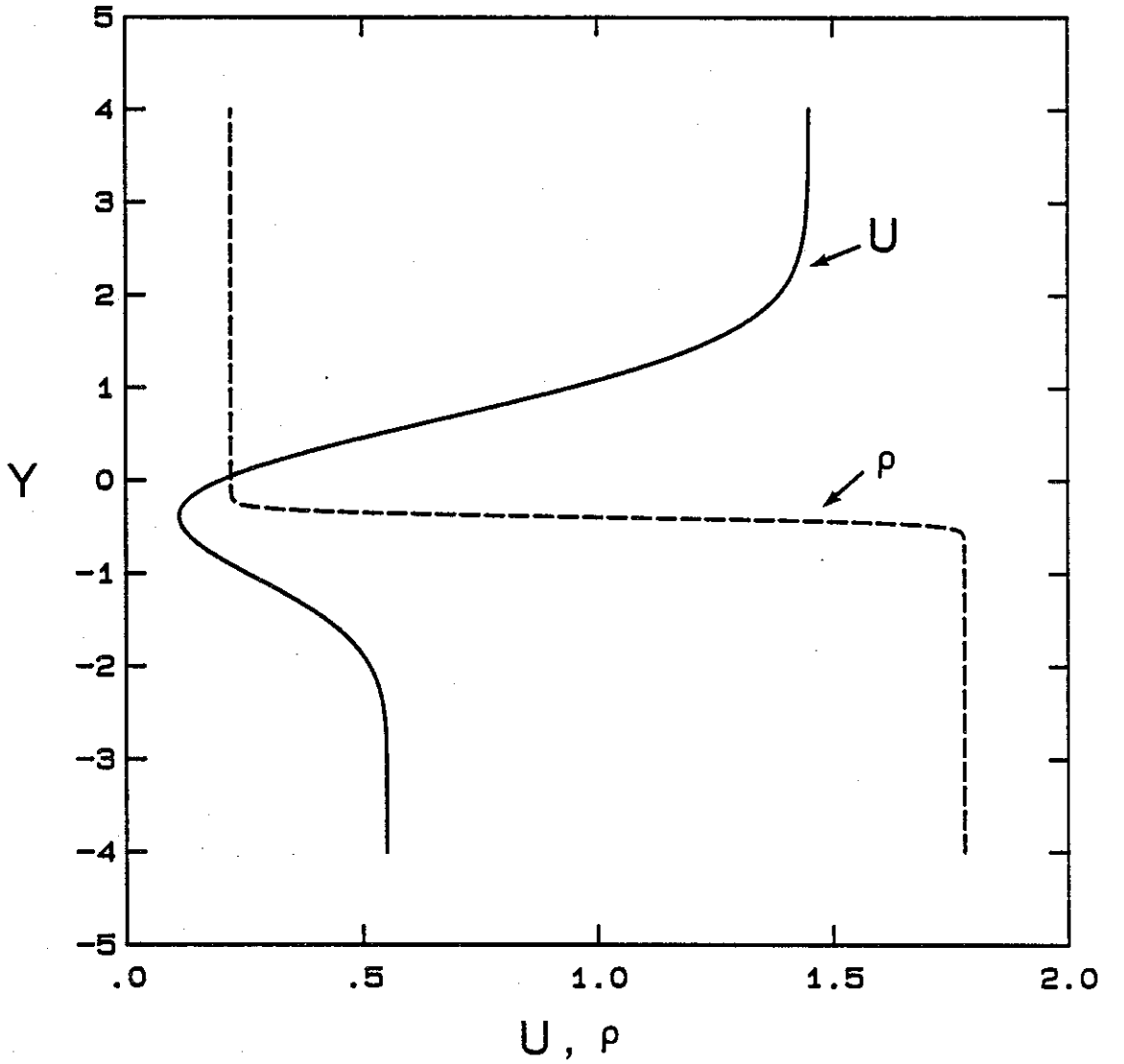

Figure 2. Mean velocity and density profiles, $\lambda_u = 0.45$ ($U_2/U_1 = 0.38$) and $\lambda_\rho = -0.78$ ($\rho_2/\rho_1 = 8$).

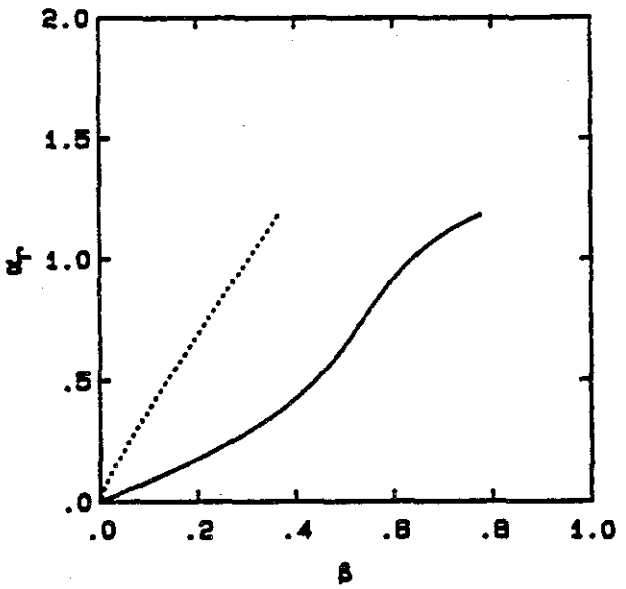

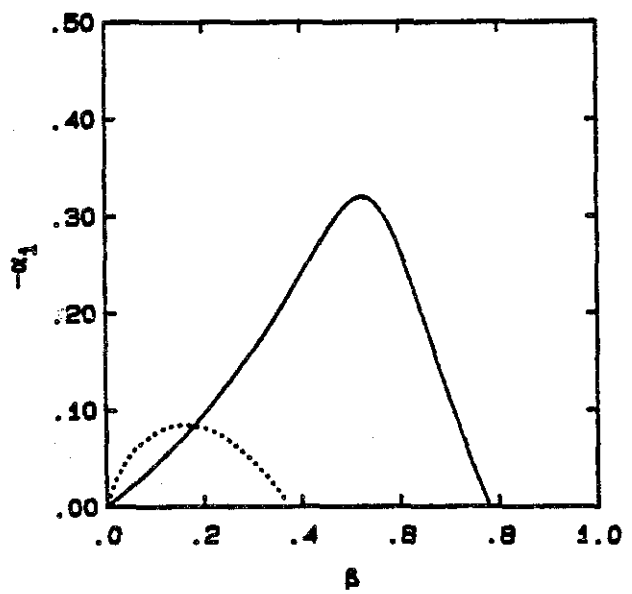

Figure 3a. Instability characteristics of the mean velocity profile of figure 2 with uniform density.

——— shear layer branch
..... wake branch

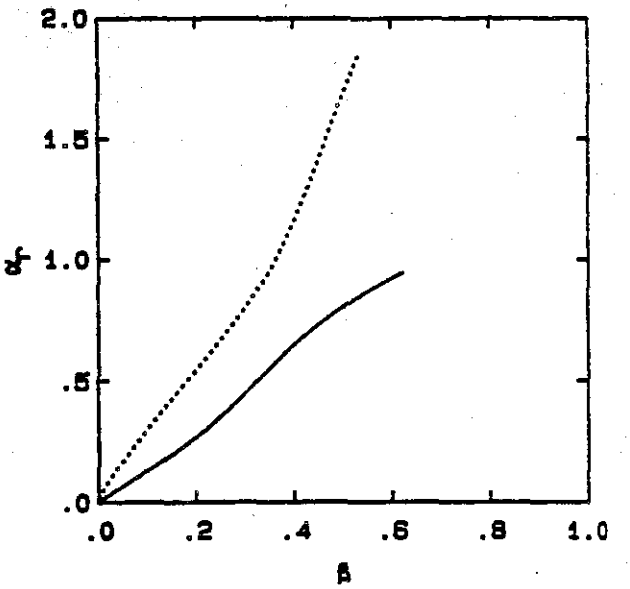

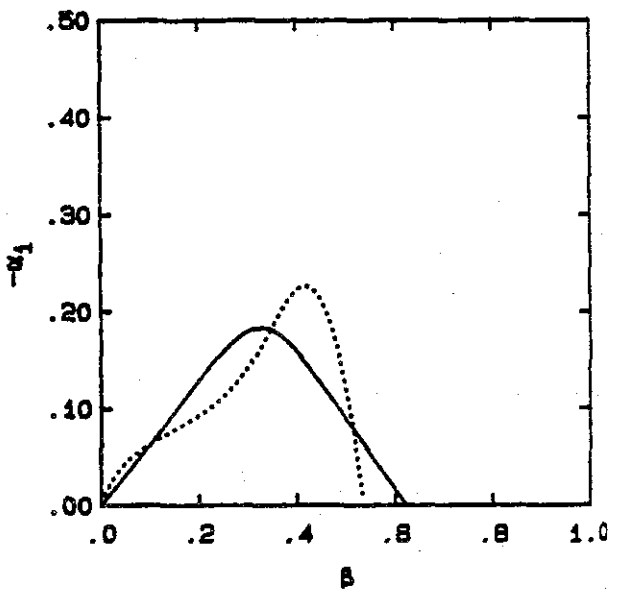

Figure 3b. Instability characteristics of the mean velocity and density profiles of figure

——— shear layer branch
..... wake branch

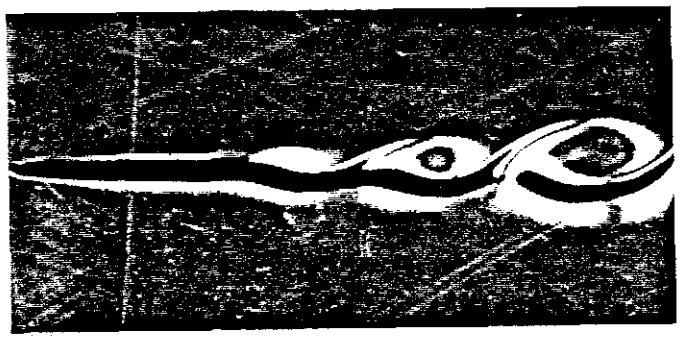

(a)

(b)

Figure 4. Schlieren photographs of the shear layer mode (a) and the wake mode (b). Flow is from left to right with high-speed stream on top ($U_2/U_1 \simeq 0.38$, $\rho_2/\rho_1 \simeq 10$).

APPENDIX B

The Effects of Damkohler Number on a Turbulent Shear Layer - Experimental Results

by

M. G. Mungal and C. E. Frieler

31 December 1985

GALCIT Report FM85-01

Graduate Aeronautical Laboratories

California Institute of Technology

Pasadena, CA 91125

The Effects of Damkohler Number on a Turbulent Shear Layer - Experimental Results

M. G. Mungal and C. E. Frieler

ABSTRACT

A chemical reaction for which the reaction rate can be varied is studied in a fully developed, two-dimensional, turbulent mixing layer. The layer is formed between two nitrogen streams, one carrying low concentrations of fluorine and the other hydrogen and nitric oxide. For fixed concentrations of fluorine and hydrogen and for nitric oxide concentrations that are small fractions of the fluorine concentration, the heat release is fixed but the overall reaction rate is controlled by the nitric oxide concentration. Therefore, for fixed flow conditions, the nitric oxide concentration determines the ratio of the reaction rate to the mixing rate. For large values of this ratio, the amount of product, at a given downstream location, measured by the mean temperature rise, is independent of the reaction rate, i.e., the reaction is mixing limited. As the reaction rate is reduced the major effects are: (1) amount of product declines (as expected), (2) the mean temperature profile, which is initially somewhat unsymmetrical because the hydrogen-fluorine freestream concentration ratio is set at a large value, becomes symmetrical, and (3) the ramp-like instantaneous temperature traces within the large structure gradually become more top-hat.

The Effects of Damkohler Number on a Turbulent Shear Layer - Experimental Results

M. G. Mungal and C. E. Frieler

1. Introduction

This work represents the third in a series of studies aimed at achieving an understanding of mixing and combustion in a fully developed, two-dimensional, turbulent mixing layer, Fig. 1. In these experiments, the reactants are low concentrations of hydrogen and fluorine carried in separate nitrogen freestreams. Nitric oxide, in concentrations that are small compared to the fluorine, is carried with the hydrogen stream. When the two streams mix, the nitric oxide dissociates a fraction of the fluorine to initiate and control the hydrogen-fluorine chain reaction. In all experiments, the heat release is sufficiently low that the heat release does not couple with the fluid mechanics, so that the overall properties of the mixing layer are not significantly changed from those of the non-reacting case. It is important to note that the present chemical system is hypergolic (low activation energy) at all concentrations, unlike hydrocarbon - air systems which require ignition sources to sustain combustion, have flammability limits and can be quenched by high values of strain rate.

The first of these efforts [1,2] examined the effects of the hydrogen-fluorine freestream concentration ratio upon the amount of product formed in the fully developed layer at a single Reynolds number of $\sim 4\times10^5$ (based on velocity difference and downstream distance). The results confirmed the central role of the large structure dynamics in mixing and combustion. The asymmetry in entrainment of the mixing layer was demonstrated through 'flip' experiments whereby the lean reactant being

carried on the high-speed or low-speed side of the layer leads to different amounts of product. The experiments also showed that when one reactant concentration is fixed, a nearly asymptotic product profile is reached when the other reactant concentration is approximately eight times the first. Under these conditions, essentially all the molecularly mixed lean reactant is completely consumed. It is instructive to note that for chemical reactions in water at similar Reynolds numbers, Koochesfahani [3] found that there was approximately 50% less (normalized) product than in the gas. This has led to the conclusion that the Schmidt number influences the amount of product formed in turbulent flows, even at Reynolds numbers as high as 4×10^5.

In the second effort [4], the dependence of the amount of product formed in the mixing layer upon Reynolds number was studied. It was found that the large organized structures are present at all Reynolds numbers investigated, irrespective of whether the boundary layer on the splitter plate is laminar or turbulent, and that the product dependence on Reynolds number is weak. There is, approximately, a 20% decrease in the amount of product formed for a factor of 10 increase in Reynolds number (or 6% decrease per factor of 2 in Reynolds number).

In both of the above investigations, the amount of nitric oxide was sufficiently large to insure that the reaction was, to a good approximation, mixing limited. In the present investigation we reduce the nitric oxide concentration to study the effects of the chemical reaction rate. A chemical kinetics code, CHEMKIN [5], was used to study the hydrogen-fluorine-nitric oxide system. The results show that the nitric oxide concentration controls the overall reaction rate, while the heat of reaction is the same. Since the runs described below are all performed at low heat, the fluid mechanics also remains unchanged.

In the investigations mentioned above, the findings were interpreted in the context of the simple model for mixing and product formation in the turbulent shear layer proposed by Broadwell & Breidenthal [6]. The

present results are interpreted in terms of this model in Broadwell & Mungal [7].

2. The Chemical Reactions

The principal reactions in the experiment consists of the hydrogen-fluorine chain reaction and the nitric oxide fluorine dissociation reaction.

$$H_2 + F \xrightarrow{k_1} HF + H, \quad \Delta Q = -32 \frac{kcal}{mole}, \quad \underline{k}_1 = 2.6\times10^{12}\underline{T}^{0.5}\exp(\frac{-610}{\underline{RT}}) \qquad (1)$$

$$H + F_2 \xrightarrow{k_2} HF + F, \quad \Delta Q = -98 \frac{kcal}{mole}, \quad \underline{k}_2 = 3\times10^{9}\underline{T}^{1.5}\exp(\frac{-1680}{\underline{RT}}) \qquad (2)$$

$$NO + F_2 \xrightarrow{k_3} NOF + F, \quad \Delta Q = -18 \frac{kcal}{mole}, \quad \underline{k}_3 = 4.2\times10^{11}\exp(\frac{-2285}{\underline{RT}}) \qquad (3)$$

where k is given in cc/mole-s, T in degrees K and R is the universal gas constant in cal/mole-K.

Reactions (1) and (2) are the so-called cold and hot reactions, respectively. The cold reaction, which carries 25% of the total heat release, is faster than the hot reaction by about an order of magnitude at 300K ($k_1 \simeq 1.6\times10^{13}$, $k_2 \simeq 9.5\times10^{11}$). The rate constants k_1 and k_2 are taken from Cohen & Bott [8] and k_3 from Baulch et al. [9].

Additional reactions which must be considered are:

$$F + NO + M \xrightarrow{k_4} NOF + M, \quad \Delta Q = -57 \frac{kcal}{mole}, \quad \underline{k}_4 \simeq 3\times10^{16} \qquad (4)$$

and

$$F + F + M \xrightarrow{k_5} F_2 + M, \qquad k_5 \simeq 3.2\times10^{14} \tag{5}$$

$$H + F + M \xrightarrow{k_6} HF + M, \qquad k_6 \simeq 2.5\times10^{16} \tag{6}$$

$$H + H + M \xrightarrow{k_7} H_2 + M, \qquad k_7 \simeq 3.0\times10^{15} \tag{7}$$

where the k_4 - k_7 rates are given in $cc^2/mole^2$-s and are estimated at 300K from Baulch et al. [9].

We have used the CHEMKIN [5] computer code to study the reaction set (1) - (7) in a premixed constant pressure reactor. The initial condition 4%H_2, 0.5%F_2, 0.015%NO in a N_2 diluent simulate our normal operating conditions of 8%H_2, 0.03%NO in N_2 on the high-speed side and 1%F_2 in N_2 on the low-speed side (this nominal condition will be referred to as $[NO]^*$). The CHEMKIN code computes the species concentration and temperature as a function of time for the mixture at constant pressure or constant volume, the former being the option applicable to this work. The result of such a calculation is shown in Fig. 2. The starting temperature is 300K and the system asymptotes to a temperature of 393K. The figure shows the results if only the first three reactions (1)-(3) are used, together with that for all seven reactions (1)-(7). The agreement suggests that reactions (1)-(3) determine the behaviour of the chemical system at these temperatures, while (4)-(7) are relatively less important. We have fitted a straight line to the curve shown in Fig. 2 and taken the time required for a temperature rise from 300K to 393K to be a measure of the chemical time of the system. Fig. 2 shows that for the rate constants shown above, the chemical time for our nominal condition, τ^*, is 0.53 ms. (It is worthwhile to note that if we simulate an operating condition of 1%K_2, 0.03% NO together with 1%F_2 in a N_2 diluent, as was performed in Reference 2, the chemical time increases by about 15%.)

Table 1 shows (among other results) the overall chemical rate, k (the inverse of the chemical time, τ) as computed by CHEMKIN, for various concentrations of nitric oxide for the reaction set (1)-(7). As is shown

analytically in Appendix 1, the chemical rate is nearly proportional to [NO] at very low concentrations (relative to $[F_2]$) and varies as the square root of [NO] at higher concentrations. In summary, the chemical system (1)-(7) describes, for our conditions, a reaction in which the heat release is fixed by the hydrogen and fluorine concentrations but the overall rate is controlled by the nitric oxide concentration.

3. Experimental Apparatus

The experimental facility has been described previously [1,2] and will only be discussed briefly here. It is of the blowdown type in which premixed volumes of hydrogen and nitric oxide in nitrogen, and fluorine in nitrogen are discharged through sonic orifices, maintaining a constant mass flux in each of the freestreams. Both streams enter a settling and contraction section for turbulence reduction with the high speed flow emerging from a 6:1 contraction at an exit area of 5 x 20 cm, and the low speed emerging from a 4:1 contraction in a 7.5 x 20 cm exit area. The flows then meet at the tip of a splitter plate as shown in Fig. 1. All measurements are recorded at a station x = 45.7 cm downstream of the splitter plate trailing edge.

Runs were performed for flow velocities of U_1 = 22 and 44 m/s with a fixed speed ratio U_2/U_1 = 0.40. The Reynolds numbers based on the velocity difference ΔU, and the 1% thickness of the layer δ_1 (distance between points at which the mean temperature rise is 1% of the maximum mean temperature rise), and the cold kinematic viscosity of nitrogen are respectively 6.7×10^4, and 1.3×10^5. These values are all beyond the mixing transition observed by Konrad [10] and Breidenthal [11]. The high speed turbulence level is about 0.7% rms at the lower speed and decreases somewhat at the higher speed. For U_1 = 22 m/s, the high-speed boundary layer momentum thickness, θ_1, was estimated using Thwaites' method, with the Reynolds number $U_1\theta_1/\nu$ estimated to be 240. Thus at the measuring station, $x/\theta_1 \simeq 2800$.

4. Measurements

For each run, the streamwise pressure gradient is set to zero by adjustment of the low speed sidewall. Temperature rise is recorded by a rake of 8 cold wire resistance thermometers placed across the width of the layer, each driven by a constant current of 0.4mA. The wires are made of 2.5 μm diameter platinum / 10% rhodium welded to inconel prongs with a span of 1.5 mm. The ratio of the length of the wire to Betchov's cold length [12] is about 20 at the lower Reynolds number. During a run, each wire is sampled at 10 and 12.5 kHz for the two speeds, corresponding to total data rates of 80 and 100 kHz.

As described in [2], the cold wires are calibrated directly before each run and record an accurate mean temperature profile, while excursions from the mean suffer from conduction error due to the prongs and the thermal lag of the wire itself [13], [14]. The mean temperature profiles were spot checked by a 0.25 mm diameter chromel-alumel thermocouple at a single point on the mean temperature rise profile, with the agreement being generally within 3% or better. The mean temperature profiles shown below are repeatable from run to run to within 2 percent. The absolute reactant concentrations however, are known only to approximately 3-5%, and thus the absolute value of the potential heat release has an uncertainty of the same order.

5. Experimental Results and Discussion

For the runs reported here, the high-speed stream consisted of 8%H_2, 92%N_2 together with varying small concentrations of NO, while the low-speed stream consisted of 0.96%F_2 and 99%N_2 (passivation of upstream screens and plates removed an estimated 0.04%F_2 from the nominal value of 1%F_2), with an adiabatic flame temperature rise of 159K. As was noted above, this choice of reactant concentrations guarantees that, when the reaction rate is sufficiently high, the fluorine (lean reactant) which is

molecularly mixed with the hydrogen is almost totally consumed.

Figure 3a shows the mean temperature rise profiles obtained at the $x - x_0 = 45.7$ cm station for the cases of decreasing nitric oxide concentration, namely $[NO]/[NO]^* = 1, 1/2, 1/4, 1/8, 1/16, 1/23, 1/32, 0$ at $U_1 = 22$ m/s (note that the accuracy in loading our nominal concentration of NO is probably within 3% but becomes progressively worse as the amount of NO decreases). The symbols indicate the measured average temperature rise at the positions of the eight probes, and represents the average of 12,288 points per probe during which time at least 100 structures would have passed the measuring station. The smooth curve is an exponential fit of the type

$$\bar{T}(\eta)/Tflm = \exp (c_0 + c_1\eta + c_2\eta^2 + c_3\eta^3 + c_4\eta^4)$$

where T is the local mean temperature rise, Tflm is the adiabatic flame temperature rise, $\eta \equiv y/(x-x_0)$, and the point $\eta = 0$ corresponds to the position of the dividing streamline (see Table 3).

We see that, as [NO] decreases, there is a gradual loss in area under each of the product profiles, together with a tendency for the profile to become more symmetric. In fact, for the case $[NO]/[NO]^* = 1/32$, the profile is remarkably symmetric in spite of the fact that the high-speed reactant is eight times more concentrated than the low-speed reactant. This trend towards symmetry is shown more directly in Fig. 3b where all profiles have been scaled to the same height and Fig. 3c where the cases $[NO]/[NO]^* = 1, 1/32$ are shown. It should also be noted that the case $[NO]/[NO]^* = 0$ shows no product both experimentally and in computation with the CHEMKIN code.

Figure 4 shows the mean temperature rise profiles for the cases of increasing the nitric oxide concentration, namely $[NO]/[NO]^* = 1, 3/2, 2$. Table 1 indicates that the effective reaction rates for the latter two runs are larger than the nominal by factors of 1.3 and 1.5 respectively.

The similarity of the profiles implies that the reaction is mixing rate limited for [NO] at the nominal value and above.

Figure 5a shows similar results taken at the same measuring station, but with U_1 = 44 m/s (and $U_2 = 0.4U_1$ to maintain the same speed ratio) for the cases $[NO]/[NO]^*$ = 2, 1, 1/4, 1/16 (see also Table 2,4). The scaled profiles for the cases $[NO]/[NO]^*$ = 1, 1/16 are shown in Fig. 5b to again demonstrate the symmetrizing of the mean temperature profile. It is worthwhile to note that, in the fast chemistry limit, the absolute area under the temperature profile for the U_1 = 44 m/s case is less, by about 10 percent, than that for U_1 = 22 m/s. As is discussed in [4], this is believed to be a Reynolds number effect and not a Damkohler number effect, since increasing the [NO] concentration by a factor of 2 at both Reynolds numbers with the corresponding increase in chemical rates, does not eliminate the difference.

The amount of product generated by the reaction is characterized by the product thickness

$$\delta_p \equiv \int_{-\infty}^{\infty} \frac{c_p(y)}{c_\infty}\, dy = \int_{-\infty}^{\infty} \frac{C_p\, \bar{T}(y)}{c_\infty\, \Delta Q}\, dy$$

where $c_p(y)$ is the concentration of product and c_∞ is the freestream fluorine concentration. Since product is analogous to temperature rise, the second expression is obtained by making use of the mean temperature rise profile $\bar{T}(y)$, the molar heat capacity of the carrier gas, C_p, and the heat release per mole of reactant, ΔQ. The product thickness of the curves of Figs. 3a, 4 normalized by the 1% thickness is shown in Fig. 6a as a function of the nitric oxide concentration. For small values of [NO], there is a rapid increase in the amount of product with the kinetic rate in what could be called the 'slow-chemistry' regime. At the larger values of [NO], the product amount is nearly independent of [NO] implying that the reaction is mixing limited, i.e. that the chemical rate is fast relative to the mixing rate. Also shown in Fig. 6 are the results for the

U_1 = 44 m/s case. The same data are shown in Fig. 6b as a function of the Damkohler number, Da (defined as the ratio of the mixing time to the chemical time). We have chosen the time of flight at the mean convection speed $(U_1+U_2)/2$ from the mixing transition, x_t, to the measuring station, x, to be an appropriate measure of the mixing time (see Broadwell &Mungal [7]). The CHEMKIN results are used for the chemical time. This choice gives the Damkohler number Da_x shown in Fig. 6b. Based on a transition Reynolds number of 2×10^4 we estimate x_t = 13.6 cm for the U_1 = 22 m/s case and x_t = 6.8 cm for the U_1 = 44 m/s case, so that the mixing times are 20.8 msec and 12.6 msec respectively. Based on this criterion, the mixing limited (fast chemistry) regime occurs past $Da_x \sim 40$. Finite rate effects occur below this value with a symmetric profile occuring for $Da_x \sim 4$.

Alternately, one may choose the local large scale turnover time to be the mixing time $(\delta_1/\Delta U)$ to define a different Damkohler number, Da_1. By this definition, Da_1 varies from 0.8 to 17 for the range of [NO] investigated. This suggests that past $Da_1 \sim 10$, the reaction is mixing limited while for $Da_1 \sim 1$, the reaction profile is symmetric. Wallace [15] for a nitric oxide - ozone mixing layer was able to achieve $1 < Da_1 < 16$ at high Reynolds number, while Masutani [16] achieved $2 < Da_1 < 28$ at pre-transitional Reynolds numbers using the same chemical system as Wallace. A further discussion of Fig. 6b will be made in Broadwell & Mungal [7] when a detailed comparison of the results are made with the model.

Figures. 7a, 7b show sample temperature vs time traces obtained from the eight cold wires at U_1 = 22 m/s, for $[NO]/[NO]^*$ = 1 and 1/32, i.e. for fast and slow chemistry. The time traces show the instantaneous temperature rise recorded by each probe as a function of time, normalized by the highest temperature rise of any probe during this time interval (labeled Tmax). The vertical distance between a consecutive pair of horizontal axes therefore represents Tmax. The horizontal axis corresponds to 51.2 ms of real time. Flow can be viewed as being from right to left with the high-speed fluid at the top. The time axis is greatly compressed in the sense that such a plot would be to geometric scale only if the

horizontal distance were about nine times the distance between the high-speed and low-speed probes.

We have discussed such traces in [1,2,4] and noted the presence of large regions of high temperature, associated with the large scale structure, separated by tongues of unreacted, cool gas. Here however, we wish to discuss the ramp-like temperature traces shaded in Fig. 7a, the data for the high kinetic rate, and, to point out that they are not present when the rate is slow, Fig. 7b.

If one pictures a large structure undergoing reaction, then for the present choice of reactant concentrations, the large structure is hydrogen rich. The effect of free-stream addition of fluid to the structure is to create a situation whereby the composition of the upper and downstream edges of the structure is biased toward the high-speed fluid, while the composition of the upstream and lower edges are biased toward the low-speed, lean reactant fluid. This leads to lateral (y) and axial (x) gradients in composition, and hence in temperature. In the fast chemistry case the consequences are the ramp-like structures and time traces which on the lean reactant edge reach generally higher instantaneous temperatures than those of the rich reactant edge. The skewed mean temperature profiles as shown in Fig. 3b result from long time averages of such traces. These features are to be contrasted with the time traces of Fig. 7b, for a slow reaction rate. Here the ramp-like features are much less apparent (become more top-hat) and the time traces of all probes generally reach the same maximum instantaneous temperatures from one edge of the layer to the other. The long time average of such traces leads to the symmetric mean temperature profiles of Fig. 3a. We note that ramps do not occur for every structure in the fast-chemistry limit but tend to be observed more often than not. Similarly, ramps are sometimes present when the reaction rate is low, but their occurance is quite infrequent.

We also note that since the fluid mechanics is unaffected by these low values of heat release, the instantaneous mixture fraction distribution of high-speed to low-speed fluid in the mixing layer is similar for the fast and slow chemistry cases. In the fast chemistry limit, the instantaneous mixture fraction uniquely determines the temperature at every point in the layer (see Bilger [17] and [2]). For lower reaction rates, this is no longer true - the temperature at any given point being determined by its history. We also note that the two main features of the slow chemistry results discussed above - namely, a symmetric mean temperature profile and the lack of ramp-like structures are in agreement with the measurements of Koochesfahani [3] in a chemically reacting liquid mixing layer, in the limit of fast chemistry, at comparable Reynolds numbers. The connection between these seemingly unrelated observations (slow chemistry in gases and fast chemistry in liquids) and a further discussion of these results appear in Broadwell & Mungal [7].

6. Conclusions

The experiments discussed above describe the behavior of the product field in a two-dimensional, turbulent mixing layer as the overall chemical rate is varied while the fluid mechanics and the heat of reaction remain unchanged. As we proceed from the mixing limited regime to the chemical rate limited regime, three main effects are observed: (1) the amount of product declines, (2) the mean-temperature profile, which is initially somewhat unsymmetrical because of the large hydrogen-fluorine reactant concentration ratio, becomes symmetrical, and (3) the ramp-like instantaneous temperature traces within the large structures become more top-hat. At the mixing limited (fast chemistry) regime, the Damkohler number based on time of flight from the mixing transition exceeds about 40. Below this value we enter the rate limited regime with a symmetric profile attained at a Damkohler number of about 4 (based on the local large scale turnover time, the Damkohler numbers become 10 and 1 respectively). Detailed comparison of these results with a theoretical model is presented

in Broadwell & Mungal [7].

7. Acknowledgments

The authors wish to thank Dr. J. E. Broadwell (who is an unofficial co-author) for numerous technical discussions, Dr. P. E. Dimotakis, Dr. W. L. Shackleford, Dr. R. C. Miake-Lye and Mr. Earl Dahl for help in conducting the experiments. This work is sponsored by the Air Force Office of Scientific Research under Grant No. 83-0213.

Table 1 - Summary of Results, U_1 = 22 m/s.

$\frac{[NO]}{[NO]^*}$	$\frac{\delta_1}{(x-x_0)}$	$\frac{\bar{T}max}{Tflm}$	A	$\frac{\delta_p}{\delta_1}$	$\frac{k}{k^*}$
2	0.170	0.540	0.0457	0.251	1.53
3/2	0.163	0.531	0.0419	0.231	1.29
1	0.165	0.537	0.0436	0.240	1.00
1/2	0.171	0.511	0.0429	0.236	1/1.49
1/4	0.165	0.488	0.0408	0.225	1/2.37
1/8	0.165	0.443	0.0365	0.201	1/3.98
1/16	0.165	0.396	0.0330	0.182	1/6.80
1/23	0.169	0.253	0.0220	0.121	1/9.11
1/32	0.168	0.197	0.0169	0.093	1/12.2
0	-	0	0	0	0

Table 2 - Summary of Results, U_1 = 44 m/s.

$\frac{[NO]}{[NO]^*}$	$\frac{\delta_1}{(x-x_0)}$	$\frac{\bar{T}max}{Tflm}$	A	$\frac{\delta_p}{\delta_1}$	$\frac{k}{k^*}$
2	0.165	0.491	0.0405	0.223	1.53
1	0.163	0.475	0.0391	0.215	1.00
1/4	0.169	0.433	0.0364	0.200	1/2.37
1/16	0.168	0.301	0.0264	0.145	1/6.80
0	-	0	0	0	0

Tflm ≡ adiabatic flame-temperature rise = 158.7K; Tmax ≡ maximum value of T; δ_1 ≡ width of layer where $\bar{T}$ = 1% of Tmax; $A \equiv \frac{1}{Tflm}\int \bar{T} d\eta$; $\eta \equiv \frac{y}{(x-x_0)}$; A^* = nominal condition at 22 m/s; $(x-x_0)$ = 45.7 cm for all runs; $k = 1/\tau$ = overall chemical rate; τ = chemical time determined from CHEMKIN.

Table 3 - Curvefit constants, U_1 = 22 m/s, $\tilde{y}_o$ = -.35

$\frac{[NO]}{[NO]^*}$	c_o	c_1	c_2	c_3	c_4
2	4.0596	-0.9089	-0.5342	-0.4929	-0.6328
3/2	3.9804	-0.1009	-0.4528	-0.4400	-0.7601
1	4.0568	-0.9833	-0.5925	-0.4336	-0.6720
1/2	4.0402	-0.9582	-0.6372	-0.3622	-0.5524
1/4	4.0497	-0.8729	-0.6610	-0.4596	-0.6561
1/8	3.9407	-0.9110	-0.6674	-0.4094	-0.6425
1/16	3.9311	-0.8084	-0.8073	-0.3656	-0.5957
1/23	3.5560	-0.6492	-0.8642	-0.4248	-0.5362
1/32	3.3329	-0.5917	-0.8614	-0.3242	-0.5277
0	0	0	0	0	0

Table 4 - Curvefit Constants, U_1 = 44 m/s, $\tilde{y}_o$ = - .32

$\frac{[NO]}{[NO]^*}$	c_o	c_1	c_2	c_3	c_4
2	4.1344	-0.8340	-0.7880	-0.3105	-0.5942
1	4.1159	-0.8224	-0.8642	-0.3837	-0.6047
1/4	4.0793	-0.7320	-0.9205	-0.2822	-0.4830
1/16	3.7876	-0.4951	-0.8463	-0.4140	-0.5587
0	0	0	0	0	0

Mean Temperature Rise, T (°K) recorded in physical coordinates, $\tilde{y}$ (inches) where

$$T(\tilde{y}) = \exp\left(c_o + c_1\tilde{y} + c_2\tilde{y}^2 + c_3\tilde{y}^3 + c_4\tilde{y}^4\right)$$

$-3 < \tilde{y} < 2$, $\eta \equiv (\tilde{y}-\tilde{y}_o)/(x-x_o)$ and $(x-x_o)$ = 18.0 in. for all runs.

Appendix 1

The ideas in this section were developed by J.E. Broadwell to provide a simple understanding of how the NO concentration controls the overall reaction rate.

It was shown above that reactions (1)-(3) can be considered as being representative of the H_2-F_2-NO chemistry, since the addition of reactions (4)-(7) showed essentially no change in the behaviour of the system as seen from Fig. 2. It is possible to estimate the overall behaviour of the system by the following arguments. From (2), (3)

$$\frac{dF_2}{dt} = -k_2HF_2 - k_3NOF_2 \tag{9}$$

$$\frac{dNO}{dt} = -k_3NOF_2 \tag{10}$$

This represents two equations for the three unknowns F_2, NO, H. By using either the rate equations or conservation of atoms it is possible to show that

$$H + F + NO = \text{const} = NO_i \tag{11}$$

since the initial concentrations (subscript i) of H and F are zero. Examination of (1)-(3) together with the fact that $k_1 > k_2 >> k_3$ would suggest that any F atoms produced (slowly) in (2), (3) would be (quickly) depleted in (1), hence a reasonable approximation would be to take $F \tilde{} 0$. This approximation now simplifies (11) to $H = NO_i - NO$ which can be substituted into (9), (10) to yield

$$\frac{dF_2}{dt} = -k_2NO_iF_2 + (k_2 - k_3)NOF_2 \tilde{} -k_2NO_iF_2 + k_2NOF_2 \tag{12}$$

$$\frac{dNO}{dt} = -k_3 NO F_2 \qquad (13)$$

the system now being reduced to two equations in the two unknowns F_2 and NO.

In order to proceed further, the CHEMKIN simulations were used as a guide as they suggested two types of behaviour. In the first case, for small NO concentrations, CHEMKIN suggested that the NO would deplete while the F_2 concentration had remained relatively fixed. Thus, if we assume $F_2 \sim F_{2i}$ we solve (13) which yields $NO/NO_i = e^{-k_3 F_{2i} t}$ and substituting into (12) gives

$$\frac{dF_2}{dt} = -k_2 NO_i F_2 (1-e^{-k_3 F_{2i} t})$$

or

$$\frac{dF_2}{d\tau} = -F_2 (1-e^{-\frac{k_3 F_{2i}}{k_2 NO_i}\tau})$$

where $\tau = k_2 NO_i t$. The second term can be neglected for $NO_i << \frac{k_3}{k_2} F_{2i}$ to yield the approximate solution

$$\frac{F_2}{F_{2i}} = e^{-k_2 NO_i t}.$$

Thus for $NO_i << \frac{k_3}{k_2} F_{2i}$, the overall rate will be proportional to NO_i.

The second case suggested by CHEMKIN concerns large NO concentrations for which the amount of NO changed slightly but did not deplete during the times of interest. We therefore take $NO \sim NO_i$ in (13). To solve, we further assume in (13) that $F_2 \sim F_{2i}$. This yields the solution $NO/NO_i = 1-k_3 F_{2i} t$ (This expression would imply negative NO concentrations

for long time and must of course be valid for times $t << 1/k_3F_{2i}$. Alternately we might interpret this as the leading term in an expansion for the NO behaviour). With this expression, (12) becomes

$$\frac{dF_2}{dt} = -k_2k_3NO_iF_{2i}F_2t$$

with solution

$$\frac{F_2}{F_{2i}} = e^{-k_2k_3NO_iF_{2i}t^2/2} \qquad (15)$$

Thus for large NO concentrations, the overall rate is now proportional to $NO^{1/2}$. The overall reaction rate derived from the CHEMKIN simulations is shown in Fig. 8 as a function of NO concentration. The initial linear trend followed by the square root behaviour seems consistent with the preceeding analysis.

The arguments above suggest that the overall rate varies linearly with NO, for small NO, and then as the square root of NO for larger values of NO. This of course is a complication and raises the question of whether a single overall rate can be found for each run condition that accurately describes the behaviour of the system. Using the linear extrapolation technique shown Fig. 2 for each case yields a characteristic time, τ (see last column of Table 1). The CHEMKIN results for all cases using reactions (1)-(7) are shown in Fig. 9, where the abscissa has been scaled by the appropriate characteristic time. The similarity of shape for all curves suggests that choosing a single overall rate seems reasonable for describing the reaction set.

Appendix 2

For the record we include the following curvefit constants for the runs reported in References 2,4. The same notation as Tables 3,4 is used, and $(x-x_o) = 18.0$ for all runs.

Table 5 - Curvefit Constants of Reference 2, Table 1

ϕ	T_{flm}	c_o	c_1	c_2	c_3	c_4	$\tilde{y}_o$
1/8	165	4.2985	-0.7807	-0.6762	-0.0573	-0.5953	-0.175
1/4	149	4.2841	-0.6418	-0.8488	-0.0483	-0.5209	-0.175
1/2	124	4.2454	-0.5327	-0.9712	-0.0772	-0.4759	-0.175
1	93	4.0740	-0.1913	-1.0964	-0.2538	-0.3959	-0.175
1	93	3.9809	-0.7483	-1.2209	-0.6152	-0.4835	-0.425
2	124	4.3743	-0.5202	-1.5259	-0.9914	-0.5786	-0.425
4	149	4.5414	-0.3831	-1.6016	-1.1379	-0.5972	-0.425
8	165	4.6320	-0.2451	-1.7962	-1.4960	-0.7309	-0.425

Table 6 - Curvefit Constants of Reference 2, Table 2

ϕ	T_{flm}	c_o	c_1	c_2	c_3	c_4	$\tilde{y}_o$
1/2	137.5	3.9154	-1.0811	-0.9082	0.8426	-0.6098	+0.300
1	109.0	3.8242	-0.9398	-1.0662	0.5143	-0.3058	+0.300
2	154.0	4.3746	-0.7190	-0.8895	0.3105	-0.4022	+0.300

Table 7 - Curvefit Contants of Reference 4

Run	c_o	c_1	c_2	c_3	c_4	$\tilde{y}_o$
Re_1	4.1019	-0.7526	-0.5933	-0.5687	-0.6048	-0.325
Re_2	4.1603	-0.9880	-0.9188	-0.5182	-0.6362	-0.325
Re_3	4.1105	-0.7930	-0.9572	-0.6126	-0.6033	-0.325
Re_{2T}	4.0359	-1.7096	-1.1633	-1.0232	-3.4653	-0.210
Re_{3T}	4.0223	-1.7280	-2.0311	-0.7710	-1.9014	-0.210
Re_4	3.9053	-1.7094	-1.5894	-0.8499	-1.9001	-0.210

8. References

[1] MUNGAL, M.G., DIMOTAKIS, P.E. & BROADWELL, J.E. 1984 Turbulent Mixing and Combustion in a Reacting Shear Layer. AIAA Jr., 22 (6), 797-800.

[2] MUNGAL, M.G. & DIMOTAKIS, P.E. 1984 Mixing and Combustion with Low Heat Release in a Turbulent Shear Layer. J. Fluid Mech., 148, 349-382.

[3] KOOCHESFAHANI, M.M. 1984 Experiments on Turbulent Mixing and Chemical Reactions in a Liquid Mixing Layer. Ph.D. Thesis, Caltech.

[4] MUNGAL, M.G., HERMANSON, J.C. & DIMOTAKIS P.E. 1985 Reynolds Number Effects on Mixing and Combustion in a Reacting Shear Layer. AIAA Jr. 23 (9), 1418-1423.

[5] KEE, R.J., MILLER, J.A. & JEFFERSON, T.H. 1980 CHEMKIN: A General-Purpose, Problem-Independent, Transportable, Fortran Chemical Kinetics Code Package. SANDIA Report SAND80-8003.

[6] BROADWELL, J.E. & BREIDENTHAL, R.E. 1982 A Simple Model of Mixing and Chemical Reaction in a Turbulent Shear Layer. J. Fluid Mech., 125, 397-410.

[7] BROADWELL, J.E. & MUNGAL, M.G. 1986 The Effects of Damkohler Number on a Turbulent Shear Layer - Analysis. Submitted to 21st (Intl.) Symp. on Combustion, The Combustion Institute.

[8] COHEN, N. & BOTT, J.F. 1982 Review of Rate Data for Reactions of Interest in HF and DF Lasers. The Aerospace Corporation, Report SD-TR-82-86.

[9] BAULCH, D.L., DUXBURY, J., GRANT, S.J., MONTAGUE, D.C. 1981 Evaluated Kinetic Data for High Temperature Reactions, Vol. 4, J. Phys. Chem. Ref. Data, Vol. 10, Suppl. 1.

[10] KONRAD, J.H. 1976 An Experimental Investigation of Mixing in Two-Dimensional Turbulent Shear Flows with Application to Diffusion-Limited Chemical Reactions. Ph.D. Thesis, Caltech, and Project SQUID Technical Report CIT-8-PU.

[11] BREIDENTHAL, R.E. 1981 Structure in Turbulent Mixing Layers and Wakes using a Chemical Reaction. J.Fluid Mech., 109, 1-24.

[12] BETCHOV, R. 1948 Proc. Ned. Akad. Wetenshappen, 51, 721.

[13] PARANTHOEN, P., PETIT, C. & LECORDIER, J.C. 1982 The Effect of the Thermal Prong - Wire Interaction on the Response of a Cold Wire in Gaseous Flows (Air, Argon and Helium), J. Fluid Mech., 124, 457-473.

[14] SCADRON, M.D. & WARSHAWSKY, I. 1952 Experimental Determination of Time Constants and Nusselt Numbers for Bare-Wire Thermocouples in High-Velocity Air Streams and Analytic Approximation of Conduction and Radiation Errors, NACA TN 2599.

[15] WALLACE, A.K. 1981 Experimental Investigation of the Effects of Chemical Heat Release in the Reacting Turbulent Plane Shear Layer, Ph.D. Thesis, The University of Adelaide; also AFOSR Report AFOSR-TR-84-0650.

[16] MASUTANI, S.M. 1985 An Experimental Investigation of Mixing and Chemical Reaction in a Plane Mixing Layer, Ph.D. Thesis, Stanford University.

[17] BILGER, R.W. 1980 Turbulent Flows with Nonpremixed Reactants, in Turbulent Reacting Flows, Topics in Applied Physics, 44, Springer-Verlag.

9. Figure Captions

Fig. 1 Turbulent Shear Layer Geometry.

Fig. 2 CHEMKIN Simulation of Constant Pressure Reactor using Reactions (1)-(3) and (1)-(7). $[NO]/[NO]^* = 1$.

Fig. 3a Normalized Mean Temperature Profiles for decreasing [NO], U_1 = 22 m/s. $[NO]/[NO]^*$: □ - 1, ○ - 1/2, △ - 1/4, + - 1/8, × - 1/16, ▽ - 1/23, ◇ - 1/32, ◆ - 0.

Fig. 3b Scaled Mean Temperature Profiles for decreasing [NO], U_1 = 22 m/s. Symbols same as Fig. 3a.

Fig. 3c Scaled Mean Temperature Profiles for $[NO]/[NO]^*$ = 1 & 1/32, U_1 = 22 m/s. Symbols same as Fig. 3a.

Fig. 4 Normalized Mean Temperature Profiles for increasing [NO], U_1 = 22 m/s. $[NO]/[NO]^*$: □ - 1, ○ - 3/2, △ - 2.

Fig. 5a Normalized Mean Temperature Profiles for varying [NO], U_1 = 44 m/s. $[NO]/[NO]^*$: □ - 1, ○ - 1/4, △ - 1/16, + -2.

Fig. 5b Scaled Mean Temperature Profiles for $[NO]/[NO]^*$ = 1 & 1/16, U_1 = 44 m/s. Symbols same as Fig. 5a.

Fig. 6a Normalized Product Thickness vs Nitric Oxide Concentration.

Fig. 6b Normalized Product Thickness vs Time of Flight Damkohler Number.

Fig. 7a Temperature vs Time Trace, $[NO]/[NO]^* = 1$, U_1 = 22 m/s.

Fig. 7b Temperature vs Time Trace, $[NO]/[NO]^* = 1/32$, U_1 = 22 m/s.

Fig. 8 k/k^* vs $[NO]/[NO]^*$ from CHEMKIN simulations for Reactions (1)-(7).

Fig. 9 CHEMKIN Simulations of Constant Pressure Reactor using Reactions (1)-(7) for [NO] shown in Table 1.

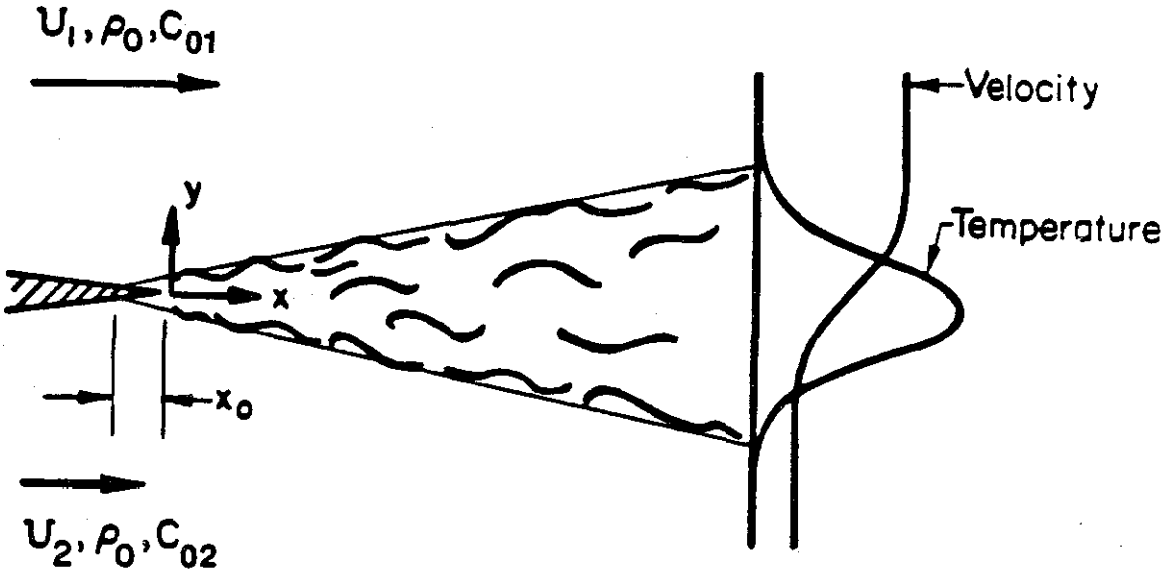

1

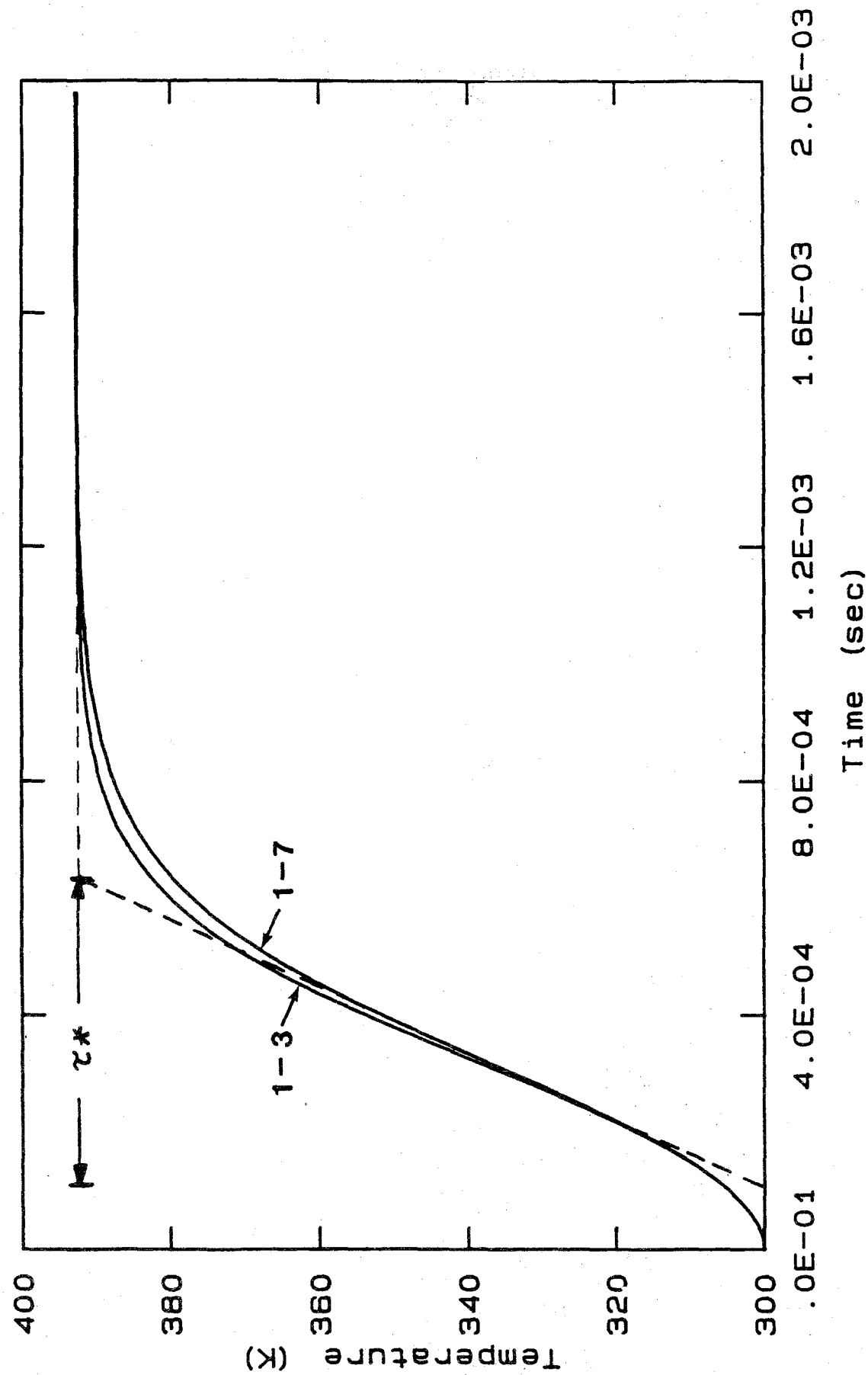
400
380
360
340
320
300
Temperature (K)
.0E-01
4.0E-04
8.0E-04
1.2E-03
1.6E-03
2.0E-03
Time (sec)
τ*
1-7
1-3

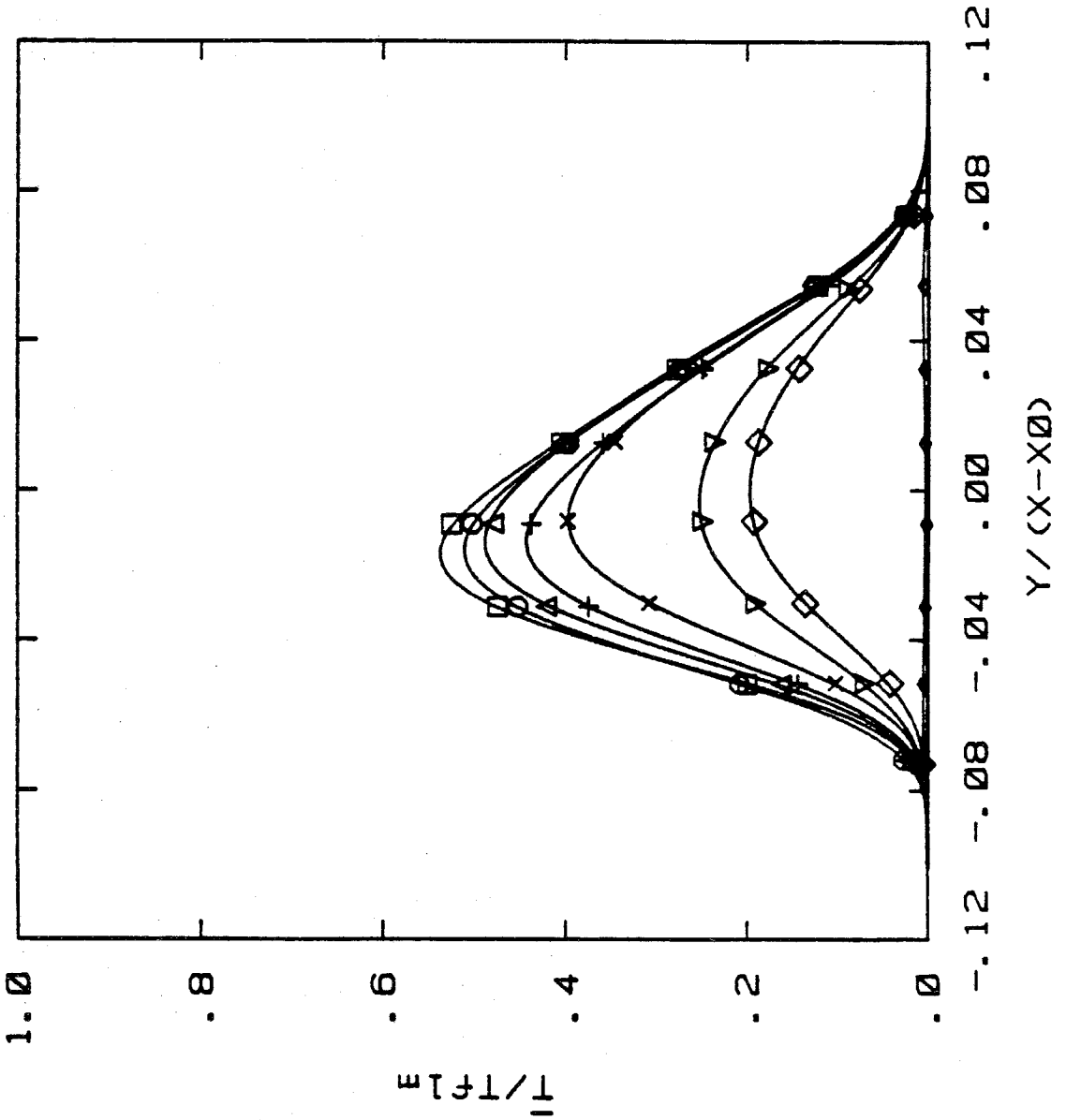
1.0
.8
.6
.4
.2
0
$\overline{T}/Tf1_\infty$
-.12
-.08
-.04
.00
.04
.08
.12
Y/(X-X0)

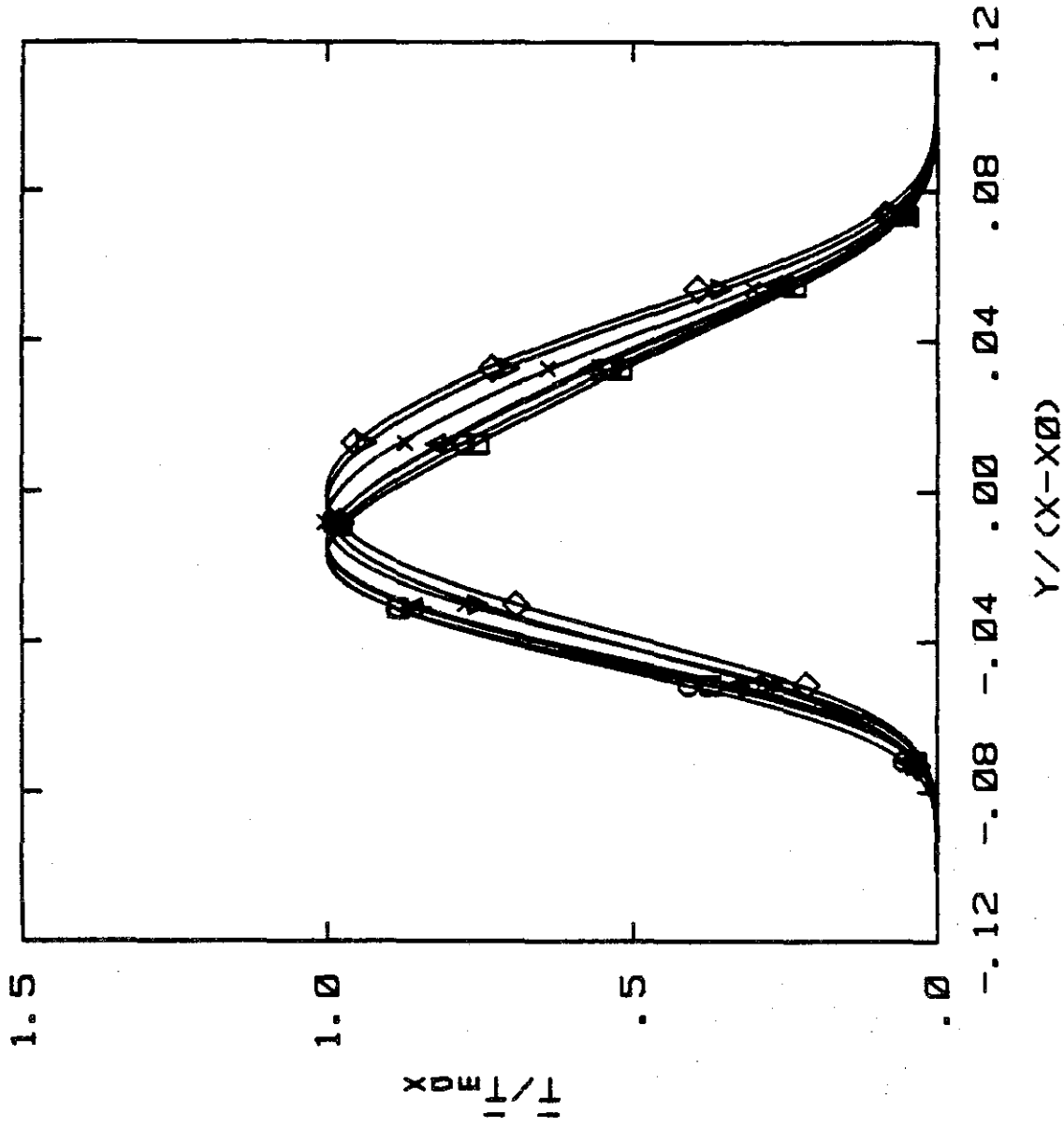
1.5
1.0
.5
.0
$\overline{T}/\overline{T}_{max}$
-.12
-.08
-.04
.00
.04
.08
.12
Y/(X-X0)

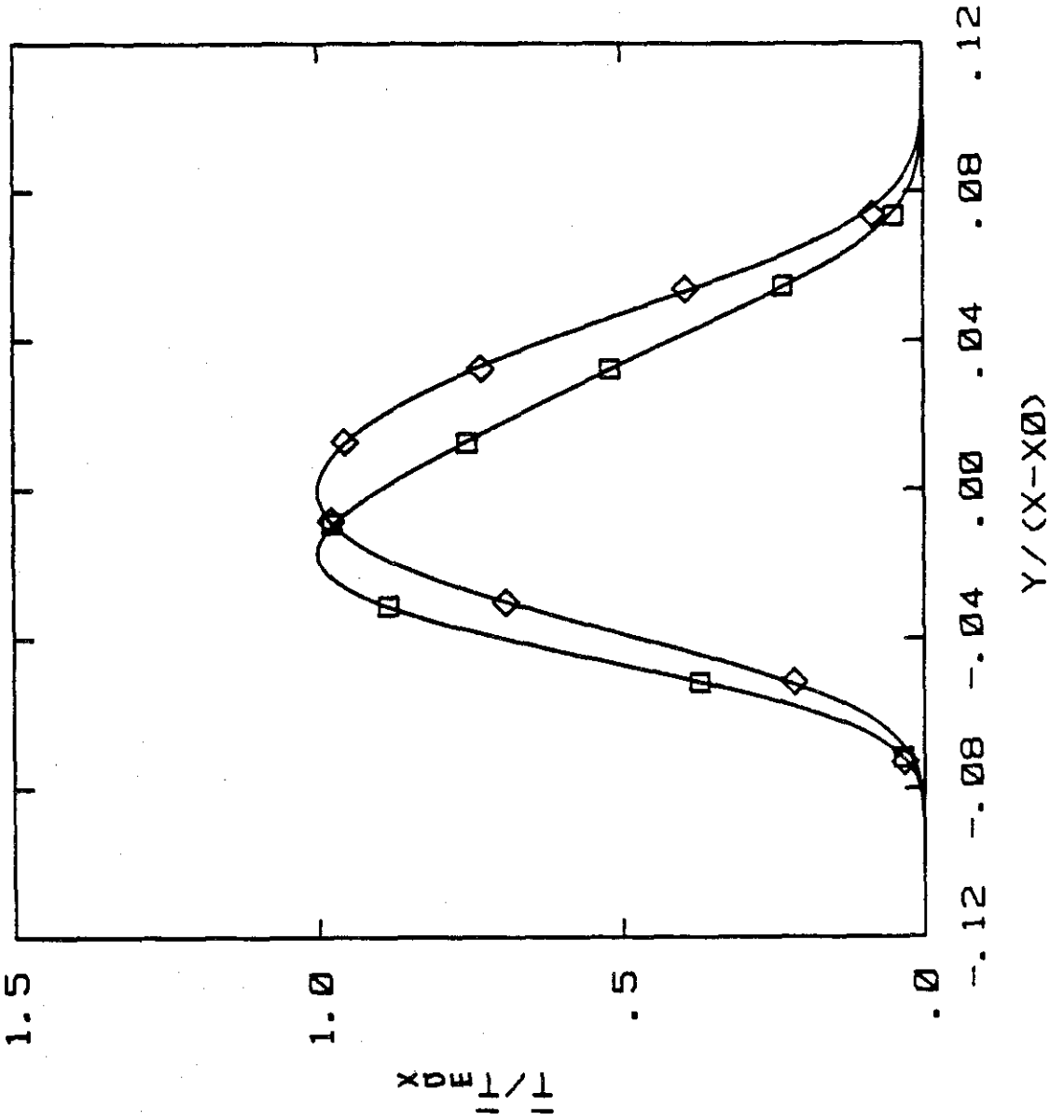
1.5
1.0
.5
.0
T/Tmax
-.12
-.08
-.04
.00
.04
.08
.12
Y/(X-X0)

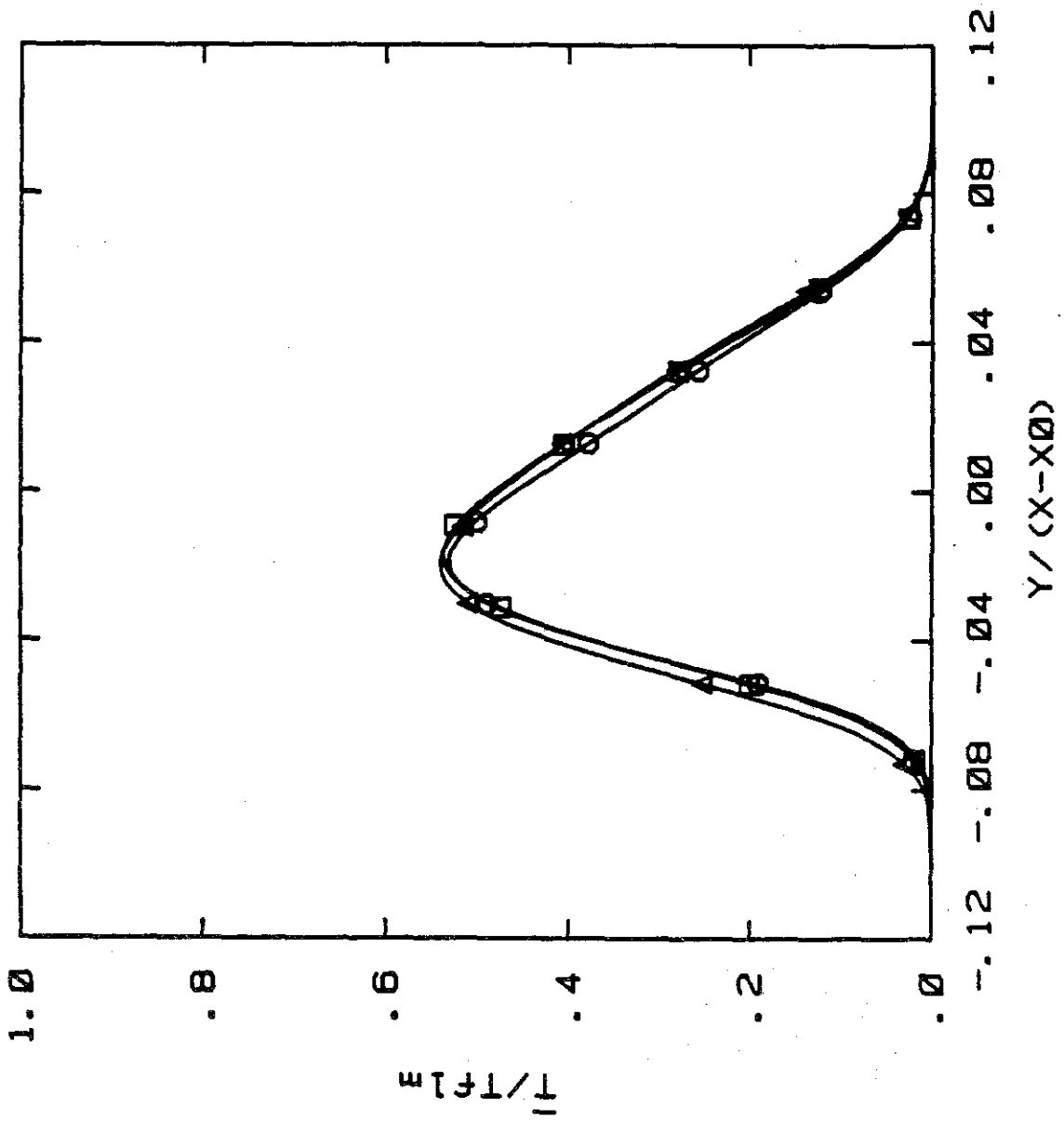
1.0
.8
.6
.4
.2
.0
T/TFlm
-.12
-.08
-.04
.00
.04
.08
.12
Y/(X-X0)

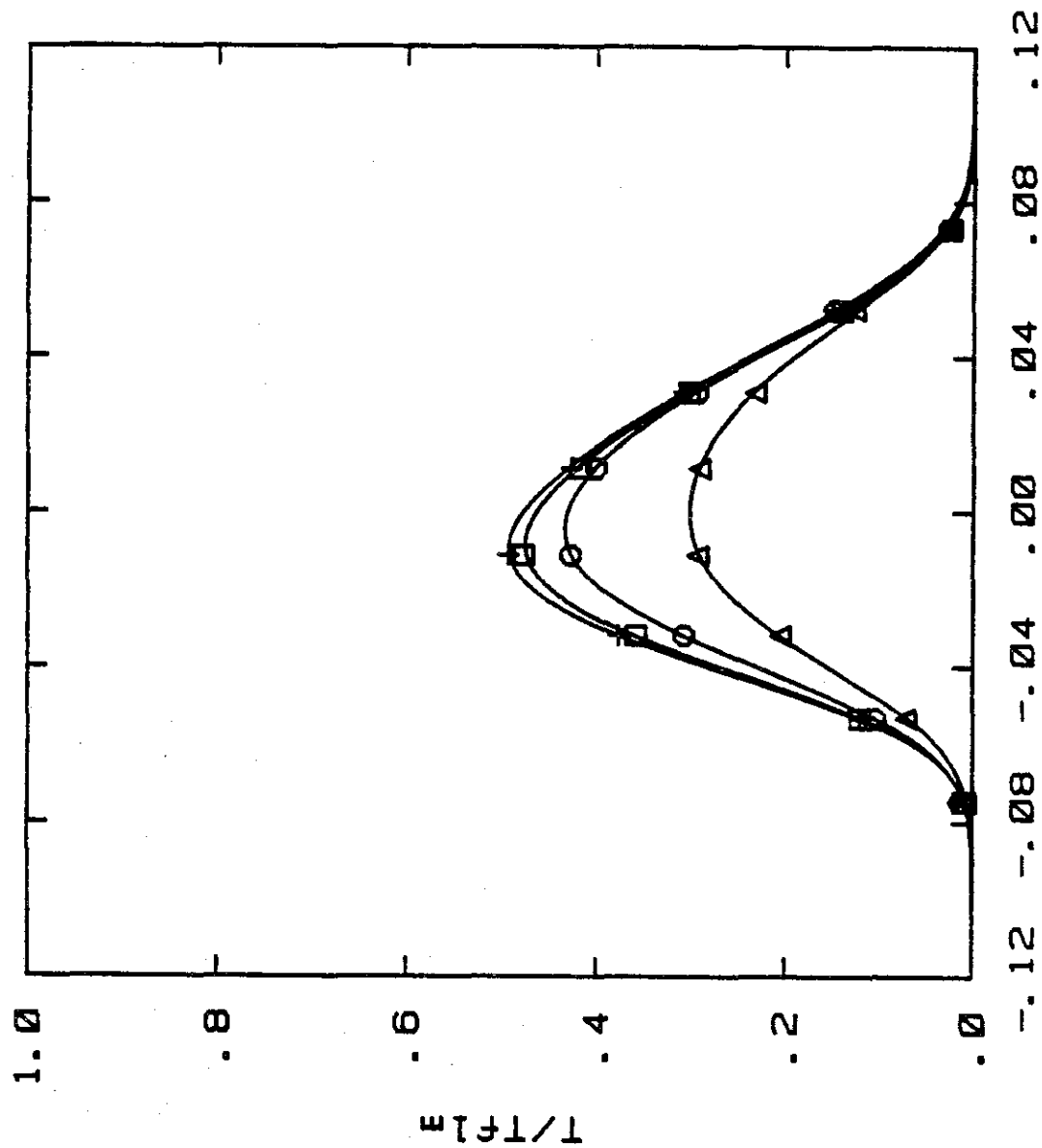

5a

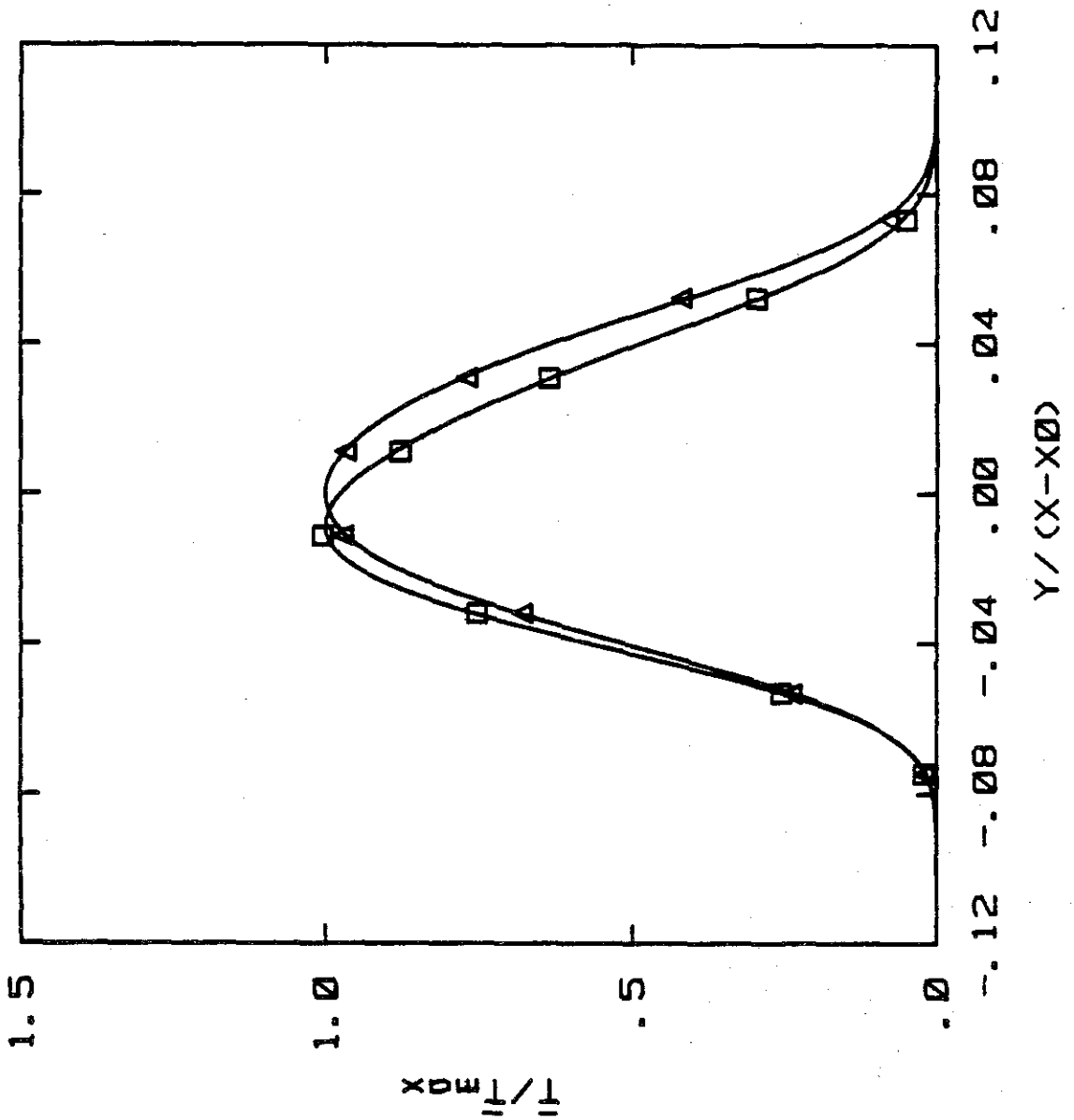

5b

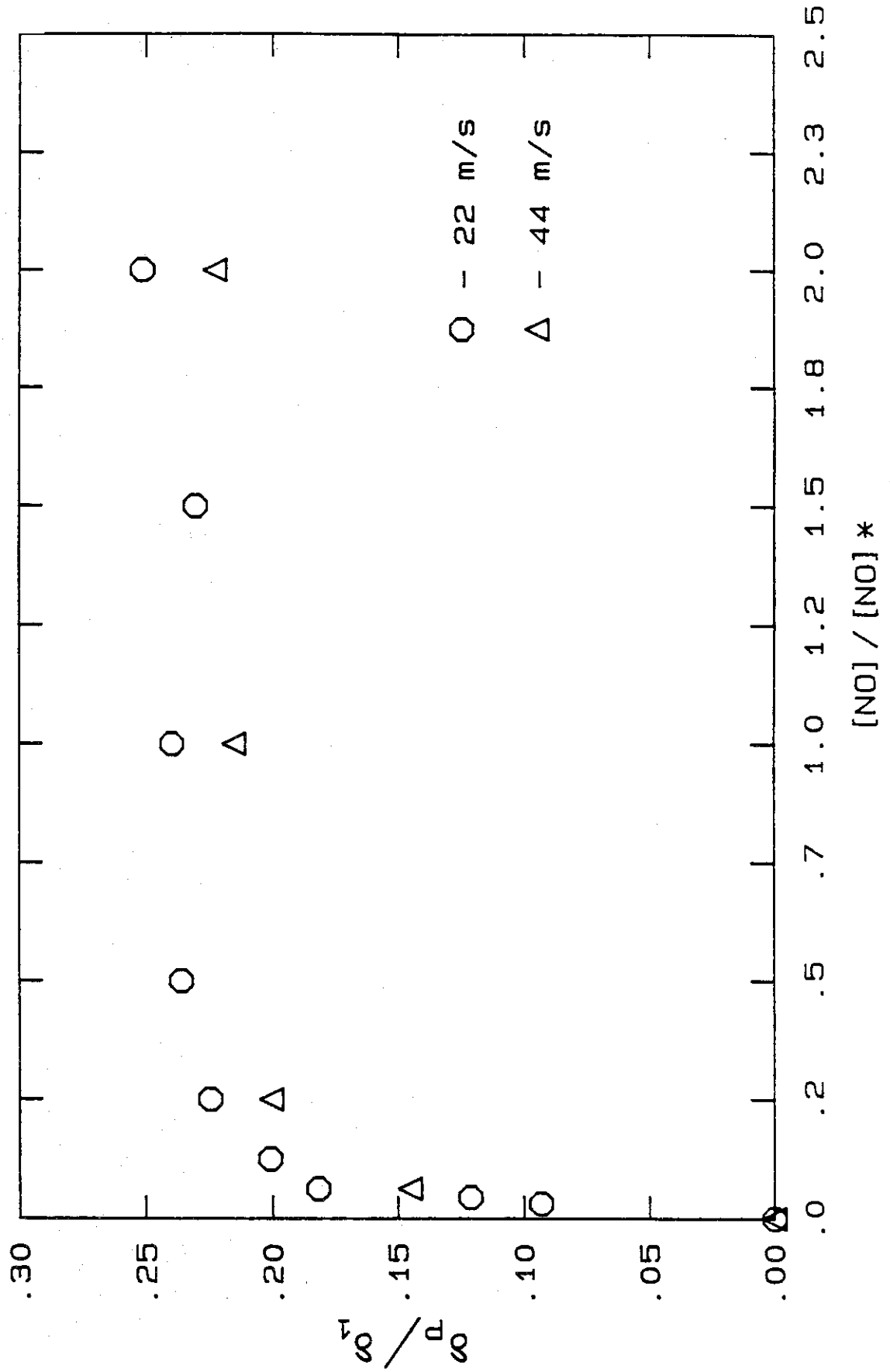
.30
.25
.20
.15
.10
.05
.00
δ_p / δ_1
.0
.2
.5
.7
1.0
1.2
1.5
1.8
2.0
2.3
2.5
[NO] / [NO] *
○ - 22 m/s
△ - 44 m/s

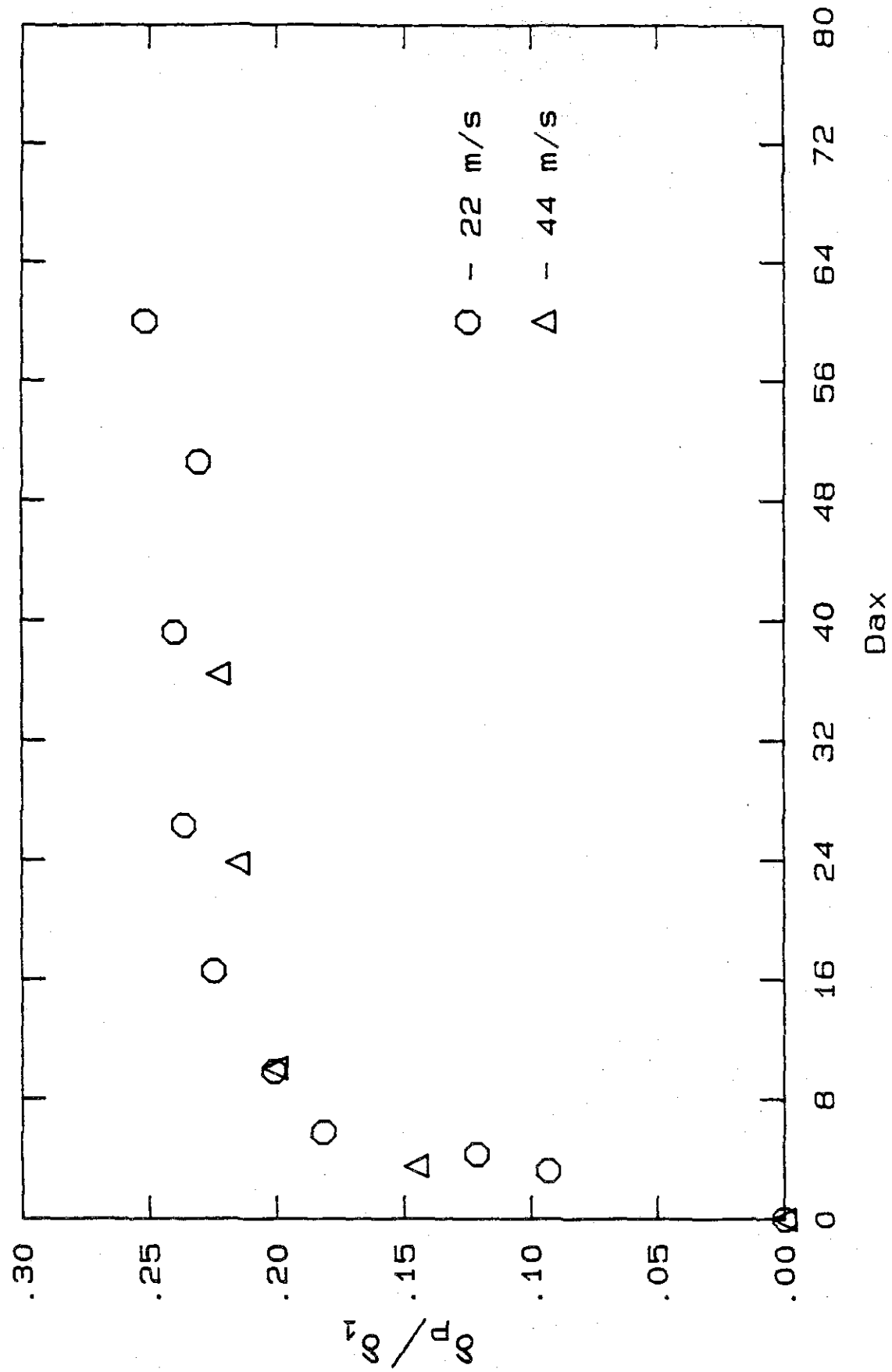
○ - 22 m/s
△ - 44 m/s
δ_p / δ_1
Dax
.30
.25
.20
.15
.10
.05
.00
0
8
16
24
32
40
48
56
64
72
80

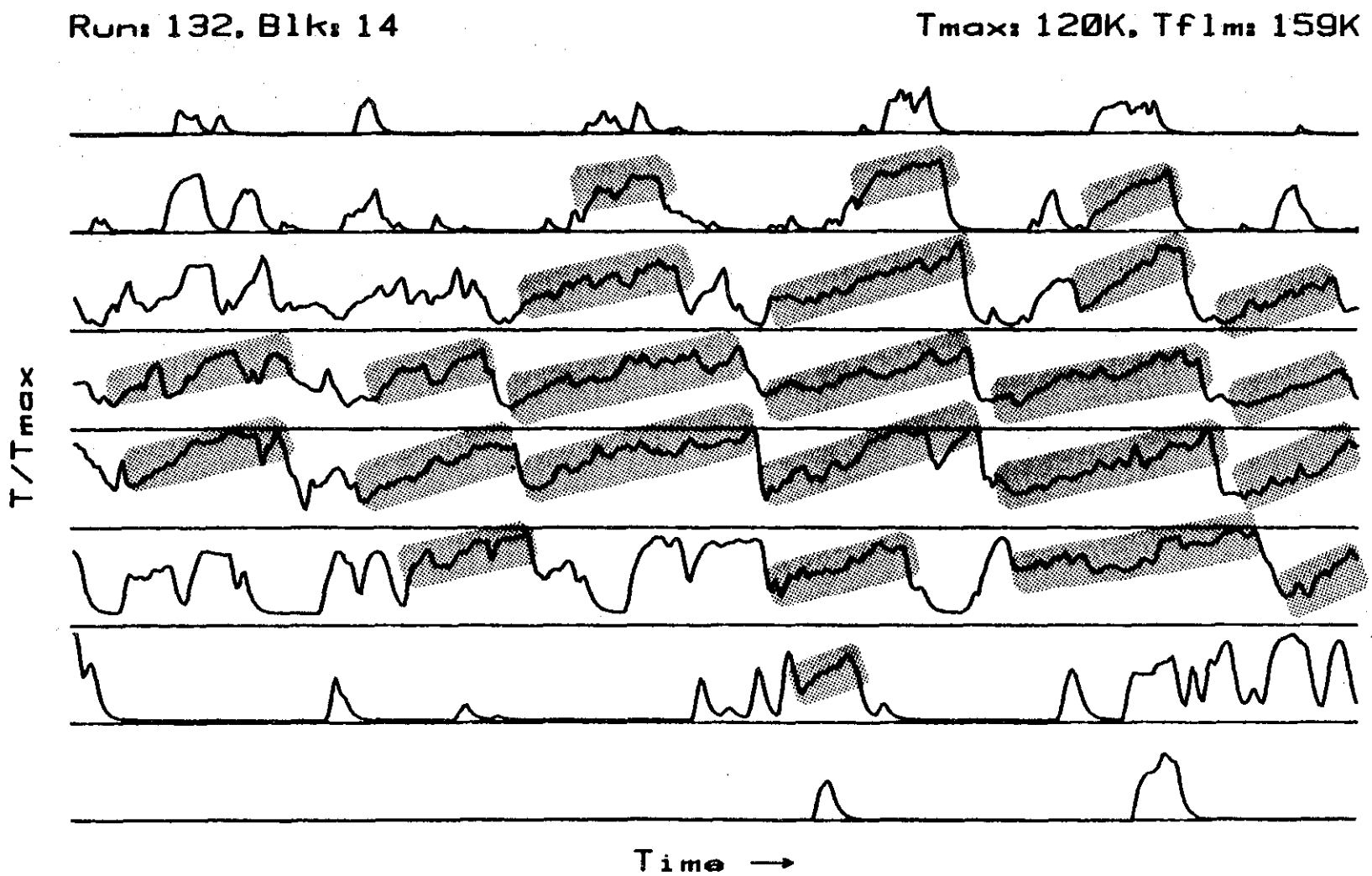

7a

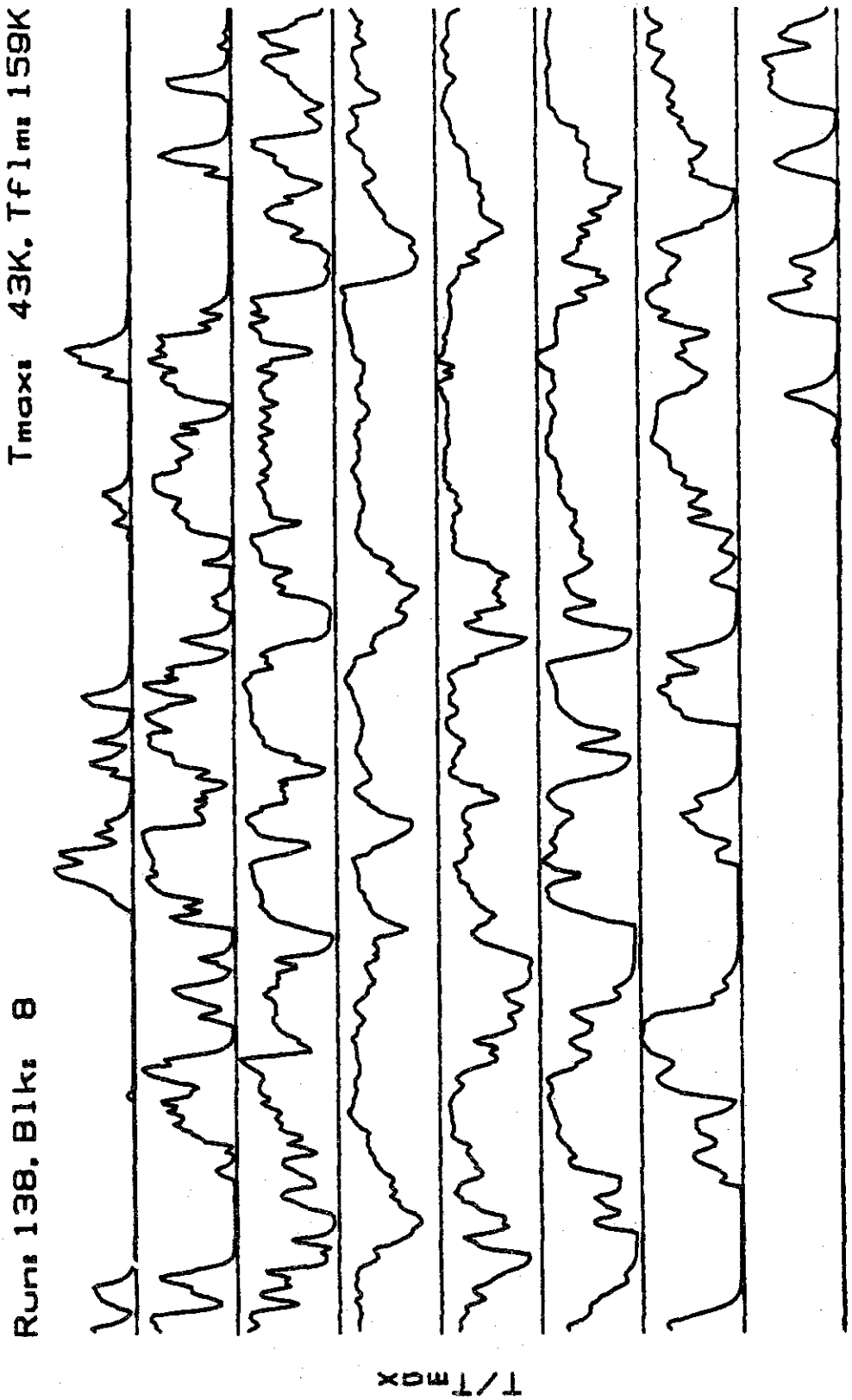
Run: 138, Blk: 8
Tmax: 43K, Tfilm: 159K
T/Tmax
Time →

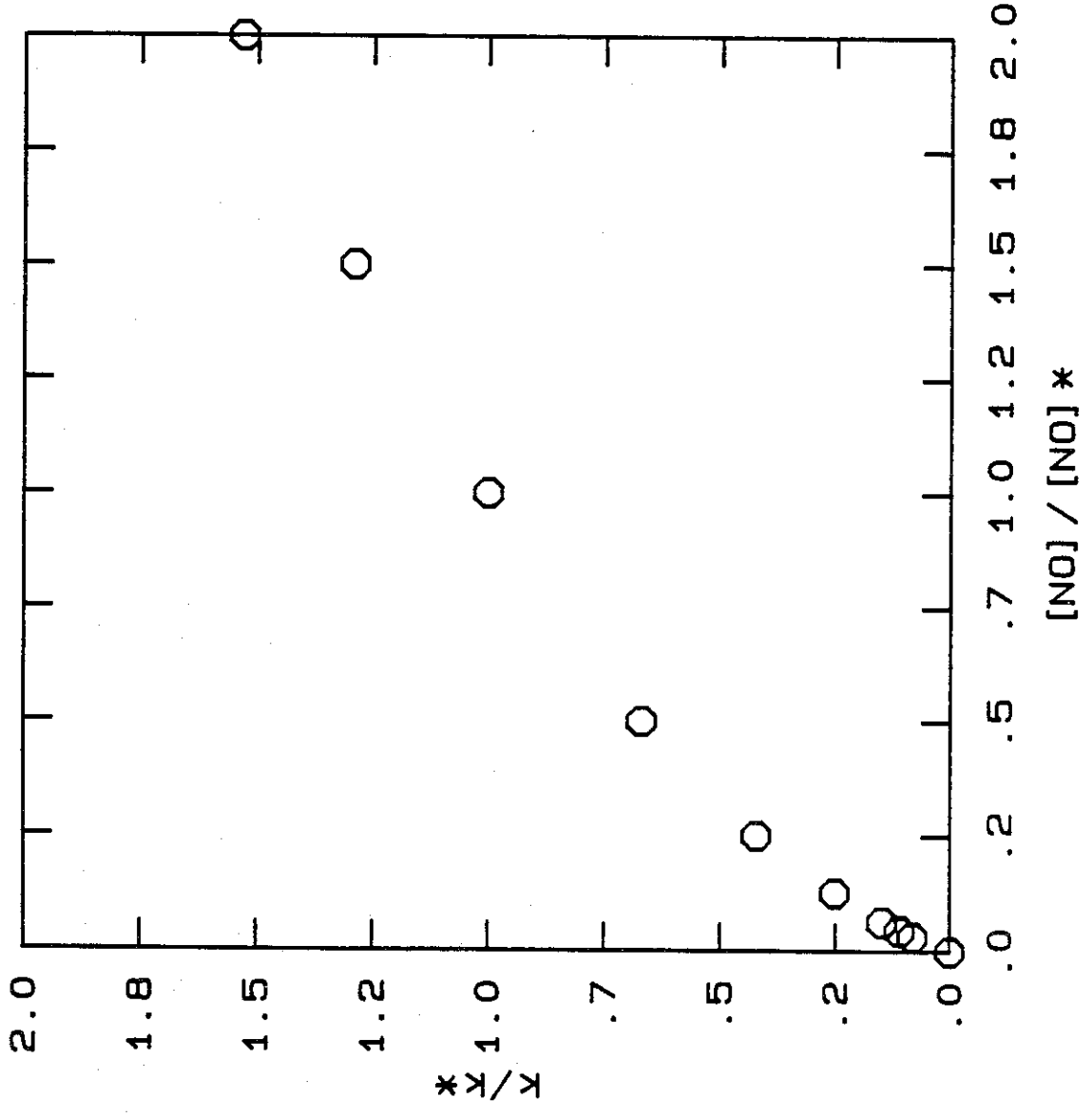
k/k*
2.0
1.8
1.5
1.2
1.0
.7
.5
.2
.0
.0
.2
.5
.7
1.0
1.2
1.5
1.8
2.0
[NO] / [NO] *

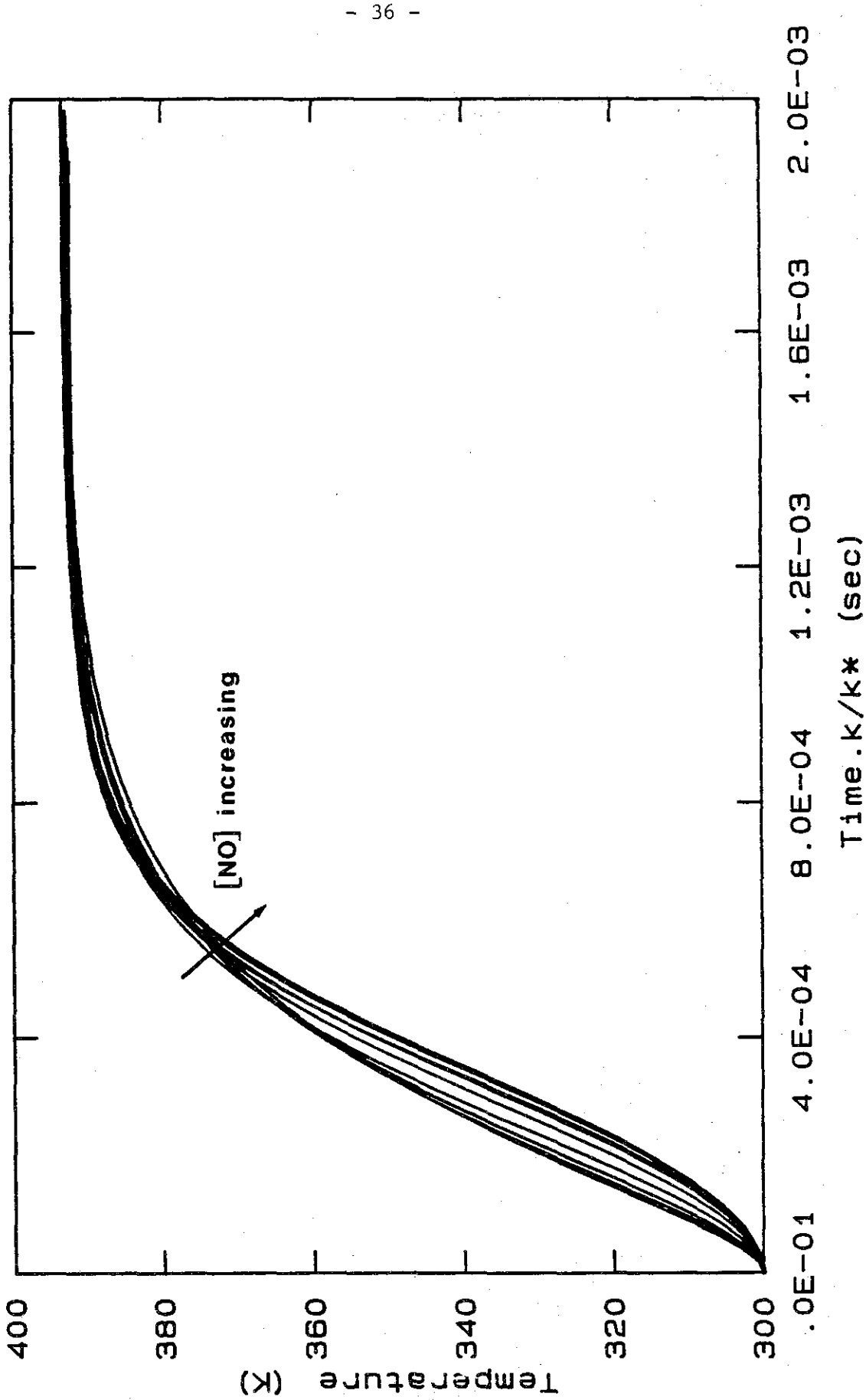
Temperature (K)
400
380
360
340
320
300
.0E-01
4.0E-04
8.0E-04
1.2E-03
1.6E-03
2.0E-03
Time.k/k* (sec)
[NO] increasing

APPENDIX C

The Effects of Damköhler Number in a Turbulent Shear Layer

by

J. E. Broadwell and M. G. Mungal*

Graduate Aeronautical Laboratories
California Institute of Technology
Pasadena, CA 91125

4 June 1986

GALCIT Report FM86-01

*Present Affiliation:
Department of Mechanical Engineering
Stanford University
Stanford, CA 94305

Abstract

A simple model describing chemical reaction in a turbulent shear layer is put in quantitative form and the model predictions compared with experiment. The reactants are not pre-mixed and the flow is two-dimensional. The dependence of the amount of product in the layer on the Schmidt, Reynolds, and Damköhler numbers and on the stoichiometric ratio is exhibited explicitly in the model. The first two parameters appear as the product (Sc Re) and influence that part of the reaction taking place in strained laminar flames. In the limit $Sc\,Re \to \infty$ (for $Sc > 1$ and $Re \gg 1$) the molecular mixing becomes independent of these parameters as it is in classical turbulence theory but the composition and spatial distribution of the molecularly mixed fluid does not resemble those given by such theories. The model predictions are in reasonable agreement with the experimental results for a Damköhler number range from zero to a mixing limited value. The comparison with a set of data for gases in which Re was varied is somewhat less satisfactory.

I. Introduction

This paper presents the results of an analytical study of chemical reactions in a two-dimensional turbulent shear layer. In particular, the experimental results for the variable rate hydrogen-fluorine reaction reported by Mungal and Frieler in Ref. 1 are interpreted in terms of the model proposed in Ref. 2. The reaction takes place between H_2 and nitric oxide, NO, carried in a high speed nitrogen stream and F_2 in a low speed nitrogen stream. In most of the experiments the high and low speed velocities were 22 m/sec and 8.8 m/sec but several runs were made at 44 m/sec and 17.6 m/sec. The H_2 concentration is eight percent molar, the F_2 concentration is one percent molar, and that of the NO (needed to initiate the reaction) varies between 0 and 0.03 percent molar. A description of the apparatus and of the experiment is given in Ref. 1.

The important reactions are:

$$F + H_2 \xrightarrow{k_1} HF + H \tag{1}$$

$$F_2 + H \xrightarrow{k_2} HF + F \tag{2}$$

$$F_2 + NO \xrightarrow{k_3} NOF + F \tag{3}$$

described by the equations:

$$\frac{d[H_2]}{dt} = -k_1 [F] [H_2]$$

$$\frac{d[F_2]}{dt} = -k_2 [F_2] [H] - k_3 [NO] [F_2]$$

$$\frac{d[NO]}{dt} = -k_3 [F_2] [NO]$$

It was shown in Ref. 1 that this kinetic system behaved as if it were a single reaction

$$H_2 + F_2 \xrightarrow{k} 2\ HF \tag{4}$$

governed by the rate equation

$$\frac{d[HF]}{dt} = k [H_2][F_2] \tag{5}$$

where k is a function of the initial nitric oxide concentration, $[NO_i]$. In the following we make use of this approximation, i.e., we assume a single reaction governed by a rate constant k.

Because the reactant concentrations are low, the density changes are neglected and the fluid motion is assumed to be unaffected by the chemical reaction.

II. Physical Ideas

The ideas on which the model is based come from a series of experiments beginning with those of Brown & Roshko[3]. Most, in fact, derive from this now widely known seminal study. The subsequent work of Konrad[4], Breidenthal[5] and Brown & Dimotakis[6] and the analyses of Corcos and Sherman[7] provided further evidence for the basic concepts. This evidence is discussed in detail in Ref. 2 and a model suggested by the observations is proposed in qualitative terms. Here the physical ideas will be reviewed briefly, the model will be put in quantitative form, and results from it compared with the experimental findings. Finally, shortcomings of the model are discussed and possible improvements suggested.

The experiments cited above show that the sequence of events by which parcels of fluid from the two streams reach the molecularly mixed state begin when the fluid elements are entrained into the shear layer by large scale coherent motions. The parcels are distributed across the layer and are entangled (using Roshko's term) by vortical motions in large scale structures. This motion, molecular mixing, and chemical reaction are governed by the equations, in non-dimensional form:

$$\nabla \cdot V^* = 0 \tag{6}$$

$$\frac{\partial V^*}{\partial t^*} + V^* \cdot \nabla V^* = \frac{1}{Re} \nabla^2 V^* - \nabla p^* \tag{7}$$

$$\frac{\partial \alpha_i}{\partial t^*} + V^* \cdot \nabla \alpha_i = \frac{1}{ReSc} \nabla^2 \alpha_i - \omega^*_i \qquad (8)$$

in which $V^* = V/\Delta u$, $p^* = p/\rho_\infty(\Delta u)^2$, $x_i^* = x_i/\delta$, $t^* = t(\Delta)/\delta)$, $Sc = \nu/D$, $Re = \Delta u\, \delta/\nu$, α_i is the mole fraction and ω_i^* the dimensionless chemical reaction term. Here Δu is the velocity difference $(u_1 - u_2)$ and δ the local layer thickness. We take the Schmidt number, Sc, to be of order unity or larger and the Reynolds number, Re, to be large. It is conventional, and presumably justifiable, at large Re to ignore the effects of the viscous terms in Eq. (7) on the motion. For the molecular mixing, however, the diffusion term is essential. In view of the nature of Eq. (8), especially in the limit $Re \to \infty$, it seems plausible that thin diffusive layers, boundary layers in the mathematical sense, would form between fluid from the two streams and that their thickness, ℓ, would be of the order $\delta/(Sc\,Re)^{1/2}$. In the model, these layers are represented by the solutions for the laminar diffusion zones formed in stagnation point flows, conventionally called strained flames.

It is argued next that as a structure moves downstream, the laminar mixing layers are lengthened and further intertwined as ever smaller scales are generated. This (Lagrangian) motion is taken to be a Kolmogorov-like cascade to λ_0, the Kolmogorov scale. When the fluctuations reach this scale, the layers merge. (During this motion, the structures are distorted and may intermingle, so that when the layers merge they do not necessarily form large, distinguishable regions in the cores as Fig. 5 in Ref. 2 may unfortunately suggest.) Since the

time to diffuse across the scale $\lambda_0 \sim \delta/Re^{3/4}$, is of the order $(\delta/\Delta u) \cdot Sc/Re^{1/2}$, at high Re the molecules in the layers interdiffuse in a time that is short compared to the cascade time, $\delta/\Delta u$, to form what is called in the model, the homogeneous mixture. Because the layers in a given structure have been distributed throughout the mixing layer by the large scale motion before they merge, we assume that the homogeneous mixture has a composition that is nearly independent of the lateral coordinate, y. Additional experimental evidence supporting this approximation is contained in the results of Mungal & Dimotakis[8], and especially, Koochesfahani[9] and Koochesfahani & Dimotakis[10]. In the model, as a further idealization, the homogeneous mixture composition is taken to be a single value: it is assumed to be composed of fluid from the two streams in the ratio, E, the ratio of high speed to low speed fluid entrained into the mixing layer.

The flame sheet area per unit volume, S, computed in the cascade by taking $S \sim 1/\lambda$, where λ in the fluctuation scale, for $\delta > \lambda > \lambda_0$, behaves as intuition suggests, i.e., S increases slowly at first and then extremely rapidly as $\lambda \to \lambda_0$. This behavior is the motivation for dividing the molecularly mixed fluid into two distinct states, flame sheets and the homogeneous mixture. In the model, then, S is the flame sheet area per unit volume at the large scale and is taken, consequently, to scale with $1/\delta$ and to be independent of Re. (The thickness, however, as already noted, depends on Re as well as Sc.)

This description of the flow, involving as it does the motion of large scale fluid elements, pictures the flow to be unsteady at spatial and temporal scales δ and $\delta/\Delta u$. Evidence for such unsteadiness is clear in the temperature-time traces in Ref. 1. In the further development of the model, however, we will be concerned only with mean values and will put the ideas, which were most naturally described in Lagrangian terms, into Eulerian form.

The ideas presented above can be summarized and clarified with the help of the diagram in Fig. 1 which is intended to represent the three fluid states in the shear layer and to show the sequence by which fluid elements pass from one to the other. Also indicated explicitly is the presence of unmixed fluid within the layer. The v's are volume fluxes per unit length into the various states, with v_1 and v_2 the fluxes from the high and low speed streams into the layer. (The entrainment ratio, E (> 1), is v_1/v_2.)

When the molecular diffusion coefficients of the contituents are equal, the flame sheets consist of equal volumes from the two streams. The excess high speed fluid, therefore, becomes part of the homogeneous mixture, directly, at the end of the cascade.

The homogeneous mixture volume flux increases with axial distance x by the addition of a volume flux per unit length, v_h, the sum of the flame sheet flux, v_f and of high speed fluid, v_d. It is easy to show that v_h is made up of v_d and v_f in the proportions

$$v_d = \frac{E-1}{E+1} v_h \quad ; \quad v_f = \frac{2}{E+1} v_h \, .$$

The justifications for the assumption that v_h is a constant independent of Re (to be determined, implicitly, by experiment as shown later) are discussed in Ref. 2; these are, essentially, the same as those given above for dividing the mixed fluid into the two states. The result is that the amount of homogeneously mixed fluid rises linearly with x as does the entrained fluid.

This description of the flow is shown schematically in Fig. 2 in which the cross-hatched regions represent the homogeneous mixture and the thin lines the flame sheets. In the present formulation it is assumed that the flame sheets are formed only between pure fluid from the two streams and, in addition, that their structure and composition is in quasi-equilibrium with the local large scale strain. (In Ref. 2 it is wrongly stated that these properties are in equilibrium with the strain at the small scales.)

III. Model Formulation

In the experiments to be discussed, the amount of product in the shear layer is characterized by the "product thickness", δ_p, defined at a particular axial measuring station by

$$\delta_p = \int_{-\infty}^{\infty} \frac{C_p(y)}{C_\infty} \, dy$$

where C_p is the molar product concentration and C_∞ is the reactant concentration in one of the streams, here taken to be the low speed fluorine bearing stream. Following the discussion above, the contributions of the flame sheets and the homogeneous mixture are considered separately as follows:

$$\delta_p = \int_{-\infty}^{\infty} \frac{C_p}{C_\infty} \, dy = \int_{-\infty}^{\infty} \frac{(C_p)_h}{C_\infty} \alpha(x,y) \, dy + \int_{-\infty}^{\infty} \frac{(C_p)_f}{C_\infty} \ell \cdot S \, dy \quad (9)$$

where $(C_p)_h$ and $(C_p)_f$ denote the homogeneous mixture and average flame sheet product concentrations, in moles per unit volume of homogeneously mixed fluid and of flame sheet fluid, respectively. The fractional volume of homogeneously mixed fluid is denoted by $\alpha(x,y)$ and that of the flame sheet by $\ell \cdot S$ where ℓ is the sheet thickness.

As already noted, $(C_p)_h$ is independent of y at fixed x and $\alpha(x,y) = \alpha(\eta)$, where $\eta = y/\delta$ and δ is the shear layer thickness, here taken to be distance between the one percent of maximum of the product profiles. The homogeneous mixture term can, consequently, be written

$$\frac{(C_p)_h}{C_\infty}\,\delta \int_{-\infty}^{\infty} \alpha(\eta)\, d\eta \ .$$

Carrier, Fendell, and Marble[11] show that $\ell = a(D/\varepsilon)^{1/2}$ where a is a constant of order one, D is the molecular diffusion coefficient, and ε the strain rate. As stated above, we take ε to be the large scale strain, $\Delta u/\delta$ and assume that ℓ and $(C_p)_f$ are also independent of y at fixed x. Since S scales with $1/\delta$, we put $S = \beta(\eta)/\delta$ and write for the flame sheet term

$$\frac{(C_p)_f}{C_\infty}\,\ell \int_{-\infty}^{\infty} \beta(\eta)\, d\eta = a\,\frac{(C_p)_f}{C_\infty}\left(\frac{D\delta}{\Delta u}\right)^{1/2} \int_{-\infty}^{\infty} \beta(\eta)\, d\eta$$

$$= \frac{a\cdot(C_p)_f}{C_\infty}\,\delta(ScRe)^{-1/2} \int_{-\infty}^{\infty} \beta(\eta)\, d\eta$$

With these expressions, Eq. (9) becomes

$$\frac{\delta_p}{\delta} = A\,(C_p)_h/C_\infty + B\,(Sc\ Re)^{-1/2}\,(C_p)_f/C_\infty \qquad (10)$$

where $A = \int_{-\infty}^{\infty} \alpha(\eta)\, d\eta$ and $B = a \int_{-\infty}^{\infty} \beta(\eta)\, d\eta$ are constants to be determined as described later.

Observe that A and B have to do only with the molecular mixing; all the chemical kinetic effects appear in $(C_p)_h$ and $(C_p)_f$. Strictly, A and B must be determined for each free stream velocity and density ratio. It is likely, however, from the arguments leading to the model, that they are weak functions of these variables.

In the next two sections, methods for determining $(C_p)_h$ and $(C_p)_f$ are derived, with the flame sheets considered first.

IV. Strained Flames

A two-dimensional strained flame is formed when two streams carrying reactants meet at a stagnation point as sketched in Fig. 3. Under our conditions, the overall conservation equation is

$$\frac{\partial u}{\partial x} + \frac{\partial v}{\partial y} = 0$$

If v is a linear function of y,

$$v = -\varepsilon y \quad , \quad \frac{\partial u}{\partial x} = -\varepsilon \tag{11}$$

When ε is constant and the reaction is fast relative to diffusion, the reaction takes place on a plane parallel to x and the exact solution of Ref. 11 is available. For finite reaction rates numerical computation is required[12]. While such computations could be used here, it is instructive, instead, to use the approximate solution developed next.

A boundary layer integral approach applied to the control volume indicated by dashed lines in Fig. 3 yields the desired results. To obtain a simple approximate solution, we specialize from the beginning to large values of the ratio $(C_H)_\infty/(C_F)_\infty = 1/\phi$, where ϕ is the stoichiometric ratio (following the conventions of Ref. 8) and where the subscripts H and F denote hydrogen and fluorine. Further, consider only average values for the concentrations in the control volume. Note first that from Eqs. (11) $v(-\ell/2) = \varepsilon\, \ell/2$ and $u = \varepsilon\, \Delta x$.

The conservation equations for H_2 and F_2 in the control volume are

$$-v(+\ell/2)\ (C_H)_\infty\ \Delta x - k(C_F)_f\ (C_H)_f \cdot \ell \cdot \Delta x = (C_H)_f\ \varepsilon\ \ell \cdot \Delta x \quad (12)$$

$$v(-\ell/2)\ (C_F)_\infty\ \Delta x - k(C_F)_f\ (C_H)_f\ \ell \cdot \Delta x = (C_F)_f\ \varepsilon\ \ell \cdot \Delta x \quad (13)$$

From Eq. (12),

$$(C_H)_f = \frac{1}{2}\ \frac{(C_H)_\infty}{\left[1 + \frac{k}{\varepsilon}\ (C_F)_f\right]}$$

Putting this expression into Eq. (13), and solving for $(C_F)_f$ in the limit $(C_F)_\infty \to 0$ (to approximate $(C_H)_\infty/(C_F)_\infty \gg 1$) we get

$$(C_F)_f = \frac{1}{2}\frac{(C_F)_\infty}{\left[1 + \frac{k(C_H)_\infty}{2\,\varepsilon}\right]} \quad (14)$$

In the same limit,

$$(C_H)_f = \frac{(C_H)_\infty}{2}\ . \quad (15)$$

The product concentration, $(C_P)_f$, is obtained from the control volume concentration equation

$$k(C_F)_f\ (C_H)_f\ \Delta x \cdot \ell = u(C_P)_f\ \ell = \varepsilon\ \Delta x (C_P)_f\ \ell$$

which becomes, using Eq. (14) and (15),

$$(C_P)_f = \frac{k(C_H)_\infty}{4\varepsilon} \frac{(C_F)_\infty}{\left[1 + \frac{k(C_H)_\infty}{2\varepsilon}\right]} \tag{16}$$

a result consistent with the requirement that

$$(C_P)_f + (C_F)_f = (C_F)_\infty/2 \ .$$

To compare these results with the exact solution of Ref. 11, note first that since $\ell = a(D/\varepsilon)^{1/2}$, the amount of product per unit flame sheet area, $\kappa_P = (C_P)_f \cdot \ell$ is, from Eq. (16) with $k \to \infty$, given by

$$\kappa_P = (a/2)\ (C_F)_\infty\ (D/\varepsilon)^{1/2} \tag{17}$$

The exact solution is

$$\kappa_P = (2/\pi)^{1/2}\ (\phi+1)\ e^{-\Lambda^2}\ (C_F)_\infty\ (D/\varepsilon)^{1/2} \tag{18}$$

where $\Lambda = \mathrm{erf}^{-1}\ \frac{(\phi+1)}{(\phi-1)}$. Thus the dependence on the parameter (D/ε) is the same in the two expressions.

For small k, Eq. (16) reduces to

$$(C_P)_f = \frac{(C_H)_\infty\ (C_F)_\infty}{4}\ (k/\varepsilon)$$

a result in agreement with the analysis of Norton[13].

In summary, Eqs. (15) and (16) are approximations for all k for $(C_H)_\infty/(C_F)_\infty = 1/\phi \gg 1$, while Eq. (18) is the exact solution for $\frac{k(C_H)_\infty}{\varepsilon} \gg 1$ for all ϕ.

Arguments were given above for taking ε proportional to $\Delta u/\delta$. Variation of the proportionality constant around unity had so little effect on the overall results that unity was chosen for convenience in the following work.

V. The Homogeneous Mixture

In this section expressions for the reactant and product concentrations in the homogeneous mixture are developed. First, an expression for the flux of the homogeneously mixed fluid is written and then the fluorine conservation equation is derived.

The homogeneous mixture flux, V_h, can be written

$$V_h = \int_{-\infty}^{\infty} \alpha(y)\, u(y)\, dy = \delta \int_{-\infty}^{\infty} \alpha(\eta)\, u(\eta)\, d\eta$$

where α has the same meaning as before. To avoid introducing an additional unimportant constant, we approximate the above integral by writing

$$V_h = \delta\, \bar{u} \int_{-\infty}^{\infty} \alpha(\eta)\, d\eta = \delta\, \bar{u}\, A \tag{19}$$

where $\bar{u} = (u_1 + u_2)/2$. Therefore, this flux increases linearly with x and is equal to $v_h x$ as indicated in Fig. 1, i.e.,

$$\delta\, \bar{u}\, A = v_h\, x \tag{20}$$

When fluorine is carried in the low speed stream, no fluorine "enters" the V_H flux directly, it is homogenized only after becoming part of a flame sheet. The fluorine and hydrogen conservation equations for the homogeneous mixture are, under these conditions,

$$\frac{d}{dx}\int_{-\infty}^{\infty}(C_F)_h\,\alpha(y)\,u(y)\,dy = -\int_{-\infty}^{\infty}k(C_H)_h\,(C_F)_h\,\alpha(y)\,dy + \frac{2(C_F)_f}{E+1}\,v_h \tag{21}$$

$$\frac{d}{dx}\int_{-\infty}^{\infty}(C_H)_h\,\alpha(y)\,u(y)\,dy = -\int_{-\infty}^{\infty}k(C_H)_h\,(C_F)_h\,\alpha(y)\,dy + \left[\frac{2}{E+1}\,(C_H)_f + \frac{(E-1)}{(E+1)}\,(C_H)_\infty\right] v_h \tag{22}$$

Equation (21) describes the change in the fluorine flux in the mixture caused by the consumption of F_2 in the chemical reaction and the addition from the flame sheets. Using Eq. (19) and (20), we find,

$$\frac{d}{dx}\left[x(C_F)_h\right] = \frac{-k(C_H)_h\,(C_F)_h\,x}{\bar{u}} + \frac{2(C_F)_f}{E+1} \tag{23}$$

$$\frac{d}{dx}\left[x(C_H)_h\right] = \frac{-k(C_H)_h\,(C_F)_h\,x}{\bar{u}} + \left[\frac{2}{(E+1)}\,(C_H)_f + \frac{(E-1)}{(E+1)}\,(C_H)_\infty\right] \tag{24}$$

The approximation used in the flame sheet analysis, i.e., that the hydrogen depletion by chemical reaction can be neglected is introducted next. With $(C_H)_f = (C_H)_\infty/2$, Eq. (24) yields

$$(C_H)_h = \frac{E}{(E+1)}\,(C_H)_\infty\,, \tag{25}$$

The hydrogen from the free stream is again simply diluted in the

homogeneous mixture by the low speed free stream fluid.

With this result Eq. (23) becomes

$$\frac{d}{dx^*}\left[(x^*(C_F)_h\right] = -\frac{E}{(E+1)}\, x^*(C_F)_h + \frac{2(C_F)_f}{(E+1)} \qquad (26)$$

where $x^* = k\,(C_H)_\infty\, x/\bar{u}$.

Since $\epsilon = \Delta u/\delta$, in which Δu is simply related to $\bar{u}$ and $\delta = 0.16x$, Eq. (14) shows that $(C_F)_f$, also, is a function of x^* only. Equation (26) can, therefore, be solved by standard methods to yield $(C_F)_h$ as a function of x^* and, since

$$(C_P)_h/C_\infty + (C_F)_\infty/C_\infty = 1/(E+1)\ , \qquad (27)$$

the variation of the product concentration at the (fixed x) measuring station with the reaction rate. Interestingly, the over-all solution is dependent only upon the Damköhler-like variable, x^*, which arises naturally in the analysis.

It is helpful to note that when $x/\bar{u}$ is replaced by t in Eqs. (23) and (24), they become equations describing exactly the fluorine and hydrogen concentrations in a homogeneous (ie., well-stirred) reactor to which streams of flame sheet and free stream fluid are being steadily added.

VI. Comparison of Theory & Experiment

To compare the theoretical predictions with the experimental results of Ref. 1, values for the constants A and B are required. They have already been determined by Mungal & Dimotakis[8] from their data for fast chemical reactions. For completeness, the constants will be rederived here, in a slightly different way, with essentially the same results. In any event, no re-adjustments are made (nor are possible) to fit the variable chemical rate data of Ref. 1.

The most straight-forward and accurate procedure makes use of two sets of results: (1) the first from a run for a nominal NO concentration in Ref. 1 and (2) from the study of Koochesfahani & Dimotakis[10] of a fast chemical reaction in water. We need not be concerned here with the details of the later experiment, needing only to note that it was for $Re = 2.2 \cdot 10^4$, $\phi = 1/10$, and $Sc = 600$.

The HF experiment, for $Re = 6.6 \cdot 10^4$ and $\phi = 1/8$ yielded $\delta_p/\delta = 0.24$ and the water experiment gave $\delta_p/\delta = 0.13$.

Eq. (10) repeated from Section III, i.e.,

$$\frac{\delta_p}{\delta} = A\,(C_p)_h/C_\infty + B(ScRe)^{-1/2}\,(C_p)_f/C_\infty \qquad (10)$$

is applicable to both experiments.

For the liquid reaction $k \gg 1$ and Eqs. (26) and (16) can be used to find that $(C_P)_h/C_\infty = 1/(E + 1)$ and $(C_P)_f/C_\infty = 0.5$. For the F_2/H_2 fast reaction experiment, $k(C_H)_\infty = (0.53 \cdot 10^{-3}\ \text{sec})^{-1}$ and $\varepsilon = 176\ \text{sec}^{-1}$. We have, again using Eqs. (26), (27) and (16), $(C_P)_h/C_\infty = .997/(E + 1)$ and $(C_P)_f/C_\infty = 0.42$. With these values and $E = 1.3$, Eq. (10) applied to the two experiments yields $A = 0.28$ and $B = 64.5$.

Substitution of these values into Eq. (10) shows that the product in the gas at this Reynolds number is almost equally divided between the homogeneous mixture and the flame sheets.

The expression for finite chemical reaction rate is, therefore,

$$\frac{\delta_P}{\delta} = 0.28\ (C_P)_h/C_\infty + 64.5(\mathrm{Re})^{-1/2}\ (C_P)_f/C_\infty$$

where Sc has been put equal to unity and the quantities $(C_P)_h/C_\infty$ and $(C_P)_f/C_\infty$ are to be found from Eqs. (26), (27) and (16). Figure 4 compares the analytical and experimental results. It shows the normalized product thickness at the measuring station in terms of the Damköhler number Da, where $Da = k\ C_{H_\infty}\ s/\bar{u}$ and s is the distance between the measuring station, x = 47.7 cm, and the location of the shear layer transition to fully developed turbulence, x = 15 cm. The contributions of the homogeneous zones and the flame sheets indicated separately, show that in contrast to the homogeneous mixture, the product concentration in the flame sheet approaches its asymptotic value slowly: even at Da - 60, the reaction is not quite mixing-limited. While, as can be

seen, the agreement between the experiment and the predictions of the model is satisfactory, experiments over a wider range of conditions are needed to test the model more stringently.

It is useful next to discuss effects of the Reynolds number on this reaction because when Re is increased by increasing the velocities, there is an accompanying change in the Damköhler number. Fig. 5 shows the theoretical results for several values of the reaction rate together with the recent measurements of Mungal et al.[14] The curve marked $k/k^* = 1$ is to be compared with the experimental values. That for infinite reaction rate, $k/k^* = \infty$, illustrates the effect of Reynolds number alone. The Reynolds number range in the experiments is too limited to permit definite conclusions from the comparison at this time.

The analysis in this paper has been concerned primarily with the effects of Damköhler and Reynolds number on chemical reactions in turbulent shear layers. The application of the model to reactions in which the equivalence ratio was varied is discussed by Mungal and Dimotakis.[8]

VII. *Concluding Remarks*

We conclude with a tentative explanation of the data in Fig. 7 of Ref. 1 showing that the slope of the ramps in the temperature-time traces within the structures at high chemical reaction rate decreases as the rate is lowered becoming nearly zero at the lowest rate. Simultaneously, the asymmetry in the time-mean temperature profile disappears: Fig. 3a, Ref. 1. Observe first from Fig. 4 that the relative contribution of the flame sheets to the product declines as the reaction rate is reduced. Next Koochesfahani[12] found that in liquids, where (in the present view) the flame sheet contribution is negligible, the time-mean profiles of the product concentration are symmetric and ramps are not present in the concentration-time traces. These observations are consistent with the idea that the ramps and asymmetries are associated with flame sheets.

In the model, the sheets are formed between pure fluids from the two streams, consequently their composition is the same everywhere. This over-simplification must, therefore, be dropped if the observations described above are to be explained by reference to the flame sheet composition. The required generalization is that the newly entrained fluids form mixing layers not only between themselves but with the homogeneous fluid. Mungal and Dimotakis[9] suggest such a generalization. After reviewing the evidence that high speed fluid enters the structures along their high speed and downstream boundaries and the low speed fluid along the low speed and upstream edges, they propose that the two

streams mix, to some degree, with the homogeneous fluid as they enter. The resulting flame sheet compositions are such as to explain the observed ramp and mean profile characteristics.

These ideas may be stated another way: at finite Reynolds number, mean product profiles are symmetric and there are no ramps when the molecular mixing is delayed, i.e., does not occur in the flame sheets. In gases, this can be the consequence of a low reaction rate; in liquids, slow molecular diffusion is the cause. In the limit $(Sc\,Re) \to \infty$ (with $Sc > 1$ and $Re \gg 1$) the flame sheet thickness goes to zero; consequently liquids and gases behave similarly. That the model approaches a limit in which the mixing is independent of Re and Sc is in accord with classical turbulence theory but the distribution and composition of the mixed fluid are qualitatively different.

Ramp-like features have been observed in scalar time traces in a wide variety of experiments in the laboratory[15,16] and in the atmosphere[17]. A more extensive review of these earlier studies and a comparison with the present work is in preparation.

Acknowledgement

The authors wish to acknowledge many helpful discussions with their GALCIT colleagues and especially to thank Richard Miake-Lye for his specific valuable comments on the manuscript. This work was sponsored jointly by the Air Force Office of Scientific Research under Grant No. 83-0213 and the Office of Naval Research under Contract No. N00014-76-C-0260.

REFERENCES

1. Mungal, M. G. and Frieler, C. E.: "The Effects of Damköhler Number on a Turbulent Shear Layer - Experimental Results", GALCIT Report No. FM85-01, California Institute of Technology, Pasadena, CA, 31 December 1985.

2. Broadwell, J. E. and Breidenthal, R. E.: J. Fluid Mech. 125, 397 (1982)

3. Brown, G. L. and Roshko, A.: J. Fluid Mech. 64, 775. (1974).

4. Konrad, J. H.: An Experimental Investigation of Mixing in Two-Dimensional Turbulent Shear Flows with Application to Diffusion-Limited Chemical Reactions, Ph.D. thesis, California Institute of Technology, 1976; also available as Project SQUID Tech. Rep. CIT-8-PU, 1976.

5. Breidenthal, R. E.: J. Fluid Mech. 109, 1 (1982).

6. Dimotakis, P. E. and Brown, G. L.: J. Fluid Mech. 78, 535 (1976).

7. Corcos, G. M. and Sherman, F. S.: J. Fluid Mech. 73, 241 (1976).

8. Mungal, M. G. and Dimotakis, P. E.: J. Fluid Mech. 148, 349 (1984).

9. Koochesfahani, M. M.: Experiments on Turbulent Mixing and Chemical Reactions in a Liquid Mixing Layer, Ph.D. thesis, California Institute of Technology, 1984.

10. Koochesfahani, M. M. and Dimotakis, P. E.: AIAA J. 23(11), 1700 (1985).

11. Carrier, G. F., Fendell, F. E. and Marble, F. E.: SIAM J. Appl. Math. 28(2), 463 (1975)

12. Dixon-Lewis, G., et al.: Twentieth Symposium (International) on Combustion, p. 1893, The Combustion Institute, 1984.

13. Norton, O. P.: The Effects of a Vortex Field on Flames with Finite Reaction Rates, Ph.D. thesis, California Institute of Technology, 1983.

14. Mungal, M. G., Hermanson, J. C. and Dimotakis, P. E.: AIAA J. 23(9), 1418 (1985).

15. Fiedler, H. F.: Adv. Geophy. 18A, 93, (1974).

16. Fiedler, H. F.: Turbulent Mixing in Nonreactive and Reactive Flows, A Project SQUID Workshop, p. 381, Plenum, 1975.

17. Gibson, C. H., Friehe, C. A. and McConnell, S. O.: Phys. Fluids 20(10), Part II, S156 (1977).

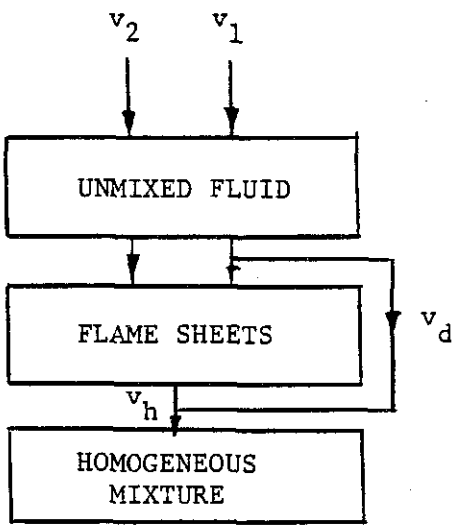

Figure 1. Fluid states in shear layer.

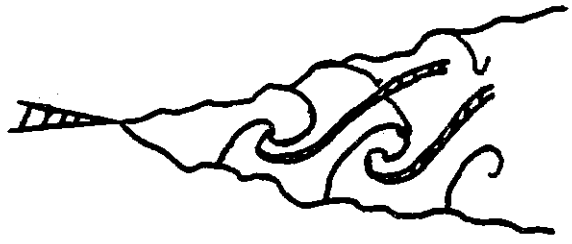

Figure 2. Strained flame sheets (solid lines) and homogeneously mixed zones (cross-hatched) in shear layer.

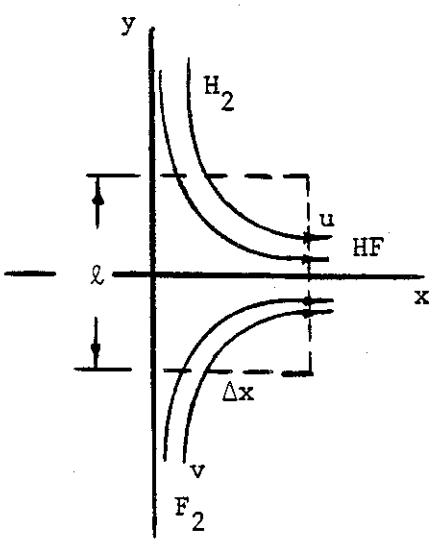

Figure 3. Strained flame control volume.

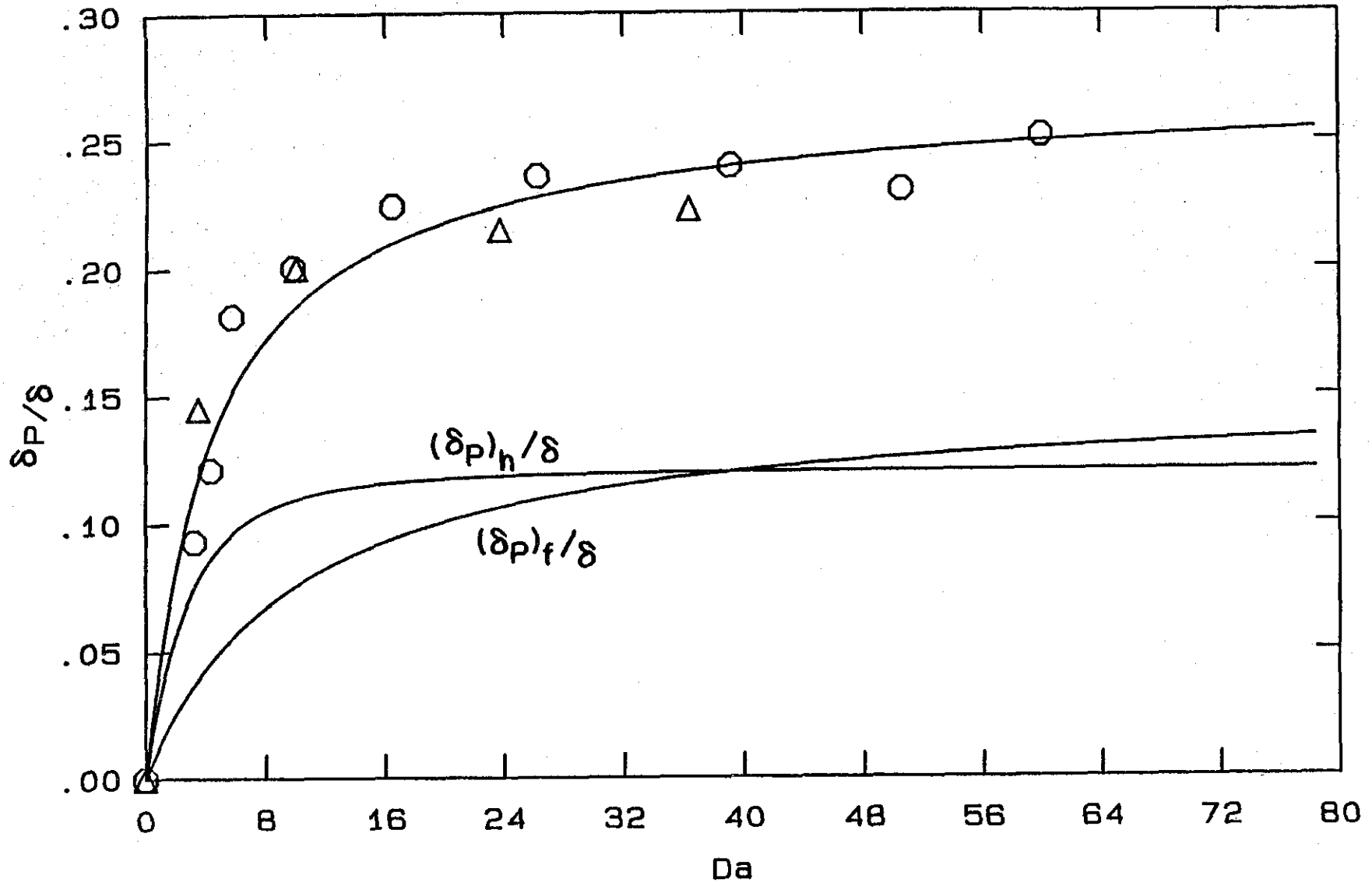

Figure 4. Dependence of product thickness on Damköhler number, Da = k C_{H_∞} s/$\bar{u}$. δ_P, total product; $(\delta_P)_f$, flame sheet product; $(\delta_P)_h$, homogeneous mixture product; δ, shear layer thickness; O , experiment[1], u_1 = 22 m/sec, u_2 = 8.8 m/sec; Δ u_1 = 44 m/sec, u_2 = 17.6 m/sec.

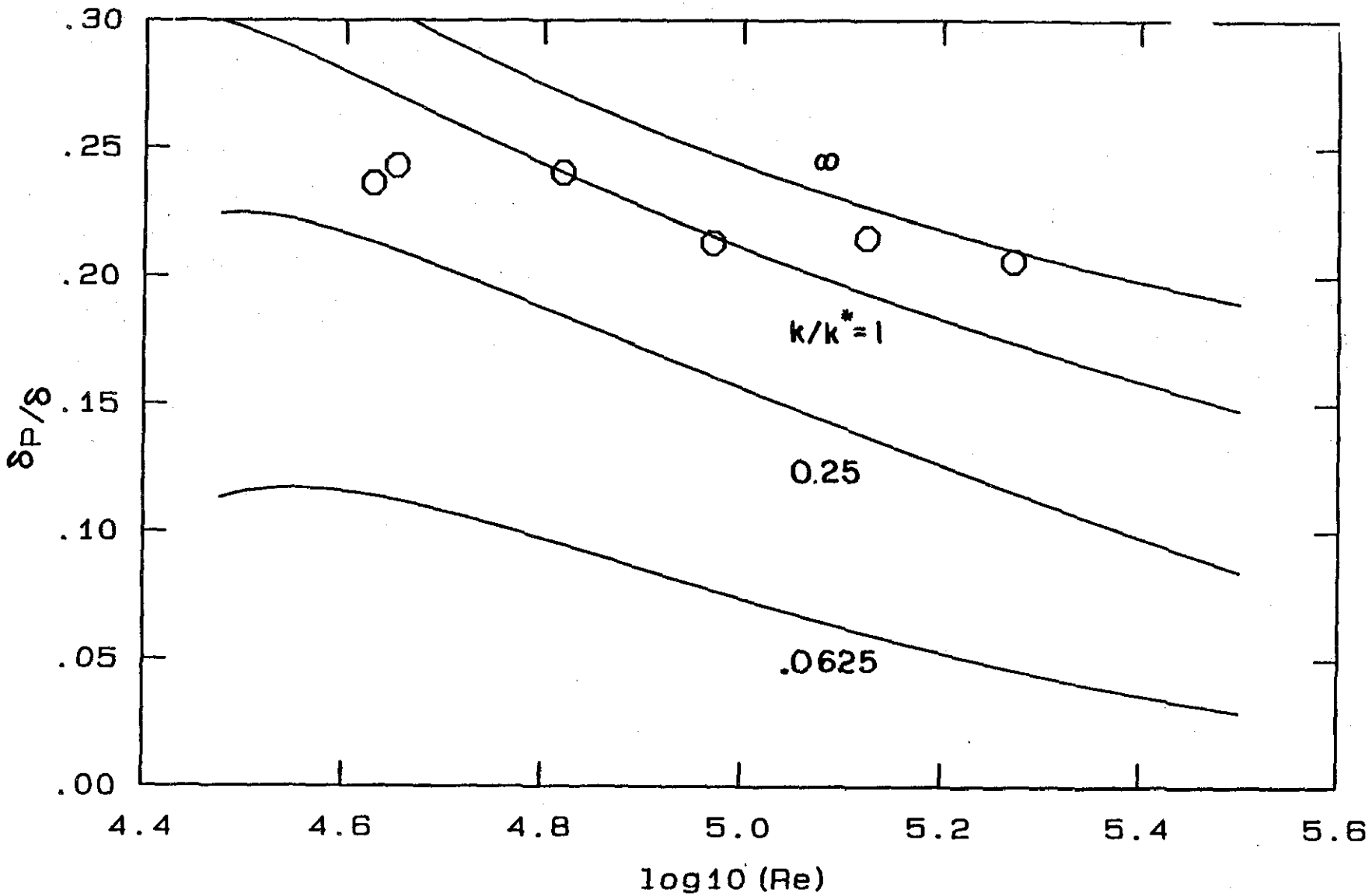

Figure 5. Dependence of product thickness on Reynolds number for various reaction rates. $(C_H)_\infty k^* = (0.53 \cdot 10^{-3}\ \text{sec})^{-1}$. O experimental results from Mungal, Hermanson and Dimotakis[14].